ornl

ORNL/CON-155

FILE COPY
DO NOT
REMOVE

OAK RIDGE
NATIONAL
LABORATORY

MARTIN MARIETTA

Linear Harmonic Analysis of Stirling Engine Thermodynamics

N. C. J. Chen
F. P. Griffin
C. D. West

OPERATED BY
MARTIN MARIETTA ENERGY SYSTEMS, INC.
FOR THE UNITED STATES
DEPARTMENT OF ENERGY

Printed in the United States of America. Available from
National Technical Information Service
U.S. Department of Commerce
5285 Port Royal Road, Springfield, Virginia 22161
NTIS price codes—Printed Copy: A07; Microfiche A01

This report was prepared as an account of work sponsored by an agency of the United States Government. Neither the United States Government nor any agency thereof, nor any of their employees, makes any warranty, express or implied, or assumes any legal liability or responsibility for the accuracy, completeness, or usefulness of any information, apparatus, product, or process disclosed, or represents that its use would not infringe privately owned rights. Reference herein to any specific commercial product, process, or service by trade name, trademark, manufacturer, or otherwise, does not necessarily constitute or imply its endorsement, recommendation, or favoring by the United States Government or any agency thereof. The views and opinions of authors expressed herein do not necessarily state or reflect those of the United States Government or any agency thereof.

ORNL/CON-155

LINEAR HARMONIC ANALYSIS OF STIRLING ENGINE THERMODYNAMICS

N. C. J. Chen F. P. Griffin
C. D. West

Date Published - August 1984

Prepared by the
Oak Ridge National Laboratory
Oak Ridge, Tennessee 37831
operated by
Martin Marietta Energy Systems, Inc.
for the
U.S. Department of Energy
under Contract No. DE-AC05-84OR21400

CONTENTS

Page

LIST OF FIGURES v

LIST OF TABLES vii

ABSTRACT 1

1. INTRODUCTION 2

2. THEORETICAL FORMULATION 6

2.1 Control Volume Representation 6

2.2 Derivation of Governing Equations 8

2.3 Integrated Energy Equations 11

2.4 Engine Performance Parameters 12

2.5 Second-Law Analysis 13

3. LHA SOLUTION METHOD 20

3.1 Pressure Linearization 20

3.2 Nondimensional Equations 22

3.3 Harmonic Oscillations 26

3.4 Truncated Fourier Series Representation 27

3.4.1 Enthalpy flux 28
3.4.2 Wall heat transfer 31
3.4.3 Work output 32
3.4.4 Rate of change of internal energy 33

3.5 System of Integrated Equations 35

3.6 System of Fluctuating Equations 37

3.7 Successive Approximations 40

3.8 Comparison with Nonlinear Solutions 41

3.9 Vector Representation 50

3.10 Summary of LHA Procedures 53

4. LOSS MECHANISMS 55

4.1 Adiabatic Effects 55

4.1.1 Thermodynamics of adiabatic cylinders 55
4.1.2 Dependence of adiabatic efficiency loss on compression ratio 59
4.1.3 Dependence of adiabatic efficiency loss on temperature difference 62

4.1.4 Mechanism for adiabatic efficiency loss..... 64

4.1.4.1 Entropy production due to external heat transfer 64

4.1.4.2 Entropy production due to mixing 67

4.2 Transient Heat Transfer Loss 70

4.2.1 Gas spring with sinusoidal motions 70

4.2.2 Working space of a Stirling engine 74

4.2.3 Entropy production due to transient heat transfer 79

4.3 Effect of Combined Adiabatic and Transient Heat Transfer Losses on Efficiency 82

4.4 Pressure Drop Loss 85

4.4.1 Effects of pressure drop on engine performance 85

4.4.2 Entropy production due to pressure drop 89

4.5 Mass Leakage Loss 90

4.5.1 Gas spring with sinusoidal motions 90

4.5.2 Effects of mass leakage on engine performance 91

4.5.3 Entropy production due to mass leakage 93

4.6 Coupling of Losses 94

5. CONCLUSIONS 97

REFERENCES 101

APPENDIX A. GAS SPRING ANALYSIS 103

APPENDIX B. DERIVATION OF THE EFFICIENCY AND PRESSURE PHASE RELATION 113

APPENDIX C. NOMENCLATURE 115

LIST OF FIGURES

Figure		Page
2.1	Schematic of RE-1000 free-piston Stirling engine	7
2.2	Control volume representation of RE-1000 engine	7
2.3	Steady state entropy balance for Stirling engine system	14
3.1	Flow chart for successive approximations	41
3.2	Efficiency comparison between LHA and CSMP solution methods for RE-1000 Modified configuration	48
3.3	Cartesian coordinate system with sine and cosine as orthogonal unit vectors	51
3.4	Vector diagram showing relevant thermodynamic variables for RE-1000 Nominal engine with adiabatic cylinders and no other losses	52
3.5	Simplified vector diagram showing only pressure and volume vectors	53
4.1	Thermodynamics of RE-1000 Nominal engine with adiabatic cylinders	56
4.2	P-V diagram for the RE-1000 Nominal engine with adiabatic cylinders	58
4.3	Effects of compression ratio and working gas on efficiency of the RE-1000 Modified configuration with isothermal and adiabatic cylinders	60
4.4	Cyclic expansion-space temperature variation for various compression ratios	62
4.5	Cyclic compression-space temperature variation for various compression ratios	63
4.6	Effects of heater temperature and working gas on efficiency of RE-1000 Nominal engine with isothermal and adiabatic cylinders	64
4.7	Irreversible gas mixing in expansion space	68
4.8	Pressure and volume vectors for gas spring with transient heat transfer loss only	71
4.9	Power output and efficiency vs heat transfer coefficients for RE-1000 Nominal engine	75
4.10	Cyclic expansion-space temperature variation for various heat transfer coefficients	76
4.11	Cyclic compression-space temperature variation for various heat transfer coefficients	77

4.12 Pressure and volume vectors for RE-1000 Nominal engine with transient heat transfer loss only 78

4.13 Efficiency loss allocation vs cylinder heat transfer 83

4.14 Power output and efficiency vs pressure drop coefficients for RE-1000 Nominal engine 86

4.15 Pressure and volume vectors for RE-1000 Nominal engine with pressure drop loss only 87

4.16 Damping and inertial components of pressure drop on displacer 88

4.17 Pressure and volume vectors for isothermal gas spring with seal leakage 91

4.18 Power output and efficiency vs mass leakage coefficients for RE-1000 Nominal engine 92

4.19 Pressure and volume vectors for RE-1000 Nominal engine with mass leakage only 93

A.1 Schematic of gas spring 103

B.1 General relationship between pressure and volume vectors in Stirling engine 113

LIST OF TABLES

Table		Page
3.1	RE-1000 Nominal engine dimensions and parameters	42
3.2	RE-1000 Nominal engine operating conditions	43
3.3	RE-1000 Modified engine dimensions and operating conditions	43
3.4	Predicted performance comparison between LHA and CSMP for the RE-1000 Nominal engine with decoupled losses	45
3.5	Predicted performance comparison between LHA and CSMP for the RE-1000 Nominal engine with coupled losses ...	47
3.6	Predicted performance comparison between LHA and CSMP for the RE-1000 Modified configuration with adiabatic cylinders and no other losses	49
4.1	RE-1000 Nominal engine performance comparison: adiabatic vs isothermal cylinders	59
4.2	Loss coefficients for coupling studies	94
4.3	Coupled efficiency loss for RE-1000 Nominal engine	95
4.4	Coupled power loss for RE-1000 Nominal engine	95

LINEAR HARMONIC ANALYSIS OF STIRLING ENGINE THERMODYNAMICS

N. C. J. Chen F. P. Griffin
C. D. West

ABSTRACT

With the objective of gaining a better understanding of Stirling machine processes and especially of free-piston engines, a linearized harmonic analysis method has been developed. The analysis involves linearization of the pressure waveform and represents each term in the conservation equations by a truncated Fourier series, including enthalpy flux discontinuity.

Second-Law analysis is presented of four important loss mechanisms that result from adiabatic cylinders, transient heat transfer in semiadiabatic cylinders, pressure drop through the heat exchangers, and gas leakage from the compression space. The four loss mechanisms, all leading to efficiency reduction below the Carnot level, are characterized by irreversible thermodynamic processes that occur when heat is transferred across a finite temperature difference; when gases at two different temperatures are mixed; or when there is a mass flow through a pressure difference.

The allocation of each individual loss mechanism is derived precisely in terms of entropy production but evaluated by use of pressure, temperature, and mass oscillations calculated from the linear harmonic approximation. When the theory is applied to an engine of Sunpower's RE-1000 dimensions, it reveals clearly that the "adiabatic loss" (due to temperature fluctuations in the cylinders) consists of two components: gas mixing and heat transfer across a temperature difference. The theory further shows that the adiabatic effect is more important than the transient heat transfer loss if the gas-to-cylinder heat transfer rate is small (i.e., nearly adiabatic conditions); the reverse is true for intermediate heat transfer rates; and both losses vanish at very high heat transfer rates. In addition, entropy analyses of pressure drop and mass leakage for isothermal cylinders shed some light on coupling between the different individual loss mechanisms.

1. INTRODUCTION

Analyses of free-piston Stirling engines require a thorough treatment of both the thermodynamics and the dynamics because these two interact in a highly complex manner. As a prerequisite to dealing with this complicated problem, a thermodynamic analysis has been developed that considers the effects of four important loss mechanisms on engine thermodynamic performance through a newly developed method, linear harmonic analysis (LHA), which provides a semi-closed-form solution in contrast to a numerical approach. By the nature of its closed-form solution, the analysis offers additional insights into the underlying physical processes. The method also permits an analysis of the engine dynamics, and such an analysis will be considered in a later publication.

The objectives of this report are twofold: to gain a better understanding of the four loss mechanisms and to provide the basis for future free-piston analysis. The four loss mechanisms that affect engine performance significantly are adiabatic cylinder effects, transient heat transfer in semiadiabatic cylinders, pressure drop through the heat exchangers, and gas leakage from the compression space. All other aspects of the engine are considered ideal at this stage of the analysis. These four loss mechanisms are studied in a coupled mode by the LHA method; that is, their interactions are fully taken into account so that the method is "third order." The basic theoretical formulation, solution method, and variable definitions are provided in great detail for future reference; thus, the report will serve as a solid basis for further development of free-piston engine theory.

As stated, this report will concentrate on the engine thermodynamics. All relevant discussions will be based on a well-tested and well-documented reference engine. This reference engine, a Sunpower RE-1000 free-piston Stirling engine, is analyzed in a kinematic mode. Analyzing an engine in a kinematic mode means that the volume variations are specified. The report also includes three important analyses: allocation of losses according to the Second Law of Thermodynamics, behavior of nonideal gas spring, and nonlinear thermodynamic analyses. The Second-Law analysis provides a rational method to allocate individual loss mechanisms when

two or more of the mechanisms are coupled together. Three irreversible thermodynamic processes that are caused by the four loss mechanisms are identified. Irreversibilities occur wherever there is heat transfer across a finite temperature difference, wherever gases at two different temperatures mix together, and whenever mass flows through a pressure drop. These processes that occur in a typical real machine are quantified in terms of entropy production, thereby making the allocation of efficiency and power losses possible.

A gas spring plays a vital role in free-piston engine performance; therefore, it is included as an integrated part of the thermodynamic analysis. Because a gas spring is simpler in configuration than an engine, an elegant closed-form solution can be obtained that illustrates the transient heat transfer loss much better than numerical methods. This leads to a clear understanding of the transient heat transfer loss associated with the working space in an engine, where mass shuttles continuously between expansion (hot) and compression (cold) spaces.

Even assuming that the amplitudes of all thermodynamic state variables are small relative to their respective mean values, a systematic error could perhaps be introduced by the LHA method. To assess the LHA solution accuracy, a nonlinear analysis that uses the identical set of governing equations, but does not linearize, has been studied independently. The nonlinear analysis applies a well-established numerical software package, the Continuous System Modeling Program[1] (CSMP), to avoid unnecessary programming effort and to concentrate on the problem formulations. The comparison between LHA and CSMP thus establishes the LHA numerical credibility.

A brief literature survey of Stirling engine analyses seems to be appropriate. For kinematic engine analyses, Schmidt's isothermal analysis for sinusoidal volume variations provides a closed-form solution and establishes a standard for Stirling engine theoretical studies.[2] However, it is far from representing real engines because the gas inside the cylinders behaves more adiabatically than isothermally. Unfortunately, if any departures from the isothermal assumption are made, then the equations describing the gas behavior become a nonlinear set of differential equations. Finkelstein[3] was the first to study the effects of adiabatic

cylinders. Subsequently, Qvale,[4] Rios,[5] and Urieli and Berchowitz[2] have all contributed to the understanding of engine performance under various loss mechanisms. These and other numerical analyses, such as Martini's important new work reported in the second edition of his well known "Stirling Engine Design Manual,"[6] have been reviewed by Chen and Griffin.[7] The book by Urieli and Berchowitz[2] was reviewed in draft form prior to publication. A few works have used approximate methods (e.g., Fokker and Van Eekelen[8] and Rauch[9]) or simplified cycles (e.g., Rallis and Urieli[10] and West[11]) to arrive at analytical or closed-form solutions for the performance of engines with nonisothermal cylinders.

When considering free-piston machines, we may conveniently define two categories of analytical approach: isothermal and nonisothermal cylinders. Most previous approaches to the analysis of coupled engine dynamics/thermodynamics begin with the isothermal assumption; representative works include these of Cooke-Yarborough,[12] Rauch,[13] Marusak and Chiu,[14] Berchowitz and Wyatt-Mair,[15] Goldberg,[16] Vincent et al.,[17] West,[18] and Urieli and Berchowitz[2] (Chap. 3). When the analysis is extended to nonisothermal cylinders, as it must be if a physical realistic formulation is to be made, most of the work has depended entirely on numerical solutions to the equations (e.g., Gedeon,[19] Giansante,[20] GE[21]). The work of Rauch[22] is among the few that attempt to treat by nonnumerical methods the coupled dynamics and thermodynamics of free-piston machines with nonisothermal cylinders, but few details have been released because of proprietary restrictions. Rauch's approach, like Fokker and Van Eekelens'[8] successful treatment of the kinematic engines and Cooke-Yarborough's[12] equally successful analysis of the isothermal free-piston engines, uses a linearized approximation in which the variables are represented by harmonic functions.

Our literature survey has convinced us that there is a need for further development of the linearized analyses because closed-form analytical solutions provide a much clearer physical understanding of processes occurring in Stirling machines. However, a closed-form, or nearly closed-form, solution should not oversimplify the physics of the problem; major losses and their interactions should be included to provide a realistic representation of Stirling engine behavior. Therefore, an LHA that takes

into account interactions of major losses has been chosen for studying Stirling engine performance.

This report is rather detailed and mathematical: it should be regarded as a textbook, or at least a primer, on the theory and use of LHA for Stirling engine thermodynamics. We plan to prepare, if this work continues, other reports and papers describing the verification and application of the method in simpler and more descriptive terms; this report will be the main source document. We also plan to publish the extension of the analysis, which is fairly straightforward, to include the dynamics of free-piston engines in certain simplified circumstances.

2. THEORETICAL FORMULATION

Based on a control volume approach, a system of nonlinear differential equations governing the thermodynamic performance of a Stirling engine has been formulated. To simplify the formulation but preserve the physics, the formulation retains an essential minimum of three control volumes (expansion space, compression space, and dead volume). This report encompasses four of the loss mechanisms (adiabatic effects, transient heat transfer, pressure drop, and mass leakage) that are expected to have significant effects on the engine dynamics. All other aspects of the machine are considered to be ideal, although other factors (including appendix gap losses and imperfect heat exchanger elements) that will affect the thermodynamics and, perhaps to a lesser extent, the dynamics will be considered in future work. With proper assumptions, the formulation will lead to a semi-closed-form solution that can greatly enhance theoretical understanding of Stirling-cycle machines.

2.1 Control Volume Representation

With an initial objective of a better understanding of pertinent thermodynamics (and later of dynamics), the formulation effort has concentrated on the Sunpower RE-1000 free-piston Stirling engine, but the engine has been analyzed in a kinematic mode. By kinematic mode, it is meant that the engine is analyzed with specified piston motions.

Shown schematically in Fig. 2.1, the RE-1000 engine manufactured by Sunpower Inc. is a 1-kW single-cylinder machine containing a piston and a displacer sprung to a relatively massive engine casing. The displacer rod is supported by a bracket mounted to the pressure vessel walls. The bounce space contains a large volume of gas and thus remains at a nearly constant pressure. A dashpot loading device, controlled by a variable orifice, has been used to absorb power. Readers seeking detailed information on engine characteristics should refer to a report by Schreiber,[23] but some basic dimensions are included in Table 3.1 of this report.

The working space is divided into three control volumes as depicted in Fig. 2.2. Here the working space refers to the ensemble of variable

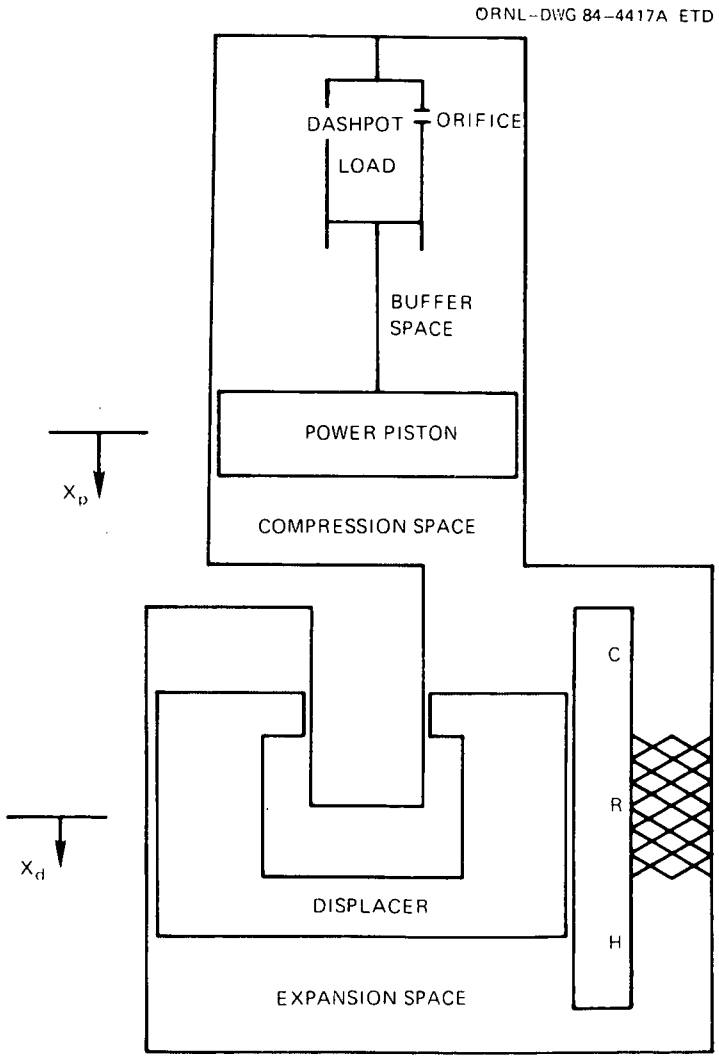

Fig. 2.1. Schematic of RE-1000 free-piston Stirling engine.

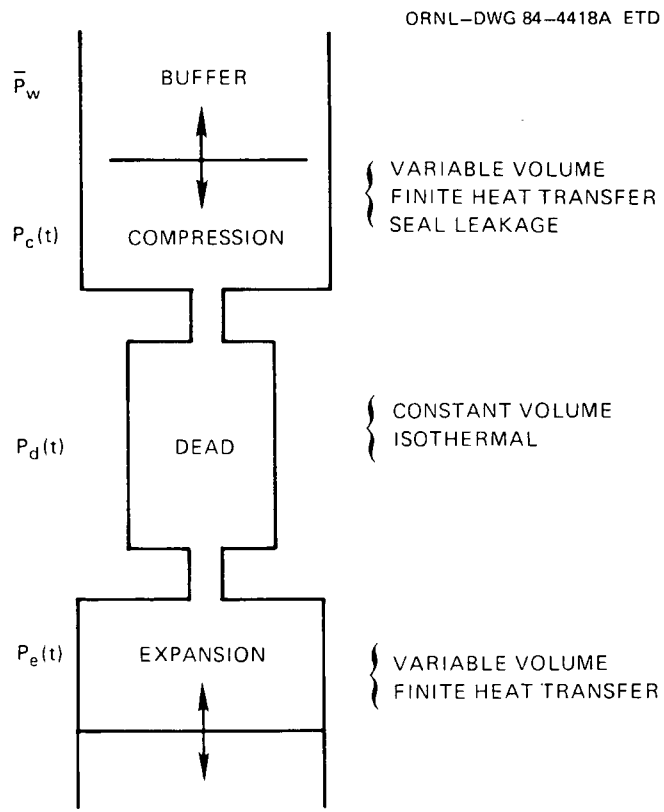

Fig. 2.2. Control volume representation of RE-1000 engine.

and constant volumes. The three control volumes are an expansion space, a compression space, and a dead volume. The volumes of the expansion and compression spaces are time varying and nonisothermal. On the other hand, the dead volume consisting of the heater, regenerator, and cooler is fixed and assumed to be isothermal. In addition, mass leakage is permitted between the compression space and buffer space.

2.2 Derivation of Governing Equations

In the formulation, five basic variables are chosen to define the thermodynamic state of the engine at any instant — the time-dependent masses and temperatures in the control volumes; there are only five variables because the temperature in the dead space is not time dependent. These five unknowns require five governing equations, which are provided by the conservation of mass and energy. The pressure in each space is treated as a parameter and determined by the ideal gas law from the mass, temperature, and volume. The derivations of the governing equations will be described, first on the mass distribution and then on the energy equations.

Of three mass equations, the first two account for pressure drop and the last one includes mass leakage. Starting from mass variation in the expansion space, by continuity, the change of mass inventory in any control volume must equal the net mass flux across that control volume boundary. The mass flux is assumed to be linearly proportional to the pressure difference between adjacent spaces. In Fig. 2.2, there is no outgoing mass flow, and thus the rate of mass increase in the expansion space is equal to the incoming mass flux:

$$\frac{dm_e}{dt} = \frac{1}{k_{pe}} (P_d - P_e) \ . \tag{2.1}$$

An excess pressure in the dead volume over the expansion space leads to an increase in the mass of gas in the expansion space. The proportionality constant k_{pe}, a measure of flow resistance, must be obtained from experimental data. A higher value of k_{pe} indicates a higher pressure drop for the same flow rate.

Likewise, considering the combined spaces of the expansion and dead volume with respect to an incoming mass flux, the mass variation is given by

$$\frac{dm_e}{dt} + \frac{dm_d}{dt} = \frac{1}{k_{pc}} (P_c - P_d) \ . \tag{2.2}$$

The final equation establishes the mass leakage relationship between the working space and buffer space through a rate constant k_{mc}. The buffer space of the RE-1000, characterized by a large volume (about 200 times that of the working space), is assumed to have a constant temperature (approximately equal to the cooler temperature T_K) and pressure $\overline{P}_w$. Coupled with these facts, the rate of the change of mass inventory in the working space shows that

$$\frac{dm_e}{dt} + \frac{dm_d}{dt} + \frac{dm_c}{dt} = k_{mc} (\overline{P}_w - P_c) \ . \tag{2.3}$$

For a perfect seal ($k_{mc} = 0$), there is no leakage. Consequently, the total mass in the working space would remain constant, as expected.

Next, consider the derivation of the two energy equations, first in the expansion and then the compression space. Stirling-cycle machines are characterized by an enthalpy flux discontinuity, which not only presents a conceptual difficulty but also complicates the analysis. An appropriate representation of this discontinuity is vital to the success of any analysis. Our choice is a truncated Fourier series representation; the reasons for this and other related topics will be presented in detail in Chap. 3.

By the First Law of Thermodynamics, the instantaneous energy balance in the expansion space states that

$$c_p T_H \frac{dm_e}{dt} + h_e A_{se} (\overline{T}_{we} - T_e) = P_e \frac{dV_e}{dt} + c_v \frac{d(m_e T_e)}{dt} \ ,$$

$$\text{for } \frac{dm_e}{dt} > 0 \ . \tag{2.4}$$

This is true over that part of the cycle where the working gas emerges from the heater and enters into the expansion space or when the mass of gas in the expansion space is increasing. The first term on the left-hand side of Eq. (2.4) signifies the incoming enthalpy flux at the heater temperature (assuming that the heater acts perfectly), and the second term accounts for heat transfer between the cylinder wall and the gas. The first and second terms on the right-hand side of Eq. (2.4) indicate work done by the gas and the rate of change of internal energy, respectively.

For that part of the cycle where the gas leaves the expansion space and enters into the heater (i.e., for decreasing expansion-space mass), a similar equation will describe the process except that the temperature of the gas leaving the space is not the heater temperature T_H but the instantaneous expansion-space gas temperature T_e.

$$c_p T_e \frac{dm_e}{dt} + h_e A_{se}(\overline{T}_{we} - T_e) = P_e \frac{dV_e}{dt} + c_v \frac{d(m_e T_e)}{dt} ,$$

$$\text{for } \frac{dm_e}{dt} < 0 . \qquad (2.5)$$

The counterpart of the instantaneous energy equations in the compression space may be derived in a similar fashion:

$$c_p T_K \frac{dm_c}{dt} + h_c A_{sc}(\overline{T}_{wc} - T_c) = P_c \frac{dV_c}{dt} + c_v \frac{d(m_c T_c)}{dt} ,$$

$$\text{for } \frac{dm_c}{dt} > 0 ; \qquad (2.6)$$

$$c_p T_c \frac{dm_c}{dt} + h_c A_{sc}(\overline{T}_{wc} - T_c) = P_c \frac{dV_c}{dt} + c_v \frac{d(m_c T_c)}{dt} ,$$

$$\text{for } \frac{dm_c}{dt} < 0 . \qquad (2.7)$$

For further simplification, the heat transfer areas in the wall-gas heat transfer terms in both spaces are assumed to be constant so that

$$A_{se} = \overline{A}_{se} \ , \tag{2.8}$$

$$A_{sc} = \overline{A}_{sc} \ . \tag{2.9}$$

2.3 Integrated Energy Equations

A complete transient treatment of the system of the governing equations [Eqs. (2.1)–(2.7)] is not pursued; only a steady state solution is desired. A steady state solution represents a series of processes whereby the working gas passes through a succession of changes in pressure, volume, temperature, and mass in such a way that, at the completion of the operation, the gas returns to its initial state.

For a solution to be steady state, there should be no net change in the internal energy over a cycle. Satisfying the steady state condition leads to the integrated energy equations. They are derived by performing a cyclic average over each term in the instantaneous energy equations [i.e., Eqs. (2.4)–(2.7)]; symbolically,

$$\overline{\dot{H}}_e + \overline{\dot{Q}}_{we} = \overline{\dot{W}}_e \tag{2.10}$$

in the expansion space, and

$$\overline{\dot{H}}_c + \overline{\dot{Q}}_{wc} = \overline{\dot{W}}_c \tag{2.11}$$

in the compression space.

In these relations $\overline{\dot{H}}$, $\overline{\dot{Q}}_w$, and $\overline{\dot{W}}$ represent, respectively, the cyclic enthalpy flux, the wall-to-gas heat transfer, and the work output. Note that the cyclic internal energy vanishes in the respective spaces and, thus, there is no net change in the overall internal energy over a full cycle; this is the requirement set forth by the steady state condition.

Equation (2.10) contains the information on the source of heat necessary for a Stirling machine. The equation states that over a complete

cycle, the total heat supplied must equal the work performed in the expansion space. It further reveals that there are two distinct heating modes: enthalpy flux from the heater $\overline{\dot{H}}_e$ and the wall-to-gas heat transport $\overline{\dot{Q}}_{we}$. The enthalpy flux represents the amount of heat passed between the heater and the expansion space, while the wall-to-gas heat transfer occurs inside the cylinder. For adiabatic cylinders, there is no wall-to-gas heat transport, and the heat supply comes exclusively from the heater by convection. On the other hand, for isothermal cylinders, no heater is needed; there is no enthalpy flux, and the heat input comes solely from wall-to-gas transfer. However, the quantity of heat provided by wall-to-gas transport remains finite for a perfect isothermal cylinder, although the heat transfer coefficient approaches infinity; this is apparent because a finite amount of work will be performed by the working gas in the expansion space. Finally, for semiadiabatic cylinders, both heating modes are in effect, and the contribution from each component depends on the wall-to-gas heat transfer rate inside the expansion space. Equation (2.11), containing information on the source of cooling, can be discussed in exactly the same way.

2.4. Engine Performance Parameters

The quantities representing cyclic averages in the integrated energy balance equations are significant in defining engine performance. The engine performance is measured by two main parameters: indicated power output and indicated efficiency. The power output is calculated by evaluating the cyclic work integral from the expansion space plus the cyclic work integral from the compression space (generally a negative value). In notations,

$$\overline{\dot{W}}_e = \oint P_e \, dV_e \ , \tag{2.12}$$

$$\overline{\dot{W}}_c = \oint P_c \, dV_c \ , \tag{2.13}$$

$$\overline{\dot{W}}_{out} = \overline{\dot{W}}_e + \overline{\dot{W}}_c \ . \tag{2.14}$$

Because the work integral from the expansion space also represents the total heat input to the engine, the indicated thermal efficiency[24] may be defined as

$$\text{efficiency} = \frac{\text{power output}}{\text{heat input}} , \tag{2.15}$$

or

$$\eta = 1 + \frac{\bar{\dot{W}}_c}{\bar{\dot{W}}_e} , \tag{2.16}$$

or

$$\eta = 1 + \frac{\left(-\bar{\dot{Q}}_{out}\right)}{\bar{\dot{Q}}_{in}} . \tag{2.17}$$

2.5 Second-Law Analysis

The four important loss mechanisms (adiabatic effect, transient heat transfer, pressure drop, and mass leakage) that degrade engine performance result in irreversible thermodynamic processes. These processes occur when (1) there is heat transfer across a temperature difference, (2) two streams of gases at different temperatures are mixed, and (3) there is mass flow through a pressure difference. To allocate properly the losses to individual mechanisms, a Second Law analysis is necessary. The change of entropy is a measure of the amount of energy that becomes unavailable for conversion to useful work; the greater the entropy change because of an irreversibility, the greater the loss of available energy.

To facilitate the later discussions, a general introduction to the subject will be provided here. Consider a system (control volume) bounded by a closed surface (Fig. 2.3). When applied to the reference engine, the boundary of the control volume will be the outer surface of the cylinder, enclosing the heat exchanger components as well. The Second Law of Thermodynamics states that the entropy of the system will be conserved

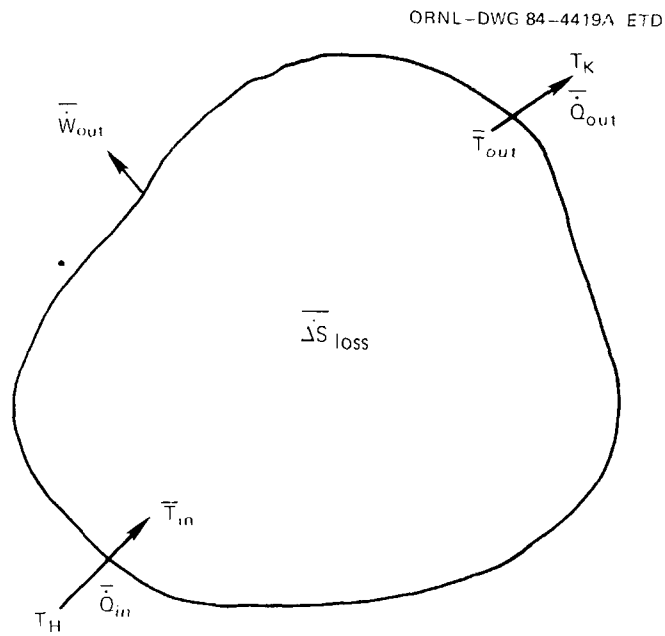

Fig. 2.3. Steady-state entropy balance for Stirling engine system.

over a cycle. Thus,

$$\frac{\overline{\dot{Q}}_{in}}{\overline{T}_{in}} + \overline{\Delta \dot{S}}_{loss} + \frac{-\overline{\dot{Q}}_{out}}{\overline{T}_{out}} = 0 \ , \tag{2.18}$$

where the first and last terms represent the entropy change due to, respectively, heat transfer into the system at temperature $\overline{T}_{in}$ and heat transfer out of the system at temperature $\overline{T}_{out}$. The second term indicates the entropy produced by the internal losses such as mixing, transient heat transfer, and pressure drop.

Substitute $\overline{\dot{Q}}_{out}$ from Eq. (2.18) into the efficiency definition Eq. (2.17), then add and subtract a term involving temperature ratio of source and sink, resulting in

$$\eta = 1 - \frac{T_K}{T_H} - \left(\frac{\overline{T}_{out}}{\overline{T}_{in}} - \frac{T_K}{T_H} \right) - \frac{\overline{T}_{out}\ \overline{\Delta \dot{S}}_{loss}}{\overline{\dot{Q}}_{in}} \ , \tag{2.19}$$

or

$$\eta = \eta_c - \Delta\eta_{EHT} - \Delta\eta_{loss} \ , \tag{2.20}$$

where

$$\eta_c = 1 - \frac{T_K}{T_H} , \tag{2.21}$$

$$\Delta\eta_{EHT} = \frac{\overline{T}_{out}}{\overline{T}_{in}} - \frac{T_K}{T_H} , \tag{2.22}$$

$$\Delta\eta_{loss} = \frac{\overline{T}_{out}\,\overline{\Delta\dot{S}}_{loss}}{\overline{\dot{Q}}_{in}} . \tag{2.23}$$

Equation (2.20) appears somewhat simple in form but offers far-reaching implications for the allocation of efficiency losses. Note that the first term is simply the Carnot efficiency because it involves only the temperatures of the heater and cooler. The second term represents the efficiency loss due to energy transfer to and from the external heat sink T_K and heat source T_H. Heat enters the system through the heater or expansion cylinder or both. $\overline{T}_{in}$ is the average temperature of the working fluid that absorbs the heat input. Heat leaves the system through the cooler or compression cylinder or both. $\overline{T}_{out}$ is the average temperature of the working fluid that rejects the heat output. This loss is derived from the fact that it takes a finite temperature difference to transfer heat in and out of the system. Finally, the last term may be considered as the efficiency reduction due to the irreversibilities in an engine.

Besides efficiency loss, the concept of power loss is both instructive and useful; in particular, the entropy change is needed to relate the various losses back to the energy balance. To do this, a referenced maximum power output (often termed the basic power output in second-order decoupled analyses), from which various identifiable power losses are deducted, should be established. This can be accomplished if Eq. (2.19)

is multiplied by $\overline{\dot{Q}}_{in}$;

$$\overline{\dot{W}}_{out} = \overline{\dot{Q}}_{in}\eta_c - \overline{\dot{Q}}_{in}\left(\frac{\overline{T}_{out}}{\overline{T}_{in}} - \frac{T_K}{T_H}\right) - \overline{T}_{out}\overline{\Delta\dot{S}}_{loss} \ . \tag{2.24}$$

The first term on the right-hand side of Eq. (2.24) represents the maximum possible power output of a Carnot cycle that has a heat input $\overline{\dot{Q}}_{in}$. This term $\overline{\dot{Q}}_{in}\eta_c$ is the basic power output that will be used as the reference value. The second term refers to the power loss due to external heat transfer irreversibilities, and the last term represents power losses due to internal irreversibilities. Note that $\overline{T}_{out}$ is the temperature to be used in determining the conversion of entropy to energy.

For the present formulation with various processes occurring simultaneously, 11 elements are responsible for changes in entropy. The first two elements come from the heat supply,

$$\frac{\overline{\dot{Q}}_{in}}{\overline{T}_{in}} = \frac{\overline{\dot{H}}_e + \overline{\dot{Q}}_{we}}{\overline{T}_{in}} = \overline{\Delta\dot{S}}_{QH} + \overline{\Delta\dot{S}}_{Qwe} \ , \tag{2.25}$$

where $\overline{\Delta\dot{S}}_{QH}$ and $\overline{\Delta\dot{S}}_{Qwe}$ are entropy production due to the heater and average expansion-cylinder-wall heat transfer, respectively. The next two come from the heat rejection,

$$-\frac{\overline{\dot{Q}}_{out}}{\overline{T}_{out}} = \frac{\overline{\dot{H}}_c + \overline{\dot{Q}}_{wc}}{\overline{T}_{out}} = \overline{\Delta\dot{S}}_{QK} + \overline{\Delta\dot{S}}_{Qwc} \ , \tag{2.26}$$

where $\overline{\Delta\dot{S}}_{QK}$ and $\overline{\Delta\dot{S}}_{Qwc}$ represent the entropy production due to the cooler and average compression-cylinder-wall heat transfer, respectively.

The last seven elements are included in the $\overline{\Delta\dot{S}}_{loss}$ term that consists of losses due to mixing, transient heat transfer, pressure drop,

and mass leakage.

$$\overline{\Delta\dot{S}}_{loss} = \overline{\Delta\dot{S}}_{mixe} + \overline{\Delta\dot{S}}_{mixc} + \overline{\Delta\dot{S}}_{TQe} + \overline{\Delta\dot{S}}_{TQc} + \overline{\Delta\dot{S}}_{PDe} + \overline{\Delta\dot{S}}_{PDc} + \overline{\Delta\dot{S}}_{MLc} \ . \qquad (2.27)$$

In the relation, mixing and transient heat transfer processes occur in the respective spaces; pressure-drop-induced entropy changes occur between the variable and constant volumes; and the mass leakage irreversibility occurs between the compression and buffer spaces.

Special attention should be called to the cylinder heat transfer irreversibility, because it involves the definitions of the average and transient components of the heat transfer. In the expansion space, the instantaneous entropy change due to this process is defined as

$$\Delta\dot{S}_{Qe} = \frac{\dot{Q}_{we}}{T_e} = \frac{h_e \overline{A}_{se}(\overline{T}_{we} - T_e)}{T_e} \ . \qquad (2.28)$$

Equation (2.28) can be further decomposed into two components.

$$\Delta\dot{S}_{Qe} = \frac{h_e \overline{A}_{se}(\overline{T}_{we} - \overline{T}_e)}{T_e} + \frac{h_e \overline{A}_{se}(\overline{T}_e - T_e)}{T_e} \ . \qquad (2.29)$$

It is convenient, although somewhat arbitrary, to define the first and second terms as the average expansion-cylinder-wall heat transfer and transient heat transfer component, respectively. Their cyclic values are denoted as $\overline{\Delta\dot{S}}_{Qwe}$ and $\overline{\Delta\dot{S}}_{TQe}$ and will be derived in Chap. 4. Similar expressions for the compression space can be derived without further effort.

The specific derivation of these entropy production terms will not be given until Chap. 4, where the effects of various loss mechanism are to be discussed fully. However, some general background review is provided here.

From the Maxwell relations,[25] one of the general equations for change of entropy may be written

$$dh = Tds + vdP \ , \tag{2.30}$$

or

$$ds = \frac{dh}{T} - \frac{v}{T}\, dP \ . \tag{2.31}$$

Note that s, h, and v are intensive properties that are independent of mass and represent, respectively, the specific entropy, enthalpy, and volume.

For an ideal gas,

$$Pv = RT \ , \tag{2.32}$$

$$h = c_p T \ . \tag{2.33}$$

Substitute Eqs. (2.32) and (2.33) into Eq. (2.31) and integrate over initial and final states, resulting in

$$\int ds = \Delta s = c_p \int \frac{dT}{T} - R \int \frac{dP}{P} \ . \tag{2.34}$$

For a flow process, the variation of entropy becomes

$$\dot{m}\Delta s = \Delta\dot{S} = \dot{m}\left(c_p \int \frac{dT}{T} - R \int \frac{dP}{P}\right). \tag{2.35}$$

To obtain the cyclic entropy change, perform the integration over a complete cycle,

$$\overline{\Delta\dot{S}} = \frac{1}{2\pi} \int_0^{2\pi} \dot{m}\left(c_p \int \frac{dT}{T} - R \int \frac{dP}{P}\right) dt^* \ , \tag{2.36}$$

which represents a general relationship for flow processes. In processes where pressure is constant, such as mixing, the cyclic entropy change

simplifies to

$$\overline{\Delta\dot{S}} = \frac{c_p}{2\pi} \int_0^{2\pi} \dot{m} \ln \left(\frac{T_{final}}{T_{initial}} \right) dt^* \ . \tag{2.37}$$

On the other hand, in processes where enthalpy is constant, such as throttling processes, the cyclic entropy change reduces to

$$\overline{\Delta\dot{S}} = - \frac{R}{2\pi} \int_0^{2\pi} \dot{m} \ln \left(\frac{P_{final}}{P_{initial}} \right) dt^* \ . \tag{2.38}$$

3. LHA SOLUTION METHOD

This chapter will reveal the methodology that makes the semi-closed-form solution for Stirling engine thermodynamic analysis possible. The chapter consists of ten sections to illustrate the basic principles step-by-step in their most logical sequence. First, the analysis imposes a linearized working gas pressure that, in turn, leads to a system of nondimensional governing equations. Subsequently, a simple harmonic solution is assumed for the relevant variables, paving the way for Fourier series representation of all nonharmonic terms in the governing equations, including the enthalpy flux discontinuity. The development further leads to two coupled systems of equations — the integrated and fluctuating energy balances — that the working gas must satisfy simultaneously. Thus, a successive approximation is inevitable for nonisothermal calculations. Above all, vector representation, a direct product of the harmonic analysis, is introduced for future presentation of significant loss mechanisms. Finally, the chapter is closed by a cookbooklike summary for LHA procedures.

3.1 Pressure Linearization

Pressure linearization is a key to the present analysis. The validity of the linearization, in turn, relies on the underlying assumptions that the amplitudes of the thermodynamic variables are smaller than their respective mean values. Stirling engines with both low- and (more surprisingly) high-compression ratios have been confirmed, by a nonlinear analysis to be described later, to satisfy this criterion, so that the use of linearized pressure in the analysis is justified. Two simplified results, mean and fluctuating pressures, will now be derived.

The ideal gas law states that

$$PV = mRT \ . \tag{3.1}$$

As mentioned, all variables will be represented by

$$
\begin{aligned}
P &= \overline{P} + \Delta P \ , \\
V &= \overline{V} + \Delta V \ , \\
m &= \overline{m} + \Delta m \ , \\
T &= \overline{T} + \Delta T \ ,
\end{aligned}
\tag{3.2}
$$

where the barred and the delta quantities refer to the mean and perturbed components, respectively, satisfying inequalities:

$$
\frac{\Delta P}{\overline{P}} \ll 1 \ , \quad \frac{\Delta m}{\overline{m}} \ll 1 \ , \quad \frac{\Delta T}{\overline{T}} \ll 1 \ , \quad \text{and } \frac{\Delta V}{\overline{V}} \ll 1 \ . \tag{3.3}
$$

Substitute Eq. (3.2) into Eq. (3.1), resulting in

$$
\overline{P}\left(1 + \frac{\Delta P}{\overline{P}}\right) = \frac{\overline{m}R\overline{T}}{\overline{V}} \frac{\left(1 + \frac{\Delta m}{\overline{m}}\right)\left(1 + \frac{\Delta T}{\overline{T}}\right)}{1 + \frac{\Delta V}{\overline{V}}} \ . \tag{3.4}
$$

Now, linearize the nonlinear term by retaining the first-order terms to obtain

$$
\overline{P}\left(1 + \frac{\Delta P}{\overline{P}}\right) \simeq \frac{\overline{m}R\overline{T}}{\overline{V}}\left(1 + \frac{\Delta m}{\overline{m}} + \frac{\Delta T}{\overline{T}} - \frac{\Delta V}{\overline{V}}\right) \ . \tag{3.5}
$$

This equation leads to two obvious but useful approximations:

$$
\overline{P} = \frac{\overline{m}R\overline{T}}{\overline{V}} \ , \tag{3.6}
$$

$$
\frac{\Delta P}{\overline{P}} = \frac{\Delta m}{\overline{m}} + \frac{\Delta T}{\overline{T}} - \frac{\Delta V}{\overline{V}} \ . \tag{3.7}
$$

Equation (3.6) states that under the linearization, the mean pressure may be computed by the product of mean values of other variables. When applied to Stirling machines, static equilibrium conditions require that

the same mean pressure should prevail in all control volumes and satisfy

$$\bar{P}_w = \frac{\bar{m}_e R \bar{T}_e}{\bar{V}_e} = \frac{\bar{m}_c R \bar{T}_c}{\bar{V}_c} = \frac{\bar{m}_d R \bar{T}_d}{\bar{V}_d} . \tag{3.8}$$

Equation (3.7) further states that the pressure perturbation is a linear summation of the respective fluctuating components. More importantly for the harmonic oscillations of major interest, each term in Eq. (3.7) can be regarded as a vector, and this will greatly facilitate vector analysis. By this interpretation, Eq. (3.7) now states that the pressure vector is the resultant of the mass, temperature, and volume vectors.

Substitution of Eq. (3.2) into Eq. (3.7) yields

$$\frac{P}{\bar{P}} = \frac{m}{\bar{m}} + \frac{T}{\bar{T}} - \frac{V}{\bar{V}} . \tag{3.9}$$

This equation represents the linearized instantaneous pressure. It is this approximate pressure expression that will be used in the pressure-containing terms wherever they occur in the conservation equations.

3.2 Nondimensional Equations

To simplify subsequent analysis, it is convenient to deal with the governing equations in dimensionless form. For this purpose, a set of dimensionless parameters and variables will be introduced.

Time: $t^* = \omega t$ (3.10)

Rate constants:

$$h_e^* = \frac{h_e \bar{A}_{se}}{\omega \bar{m}_e c_v} , \quad h_c^* = \frac{h_c \bar{A}_{sc}}{\omega \bar{m}_c c_v} ,$$

$$k_{pe}^* = \frac{k_{pe} \bar{m}_w \omega}{\bar{P}_w} , \quad k_{pc}^* = \frac{k_{pc} \bar{m}_w \omega}{\bar{P}_w} , \quad k_{mc}^* = \frac{k_{mc} \bar{P}_w}{\omega \bar{m}_w} . \tag{3.11}$$

Independent variables:

$$m_e^* = \frac{m_e}{\overline{m}_e}, \quad m_d^* = \frac{m_d}{\overline{m}_d}, \quad m_c^* = \frac{m_c}{\overline{m}_c}, \quad T_e^* = \frac{T_e}{\overline{T}_e}, \quad T_c^* = \frac{T_c}{\overline{T}_c} \tag{3.12}$$

Dependent variables:

$$P_e^* = \frac{P_e}{\overline{P}_w}, \quad P_d^* = \frac{P_d}{\overline{P}_w}, \quad P_c^* = \frac{P_c}{\overline{P}_w} \tag{3.13}$$

Prescribed variables:

$$V_e^* = \frac{V_e}{\overline{V}_e}, \quad V_c^* = \frac{V_c}{\overline{V}_c}, \quad X_p^* = \frac{X_p}{X_{pm}}, \quad X_d^* = \frac{X_d}{X_{pm}} \tag{3.14}$$

Temperature constants:

$$\overline{T}_{we}^* = \frac{\overline{T}_{we}}{\overline{T}_e}, \quad \overline{T}_{wc}^* = \frac{\overline{T}_{wc}}{\overline{T}_c}, \quad T_H^* = \frac{T_H}{\overline{T}_e}, \quad T_K^* = \frac{T_K}{\overline{T}_c} \tag{3.15}$$

Enthalpy flux temperature variables:

$$T_{e\ flux}^* = \frac{T_{e\ flux}}{\overline{T}_e}, \quad T_{c\ flux}^* = \frac{T_{c\ flux}}{\overline{T}_c} \tag{3.16}$$

Volume constants:

$$a_1 = \frac{A_d X_{pm}}{\overline{V}_e}$$

$$a_2 = \frac{(A_d - A_r)\ X_{pm}}{\overline{V}_c} \tag{3.17}$$

$$a_3 = \frac{A_p X_{pm}}{\overline{V}_c}$$

Cyclic performance parameters:

$$\overline{\dot{H}^*_e} = \frac{\overline{\dot{H}}_e}{c_v \overline{m}_e \overline{T}_e \omega}, \quad \overline{\dot{Q}^*_{we}} = \frac{\overline{\dot{Q}}_{we}}{c_v \overline{m}_e \overline{T}_e \omega}, \quad \overline{\dot{W}^*_e} = \frac{(\gamma - 1)\overline{\dot{W}}_e}{\overline{P}_w \overline{V}_e \omega}$$

$$\overline{\dot{H}^*_c} = \frac{\overline{\dot{H}}_c}{c_v \overline{m}_c \overline{T}_c \omega}, \quad \overline{\dot{Q}^*_{wc}} = \frac{\overline{\dot{Q}}_{wc}}{c_v \overline{m}_c \overline{T}_c \omega}, \quad \overline{\dot{W}^*_c} = \frac{(\gamma - 1)\overline{\dot{W}}_c}{\overline{P}_w \overline{V}_c \omega} \tag{3.18}$$

When these dimensionless parameters are substituted into the linearized pressure equation, the instantaneous nondimensional pressures in the expansion, dead, and compression spaces are given by

$$P^*_e = m^*_e + T^*_e - V^*_e , \tag{3.19}$$

$$P^*_d = m^*_d , \tag{3.20}$$

$$P^*_c = m^*_c + T^*_c - V^*_c . \tag{3.21}$$

From Fig. 2.1, the expansion volume depends only on the motion of the displacer piston, while the compression volume depends on the motion of both the displacer and the power piston:

$$V_e = \overline{V}_e - A_d X_d , \tag{3.22}$$

$$V_c = \overline{V}_c + (A_d - A_r) X_d - A_p X_p . \tag{3.23}$$

$\overline{V}_e$ and $\overline{V}_c$ represent the average volumes when both pistons are at their midstroke positions. X_d and X_p are the prescribed piston motions and they are defined equal to zero when the pistons are at midstroke. The volume equations in dimensionless form are

$$V^*_e = 1 - a_1 X^*_d , \tag{3.24}$$

$$V^*_c = 1 + a_2 X^*_d - a_3 X^*_p . \tag{3.25}$$

Using those parameters just introduced, the governing conservation equations transform to a system of ordinary differential equations in non-dimensional form:

$$\frac{\bar{m}_e}{\bar{m}_w} k^*_{pe} \frac{dm^*_e}{dt^*} = m^*_d - m^*_e - T^*_e + V^*_e \ , \tag{3.26}$$

$$\frac{\bar{m}_e}{\bar{m}_w} k^*_{pc} \frac{dm^*_e}{dt^*} + \frac{\bar{m}_d}{\bar{m}_w} k^*_{pc} \frac{dm^*_d}{dt^*} = m^*_c + T^*_c - V^*_c - m^*_d \ , \tag{3.27}$$

$$\frac{\bar{m}_e}{\bar{m}_w} \frac{dm^*_e}{dt^*} + \frac{\bar{m}_d}{\bar{m}_w} \frac{dm^*_d}{dt^*} + \frac{\bar{m}_c}{\bar{m}_w} \frac{dm^*_c}{dt^*} = k^*_{mc} \ (1 - m^*_c - T^*_c + V^*_c) \ , \tag{3.28}$$

$$\gamma \ T^*_{e \ \mathrm{flux}} \frac{dm^*_e}{dt^*} + h^*_e(\bar{T}^*_{we} - T^*_e) = (\gamma - 1)(m^*_e + T^*_e - V^*_e) \times \frac{dV^*_e}{dt^*} + \frac{d(m^*_e \ T^*_e)}{dt^*} \ , \tag{3.29}$$

$$\gamma \ T^*_{c \ \mathrm{flux}} \frac{dm^*_c}{dt^*} + h^*_c(\bar{T}^*_{wc} - T^*_c) = (\gamma - 1)(m^*_c + T^*_c - V^*_c) \times \frac{dV^*_c}{dt^*} + \frac{d(m^*_c \ T^*_c)}{dt^*} \ , \tag{3.30}$$

where the enthalpy flux discontinuities are characterized by, respectively,

$$T^*_{e \ \mathrm{flux}} = \begin{cases} T^*_H \ , & dm^*_e > 0 \\ T^*_e \ , & dm^*_e < 0 \end{cases} \ , \tag{3.31}$$

for the expansion space and

$$T^*_{c\ \mathrm{flux}} = \begin{cases} T^*_K , & dm^*_c > 0 \\ T^*_c , & dm^*_c < 0 \end{cases} , \tag{3.32}$$

for the compression space.

3.3 Harmonic Oscillations

The piston motions in most kinematic Stirling engines have waveforms that are harmonic or can be approximated by harmonic functions. Thus it seems reasonable to assume that the thermodynamic variables may also be approximated by harmonic functions. This assumption will be most accurate when the amplitudes of the oscillating variables are small relative to their mean values.

Because only a steady state solution is of interest, the analysis then becomes fairly straightforward. The system can be solved by the method of undetermined coefficients if all variables undergo simple harmonic oscillations:

$$\begin{aligned}
m^*_e &= 1 + y_1 \sin t^* + y_2 \cos t^* , \\
m^*_d &= 1 + y_3 \sin t^* + y_4 \cos t^* , \\
m^*_c &= 1 + y_5 \sin t^* + y_6 \cos t^* , \\
T^*_e &= 1 + y_7 \sin t^* + y_8 \cos t^* , \\
T^*_c &= 1 + y_9 \sin t^* + y_{10} \cos t^* , \\
X^*_d &= y_{11} \sin t^* + y_{12} \cos t^* , \\
X^*_p &= y_{14} \sin t^* ,
\end{aligned} \tag{3.33}$$

where y_1—y_{10}, which concern the thermodynamic variables, are unknowns to be determined. For the present, y_{11}—y_{14}, representing the piston positions, are specified as for kinematic engines. Later, when free pistons are allowed to respond dynamically to the various forces upon them, y_{11}—y_{14} are also treated as unknowns to be determined. All the y's provide information on the amplitudes of the variables as well as phase angles with

respect to the power piston displacement, a parameter commonly used as a reference in experimental measurements. Note that y_{13} is left out intentionally, because it is reserved for load coefficients in future free-piston dynamic analyses.

3.4 Truncated Fourier Series Representation

The general strategy of the LHA method is to transform the governing equations into harmonic forms (constant terms plus sine terms plus cosine terms). When the assumed harmonic solutions [Eq. (3.33)] are substituted into the governing equations [Eqs. (3.26–3.30)], the only remaining nonharmonic terms are the enthalpy flux, work, and internal energy terms in the energy equations. These nonharmonic terms are then represented by Fourier series that are truncated after the first harmonic. Fourier series provide an accurate way to approximate arbitrary periodic functions. Moreover, Fourier series can account for discontinuities; Taylor series do not have this capability because they are restricted to continuous functions that have continuous derivatives of all orders.

To illustrate the Fourier series expansion procedures, the expansion-space energy equation will be used. In general, a truncated Fourier series can be expressed as

$$f(t^*) = \alpha_0/2 + \alpha_1 \sin t^* + \alpha_2 \cos t^* , \tag{3.34}$$

with

$$\alpha_0 = \frac{1}{\pi} \int_0^{2\pi} f(t^*)\, dt^* , \tag{3.35}$$

$$\alpha_1 = \frac{1}{\pi} \int_0^{2\pi} f(t^*) \sin t^*\, dt^* , \tag{3.36}$$

$$\alpha_2 = \frac{1}{\pi} \int_0^{2\pi} f(t^*) \cos t^*\, dt^* , \tag{3.37}$$

where α_0 is the Fourier zero-order coefficient and α_1 and α_2 are first-order coefficients.

The goal now is to represent the enthalpy flux, work, and internal energy terms in the energy equations by a truncated Fourier series. With the assumed harmonic solutions, all the Fourier coefficients can be integrated analytically. The wall heat transfer terms in the energy equations and the mass conservation equations are already in harmonic form.

3.4.1 Enthalpy flux

The function to be expanded in a Fourier series is

$$f(t^*) = \gamma\, T_{e\ \mathrm{flux}}^* \frac{dm_e^*}{dt^*} \,. \tag{3.38}$$

The constant (zero-order) term in the Fourier series is identical to the cyclic enthalpy flux $\bar{\dot{H}}_e^*$ as defined in the integrated energy balance (see Chap. 2). Because of a discontinuity in enthalpy flux in accordance with the mass flow direction, the cyclic enthalpy flux must be evaluated by two half-cycles:

$$\bar{\dot{H}}_e^* = \frac{\alpha_0}{2} = \frac{\gamma}{2\pi}\left(\int_{dm_e^* < 0} T_e^* \frac{dm_e^*}{dt^*}\, dt^* + \int_{dm_e^* > 0} T_H^* \frac{dm_e^*}{dt^*}\, dt^*\right) . \tag{3.39}$$

The first integral represents outgoing enthalpy flux when the mass leaves the expansion space at the instantaneous gas temperature T_e^*; the second one denotes incoming flux when the gas emerges from the heater and enters into the expansion space at the heater temperature T_H^*. Because the mass flow rate $\dot{m}_e^*$ is a harmonic function, it has the same magnitudes but opposite signs over the two half-cycles; more specifically,

$$\left(\frac{dm_e^*}{dt^*}\right)_{dm_e^* > 0} = -\left(\frac{dm_e^*}{dt^*}\right)_{dm_e^* < 0} . \tag{3.40}$$

Since T_H^* is a constant, it is possible to consolidate the two integrals into a single one, if integration limits can be properly defined:

$$\bar{\dot{H}}_e^* = \frac{\gamma}{2\pi}\int_{dm_e^* < 0} (T_e^* - T_H^*) \frac{dm_e^*}{dt^*}\, dt^* \,. \tag{3.41}$$

To find the integration limits over which the mass flow remains negative over one-half cycle, define θ_e as a value of t^* such that dm_e^*/dt^* vanishes. Then,

$$\theta_e = \begin{cases} \tan^{-1}(y_1/y_2) , & \text{for } y_2 > 0 \\ \tan^{-1}(y_1/y_2) + \pi , & \text{for } y_2 < 0 \end{cases} , \tag{3.42}$$

or

$$\sin\theta_e = \frac{y_1}{\sqrt{y_1^2 + y_2^2}} \quad \text{and} \quad \cos\theta_e = \frac{y_2}{\sqrt{y_1^2 + y_2^2}} . \tag{3.43}$$

The rate of change of m_e^* is negative when $\theta_e < t^* < \theta_e + \pi$.

The cyclic enthalpy flux is found by substituting the assumed harmonic solution for the expansion-space temperature and mass flow and performing the integration over the limits from θ_e to $\theta_e + \pi$. After considerable algebraic manipulations, the result reads

$$\overline{\dot{H}}_e^* = \frac{\gamma}{\pi}(T_H^* - 1)\sqrt{y_1^2 + y_2^2} + \frac{\gamma}{4}(y_1 y_8 - y_2 y_7) . \tag{3.44}$$

This equation reveals that there are two contributions to the overall cyclic enthalpy flux. The first term can be interpreted as the steady enthalpy flux and simply represents the amount of energy convected by the total mass between two constant temperature levels: the heater temperature T_H and the mean expansion-space gas temperature $\overline{T}_e$. On the other hand, the second term denotes the apparent enthalpy flux that is derived primarily from fluctuating components of the mass and temperature. Consequently, the second term depends not only on the amplitudes of m_e and T_e but also on the phase angle between them. In general, the phase angle of the mass variation leads the temperature.

The Fourier coefficient of the sine component can be evaluated in much the same way as that of the constant term in the series, but involves a more complicated integral. Again, for alternating mass flow, the cyclic

integration is decomposed into two parts:

$$\alpha_1 = \frac{1}{\pi}\int_0^{2\pi} f(t^*) \sin t^* \, dt^* = \frac{\gamma}{\pi}\left(\int_{dm_e^* < 0} T_e^* \frac{dm_e^*}{dt^*} \times \sin t^* \, dt^* + \int_{dm_e^* > 0} T_H^* \frac{dm_e^*}{dt^*} \sin t^* \, dt^*\right) . \quad (3.45)$$

Using the fact that

$$\left(\frac{dm_e^*}{dt^*}\right)_{dm_e^* > 0} = -\left(\frac{dm_e^*}{dt^*}\right)_{dm_e^* < 0} , \quad (3.46)$$

and

$$(\sin t^*)_{dm_e^* > 0} = -(\sin t^*)_{dm_e^* < 0} , \quad (3.47)$$

the two integrals can be combined as

$$\alpha_1 = \int_{\theta_e}^{\theta_e + \pi} (T_e^* + T_H^*) \frac{dm_e^*}{dt^*} \sin t^* \, dt^* . \quad (3.48)$$

By proper substitution of the harmonic expressions and performing the definite integrals, Eq. (3.48) simplifies to

$$\alpha_1 = -[FF(1)]y_1 - [\gamma \, \tau_e + FF(2)]y_2 ; \quad (3.49)$$

the dimensionless average hot-end temperature and two correction factors for nonisothermal cylinders are defined, respectively, by

$$\tau_e = \frac{1}{2}(1 + T_H^*) , \quad (3.50)$$

$$FF(1) = -\frac{2\gamma}{3\pi}(y_8 \cos^3 \theta_e - y_7 \sin^3 \theta_e) , \quad (3.51)$$

$$FF(2) = \frac{2\gamma}{3\pi} [y_7 \cos \theta_e (\sin^2 \theta_e + 2) - y_8 \sin^3 \theta_e] . \tag{3.52}$$

Interpretation of the Fourier coefficient hierarchy gets more difficult, if not impossible, when proceeding to the higher orders. In Eq. (3.49), α_1 is expressed as if a linear combination of the mass amplitudes is involved; however, the correction factors shown in Eqs. (3.51) and (3.52) indicate a highly nonlinear interaction between mass and temperature fluctuations. Consequently, it is difficult to provide an easy physical interpretation. Nonetheless, at the isothermal limit these correction factors vanish because no temperature swings would exist ($y_7 = y_8 = 0$). This fact will be used as initial conditions for adiabatic or more general calculations when successive approximations are discussed (Sect. 3.7).

For brevity, the derivation of the Fourier coefficients of the cosine components will not be repeated, but the final results are

$$\alpha_2 = [\gamma\tau_e - FF(3)] \, y_1 + [FF(1)] \, y_2 , \tag{3.53}$$

where

$$FF(3) = -\frac{2\gamma}{3\pi} [y_7 \cos^3 \theta_e - y_8 \sin \theta_e (\cos^2 \theta_e + 2)] . \tag{3.54}$$

This completes the Fourier representation of the enthalpy flux that is given by

$$\gamma \, T^*_e \, \text{flux} \, \frac{dm^*_e}{dt^*} = \overline{\dot{H}^*_e} + \alpha_1 \sin t^* + \alpha_2 \cos t^* . \tag{3.55}$$

3.4.2 Wall heat transfer

Unlike enthalpy flux, the wall heat transfer term is already in harmonic form. When the term is decomposed with respect to the mean expansion-space gas temperature,

$$h^*_e(\overline{T}^*_{we} - T^*_e) = h^*_e(\overline{T}^*_{we} - 1) + h^*_e(1 - T^*_e)$$

$$= \overline{\dot{Q}}^*_{we} + h^*_e \, (1 - T^*_e) . \tag{3.56}$$

This equation already assumes the form of a truncated Fourier series. By inspection, the first term on the right-hand side of Eq. (3.56) is the cyclic wall heat transfer by convection ($\overline{\dot{Q}}^*_{we}$) that was defined in the integrated energy Eq. (2.10). Substitution of the assumed temperature solution into the second term results in a simple harmonic function. The complete wall heat transfer expression is:

$$h^*_e(\overline{T}^*_{we} - T^*_e) = \overline{\dot{Q}}^*_{we} - h^*_e\, y_7 \sin t^* - h^*_e\, y_8 \cos t^* \ . \tag{3.57}$$

3.4.3 Work output

Generally, Fourier representation of a work term that includes pressure nonlinearity presents insurmountable difficulties because it involves evaluating nonstandard integrals. Fortunately, with the assumption of a linearized pressure, the evaluations of Fourier coefficients can be done with ease. The assumption of the pressure linearization and the errors that may possibly be introduced have been quantified by an independent nonlinear analysis of the same set of equations. The surprisingly small discrepancies are encouraging. More discussion will be given later (Sect. 3.8).

The work term to be expanded in a Fourier series is

$$f(t^*) = (\gamma - 1)\ (m^*_e + T^*_e - V^*_e)\ \frac{dV^*_e}{dt^*} \ . \tag{3.58}$$

The zero-order or constant term is the cyclic work output $\overline{\dot{W}}^*_e$ as defined in the integrated energy Eq. (2.10). After substitution into Eq. (3.35) and integration, the result is

$$\overline{\dot{W}}^*_e = \frac{\alpha_0}{2} = \frac{(\gamma - 1)a_1}{2}\ [y_{12}(y_1 + y_7) - y_{11}(y_2 + y_8)] \ . \tag{3.59}$$

Similarly, the Fourier coefficients for the sine and cosine terms are found by substituting into Eqs. (3.36) and (3.37) and integrating

$$\alpha_1 = (\gamma - 1)\ a_1\ y_{12} \ , \tag{3.60}$$

$$\alpha_2 = -(\gamma - 1)\ a_1\ y_{11} \ . \tag{3.61}$$

The complete Fourier expansion for the work term is

$$(\gamma - 1)\ (m_e^* + T_e^* - V_e^*)\ \frac{dV_e^*}{dt^*} = \overline{\dot{W}_e^*} + (\gamma - 1)\ a_1\ y_{12}\ \sin t^*$$

$$- (\gamma - 1)\ a_1\ y_{11}\ \cos t^* \ . \quad (3.62)$$

3.4.4 Rate of change of internal energy

As pointed out before, a steady state solution has been defined when there is no net change in the internal energy over a cycle, or equivalently, a vanishing constant in the Fourier series. The first-order Fourier coefficients, following the same procedures as the other terms, can be shown to be

$$\alpha_1 = -(y_2 + y_8)\ , \quad (3.63)$$

$$\alpha_2 = y_1 + y_7\ . \quad (3.64)$$

Therefore, the Fourier representation for the rate of change of the internal energy becomes

$$\frac{d(m_e^*\ T_e^*)}{dt^*} = 0 - (y_2 + y_8)\ \sin t^* + (y_1 + y_7)\ \cos t^*\ . \quad (3.65)$$

The Fourier coefficients for the compression space can be derived by repeating the same process described previously, or by transforming the expansion-space expressions by replacing the subscript e with the subscript c and by making the following substitutions:

FF(1) replaced by FF(4) ,	y_7 replaced by y_9 ,	
FF(2) replaced by FF(5) ,	y_8 replaced by y_{10} ,	
FF(3) replaced by FF(6) ,	$(a_1 y_{11})$ replaced by $(-a_2 y_{11} + a_3 y_{14})$,	(3.66)
y_1 replaced by y_5 ,	$(a_1 y_{12})$ replaced by $(-a_2 y_{12})$,	
y_2 replaced by y_6 ,	T_H^* replaced by T_K^* .	

The Fourier expressions for the compression space are summarized as follows:

Enthalpy flux:

$$\gamma T_c^* \text{ flux } \frac{dm_c^*}{dt^*} = \overline{\dot{H}_c^*} + \alpha_1 \sin t^* + \alpha_2 \cos t^* , \tag{3.67}$$

where the Fourier coefficients appear similar to that of the expansion space.

$$\alpha_1 = -[FF(4)]y_5 - [\gamma\tau_c + FF(5)]y_6 , \tag{3.68}$$

$$\alpha_2 = [\gamma\tau_c - FF(6)]y_5 + [FF(4)]y_6 , \tag{3.69}$$

where

$$\tau_c = \frac{1}{2}(1 + T_K^*) , \tag{3.70}$$

$$FF(4) = -\frac{2\gamma}{3\pi}(y_{10} \cos^3 \theta_c - y_9 \sin^3 \theta_c) , \tag{3.71}$$

$$FF(5) = \frac{2\gamma}{3\pi}[y_9 \cos \theta_c (\sin^2 \theta_c + 2) - y_{10} \sin^3 \theta_c] , \tag{3.72}$$

$$FF(6) = -\frac{2\gamma}{3\pi}[y_9 \cos^3 \theta_c - y_{10} \sin \theta_c(\cos^2 \theta_c + 2)] , \tag{3.73}$$

$$\sin \theta_c = \frac{y_5}{\sqrt{y_5^2 + y_6^2}} ,$$

$$\cos \theta_c = \frac{y_6}{\sqrt{y_5^2 + y_6^2}} . \tag{3.74}$$

Wall heat transfer:

$$h_c^* (\overline{T}_{wc}^* - T_c^*) = \overline{\dot{Q}_{wc}^*} - h_c^* y_9 \sin t^* - h_c^* y_{10} \cos t^* . \tag{3.75}$$

Work output:

$$(\gamma - 1)(m_c^* + T_c^* - V_c^*) \frac{dV_c^*}{dt^*} = \overline{\dot{W}_c^*} - (\gamma - 1)\ a_2\ y_{12} \sin t^*$$

$$+ (\gamma - 1)\ (a_2\ y_{11} - a_3\ y_{14}) \cos t^* \ . \quad (3.76)$$

Rate of change of internal energy:

$$\frac{d(m_c^*\ T_c^*)}{dt^*} = 0 - (y_6 + y_{10}) \sin t^* + (y_5 + y_9) \cos t^* \ , \quad (3.77)$$

where quantities relating to the cyclic average are

$$\overline{\dot{H}_c^*} = \frac{\gamma}{\pi}\ (T_K^* - 1)\ \sqrt{y_5^2 + y_6^2} + \frac{\gamma}{4}\ (y_5\ y_{10} - y_6\ y_9) \ , \quad (3.78)$$

$$\overline{\dot{Q}_{wc}^*} = h_c^*\ (\overline{T}_{wc}^* - 1) \ , \quad (3.79)$$

$$\overline{\dot{W}_c^*} = \frac{(\gamma - 1)}{2}\ [(a_2 y_{11} - a_3 y_{14})(y_6 + y_{10}) - a_2 y_{12}\ (y_5 + y_9)] \ . \quad (3.80)$$

3.5 System of Integrated Equations

As stated repeatedly, if a steady state solution is sought, the working gas must satisfy an overall cyclic energy balance, or the so-called integrated energy equation, in the respective spaces simultaneously. More specifically, the previous integrated energy equations [Eqs. (2.10 and 2.11) in Sect. 2.3] should be met:

$$\overline{\dot{H}_e^*} + \overline{\dot{Q}_{we}^*} = \overline{\dot{W}_e^*} \ ,$$

$$\overline{\dot{H}_c^*} + \overline{\dot{Q}_{wc}^*} = \overline{\dot{W}_c^*} \ .$$

The mean gas temperatures in each space are characterized by the respective integrated energy balances but in a coupled manner. This coupling is linked through the continuous mass shuttling between the control volumes. With harmonically varying thermodynamic variables, quasi-closed-form solutions become available as already shown, and the mean gas temperatures of the expansion $\overline{T}_e$ and compression space $\overline{T}_c$ can be solved explicitly.

$$\overline{T}_e = \frac{Z1(1)T_H + Z1(2) + h_e\overline{A}_{se}\,\overline{T}_{we} - \overline{\dot{W}}_e}{Z1(1) + h_e\overline{A}_{se}} , \tag{3.81}$$

$$\overline{T}_c = \frac{Z1(3)T_K + Z1(4) + h_c\overline{A}_{sc}\,\overline{T}_{wc} - \overline{\dot{W}}_c}{Z1(3) + h_c\overline{A}_{sc}} , \tag{3.82}$$

where all the functions of Z1's are defined in a more workable form:

$$Z1(1) = \frac{\omega}{\pi}\, c_p \overline{m}_e \sqrt{y_1^2 + y_2^2} , \tag{3.83}$$

$$Z1(2) = \frac{\gamma}{4(\gamma - 1)}\, \omega\, \overline{P}_w\, \overline{V}_e\, (y_1\, y_8 - y_2\, y_7) , \tag{3.84}$$

$$Z1(3) = \frac{\omega}{\pi}\, c_p\, \overline{m}_c \sqrt{y_5^2 + y_6^2} , \tag{3.85}$$

$$Z1(4) = \frac{\gamma}{4(\gamma - 1)}\, \omega\, \overline{P}_w\, \overline{V}_c\, (y_5\, y_{10} - y_6\, y_9) , \tag{3.86}$$

and where $\overline{\dot{W}}_e$ and $\overline{\dot{W}}_c$ were defined in Eqs. (3.18), (3.59), and (3.80). It becomes obvious that calculations of the mean temperatures cannot be done without knowing their fluctuating components, which are yet to be determined. This problem will be addressed and solved in the next section.

3.6 System of Fluctuating Equations

So far it has been established that the working gas must simultaneously satisfy the integrated energy equations and the instantaneous (full) equations. The full equations have been approximated by truncated Fourier series. Taking the difference between the full equations and the integrated equations results in the so-called fluctuating equations that, in essence, are comprised of the sine and cosine terms from the Fourier expansions.

The system of fluctuating equations is derived from the three mass distributions and two energy equations by collecting sine and cosine components.

Mass distribution 1:

$$\left(y_1 - \frac{\overline{m}_e}{\overline{m}_w} k^*_{pe}\, y_2 - y_3 + y_7 + a_1\, y_{11}\right) \sin t^* + \left(\frac{\overline{m}_e}{\overline{m}_w} k^*_{pe}\, y_1 + y_2 - y_4 + y_8 + a_1\, y_{12}\right) \cos t^* = 0 \,. \quad (3.87)$$

Mass distribution 2:

$$\left(-\frac{\overline{m}_e}{\overline{m}_w} k^*_{pc}\, y_2 + y_3 - \frac{\overline{m}_d}{\overline{m}_w} k^*_{pc}\, y_4 - y_5 - y_9 + a_2\, y_{11} - a_3\, y_{14}\right) \times \sin t^* + \left(\frac{\overline{m}_e}{\overline{m}_w} k^*_{pc}\, y_1 + \frac{\overline{m}_d}{\overline{m}_w} k^*_{pc}\, y_3 + y_4 - y_6 - y_{10} + a_2\, y_{12}\right) \cos t^* = 0 \,. \quad (3.88)$$

Mass distribution 3:

$$\left[-\frac{\bar{m}_e}{\bar{m}_w} y_2 - \frac{\bar{m}_d}{\bar{m}_w} y_4 - \frac{\bar{m}_c}{\bar{m}_w} y_6 + k^*_{mc} (y_5 + y_9) - k^*_{mc} \times (a_2 y_{11} - a_3 y_{14})\right] \sin t^* + \left[\frac{\bar{m}_e}{\bar{m}_w} y_1 + \frac{\bar{m}_d}{\bar{m}_w} y_3 + \frac{\bar{m}_c}{\bar{m}_w} y_5 + k^*_{mc} (y_6 + y_{10}) - k^*_{mc} a_2 y_{12}\right] \cos t^* = 0 \ . \quad (3.89)$$

Expansion-space energy equation:

$$[FF(1)y_1 + D(7,2)y_2 + h^*_e y_7 - y_8 + (\gamma - 1) a_1 y_{12}] \times \sin t^* + [D(8, 1)y_1 - FF(1)y_2 + y_7 + h^*_e y_8 - (\gamma - 1) a_1 y_{11}] \cos t^* = 0 \ . \quad (3.90)$$

Compression-space energy equation:

$$[FF(4)y_5 + D(9, 6)y_6 + h^*_c y_9 - y_{10} - (\gamma - 1) a_2 y_{12}] \times \sin t^* + [D(10, 5)y_5 - FF(4)y_6 + y_9 + h^*_c y_{10} + (\gamma - 1)(a_2 y_{11} - a_3 y_{14})] \cos t^* = 0 \ . \quad (3.91)$$

Recall that the solution was originally assumed in terms of 10 undetermined coefficients (y_1—y_{10}). The system of fluctuating equations is used to solve for these undetermined coefficients. Since sin t* and cos t* are orthogonal functions, the sine and cosine coefficients in Eqs. (3.87—3.91) must vanish to satisfy the equations for all t*. This leads to a set of nonhomogeneous algebraic equations that may be represented by a 10 × 10 matrix:

$$
\begin{bmatrix}
1 & -\frac{\bar{m}_e}{\bar{m}_w} k^*_{pe} & -1 & 0 & 0 & 0 & 1 & 0 & 0 & 0 \\
\frac{\bar{m}_e}{\bar{m}_w} k^*_{pe} & 1 & 0 & -1 & 0 & 0 & 0 & 1 & 0 & 0 \\
0 & -\frac{\bar{m}_e}{\bar{m}_w} k^*_{pc} & 1 & -\frac{\bar{m}_d}{\bar{m}_w} k^*_{pc} & -1 & 0 & 0 & 0 & -1 & 0 \\
\frac{\bar{m}_e}{\bar{m}_w} k^*_{pc} & 0 & \frac{\bar{m}_d}{\bar{m}_w} k^*_{pc} & 1 & 0 & -1 & 0 & 0 & 0 & -1 \\
0 & -\frac{\bar{m}_e}{\bar{m}_w} & 0 & -\frac{\bar{m}_d}{\bar{m}_w} & k^*_{mc} & -\frac{\bar{m}_c}{\bar{m}_w} & 0 & 0 & k^*_{mc} & 0 \\
\frac{\bar{m}_e}{\bar{m}_w} & 0 & \frac{\bar{m}_d}{\bar{m}_w} & 0 & \frac{\bar{m}_c}{\bar{m}_w} & k^*_{mc} & 0 & 0 & 0 & k^*_{mc} \\
D(7,1) & D(7,2) & 0 & 0 & 0 & 0 & h^*_e & -1 & 0 & 0 \\
D(8,1) & D(8,2) & 0 & 0 & 0 & 0 & 1 & h^*_e & 0 & 0 \\
0 & 0 & 0 & 0 & D(9,5) & D(9,6) & 0 & 0 & h^*_c & -1 \\
0 & 0 & 0 & 0 & D(10,5) & D(10,6) & 0 & 0 & 1 & h^*_c
\end{bmatrix}
\begin{bmatrix} y_1 \\ y_2 \\ y_3 \\ y_4 \\ y_5 \\ y_6 \\ y_7 \\ y_8 \\ y_9 \\ y_{10} \end{bmatrix}
=
\begin{bmatrix}
-a_1 y_{11} \\
-a_1 y_{12} \\
-a_2 y_{11} + a_3 y_{14} \\
-a_2 y_{12} \\
k^*_{mc}(a_2 y_{11} - a_3 y_{14}) \\
k^*_{mc} a_2 y_{12} \\
-(\gamma - 1) a_1 y_{12} \\
(\gamma - 1) a_1 y_{11} \\
(\gamma - 1) a_2 y_{12} \\
-(\gamma - 1)(a_2 y_{11} - a_3 y_{14})
\end{bmatrix}
\quad . \tag{3.92}
$$

where

$$
\begin{aligned}
D(7,1) &= FF(1), \\
D(7,2) &= -1 + \gamma\tau_e + FF(2), \\
D(8,1) &= 1 - \gamma\tau_e + FF(3), \\
D(8,2) &= -FF(1), \\
D(9,5) &= FF(4), \\
D(9,6) &= -1 + \gamma\tau_c + FF(5), \\
D(10,5) &= 1 - \gamma\tau_c + FF(6), \\
D(10,6) &= -FF(4).
\end{aligned}
\tag{3.93}
$$

Equation (3.92) can be written in tensor notation as

$$D_{ij}\, y_j = b_i \,, \tag{3.94}$$

where D_{ij}, y_j, and b_i represent the coefficient matrix, unknown vector, and nonhomogeneous vector, respectively. The coefficient matrix contains most of the thermodynamic constants. The nonhomogeneous vector contains the information about the specified volume variations.

The fluctuating equations are written as a linear system. A careful observation of the coefficient matrix reveals that the equations are not completely linear. Some of the coefficients in the matrix (enthalpy flux

Fourier functions and elements containing $\overline{T}_e$ and $\overline{T}_c$) are functions of the undetermined coefficients. The problem is solved by an iterative process where the matrix elements are treated as constants during each iteration. The values of the coefficients are then updated after the undetermined coefficients have been computed.

3.7 Successive Approximations

The coupled system of the integrated energy equations and the fluctuating equations requires an iterative solution for any case other than an isothermal one. This process includes three key elements: initialization, choice of matrix solution method, and convergence criteria. For calculations departing from the isothermal case, a reasonable initial guess has been proven to be the isothermal limit. In the current computations, the mean gas temperatures in the respective spaces are initialized by setting them equal to the adjacent heat transfer component temperatures, namely, constant heater and cooler temperatures. In addition, the six nonisothermal correction factors [FF(n), n = 1, 2,...6] are set equal to zero, which corresponds to an isothermal condition without temperature fluctuations. For the matrix solution method, the choice of subroutines and needed accuracy will determine calculation efficiency and cost. Standard IBM FORTRAN subroutines, DECOMP and SOLVE, are used to perform matrix operations, which have been proven satisfactorily in accuracy, efficiency, and economy. Finally, the solution convergence criteria rely on the initial guess as well as the specified operating conditions. By experience, fast convergence is attainable, usually in 10 to 15 iterations.

To perform the iterative solution effectively and automatically, a FORTRAN code is written. The process shown in Fig. 3.1 indicates the underlying computation procedures in sequence:

1. Initialize

$$\overline{T}_e = T_H \ ,$$

$$\overline{T}_c = T_K \ ,$$

$$FF(n) = 0, \ (n = 1, 2,...6) \ .$$

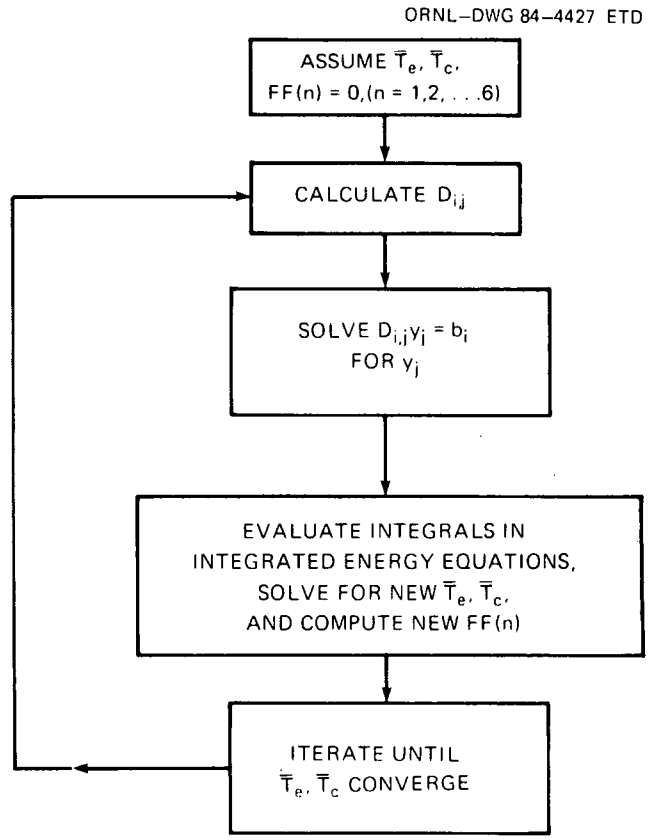

Fig. 3.1. Flow chart for successive approximations.

2. Calculate temperature-dependent ($\overline{T}_e$ and $\overline{T}_c$) elements in D_{ij} and b_i.
3. Solve the nonhomogeneous matrix equations

   $$D_{ij}\, y_j = b_i \ ,$$

   for y_j by DECOMP and SOLVE .

4. Solve for improved $\overline{T}_e$ and $\overline{T}_c$ from integrated energy equations and compute new values for FF(n), (n = 1, 2,...6).
5. Return to step 2 until $\overline{T}_e$ and $\overline{T}_c$ converge.

3.8 Comparison with Nonlinear Solutions

A key assumption in LHA is that the amplitudes of all variables are small compared with their mean values. To quantify the possible errors

that may be introduced by this assumption, an independent nonlinear analysis has been conducted. The nonlinear analysis uses the identical set of equations derived in Sect. 2.2, but does not linearize. The solution method adopted is a standard IBM numerical integrator, called the CSMP (Ref. 1). Use of this well-established software avoided unnecessary programming efforts in numerical integration. Readers who are interested in the nonlinear formulation, the method of solution, and detailed results should refer to a report by Banduric and Chen.[26]

All performance predictions in this report are based on two examples, the RE-1000 Nominal and RE-1000 Modified engines. The RE-1000 Nominal configuration simulates Sunpower's RE-1000 free-piston Stirling engine. This engine was selected because it will eventually be analyzed in free-piston mode; however, in the present report, the piston motions are specified. Table 3.1 lists the RE-1000 Nominal dimensions, and Table 3.2 lists the RE-1000 Nominal operating conditions used in the calculations. The values were estimated from a report published recently by Schreiber.[23] The RE-1000 Nominal engine has a modest volume compression ratio of about 1.30:1.

Table 3.1. RE-1000 Nominal engine dimensions and parameters

Maximum displacer stroke, m	4.04×10^{-2}
Maximum piston stroke, m	4.20×10^{-2}
Piston diameter, m	5.723×10^{-2}
Displacer diameter, m	5.723×10^{-2}
Displacer rod diameter, m	1.666×10^{-2}
Mean volume, m^3	
Expansion space	6.36×10^{-5}
Heater	3.96×10^{-5}
Regenerator	5.94×10^{-5}
Cooler	2.85×10^{-5}
Compression space	1.036×10^{-4}
Mean heat transfer surface areas	
Expansion space, m^2	1.392×10^{-2}
Compression space, m^2	2.292×10^{-2}

Table 3.2. RE-1000 Nominal engine operating conditions

Working fluid	Helium
Frequency, Hz	30
Average pressure, MPa	7
Piston stroke, m	2.80×10^{-2}
Displacer stroke, m	2.80×10^{-2}
Displacer phase angle, deg	45
Heater temperature, K	900
Expansion cylinder wall temperature, K	900
Cooler temperature, K	300
Compression cylinder wall temperature, K	300

The RE-1000 Modified configuration was designed to study the effects of higher compression ratios. The dimensions and operating conditions of the RE-1000 Modified are identical to the RE-1000 Nominal, except for the changes listed in Table 3.3. The dead volume was arbitrarily reduced in the RE-1000 Modified, and the piston strokes were varied between zero and their maximum values to simulate compression ratios between 1:1 and 1.89:1.

Table 3.3. RE-1000 Modified engine dimensions and operating conditions

Maximum displacer stroke, m	4.20×10^{-2}
Displacer rod diameter, m	0
Mean volume, m^3	
Heater	1.98×10^{-5}
Regenerator	2.97×10^{-5}
Cooler	1.43×10^{-5}
Compression space	4.77×10^{-5}
Piston stroke	Variable
Displacer stroke	Equal to piston

A sensitivity study was performed to compare the LHA and nonlinear performance predictions. The RE-1000 Nominal configuration was analyzed over a wide range of loss coefficients. The losses were examined independently (decoupled) as well as in various combinations (coupled together). Also, the RE-1000 Modified configuration was analyzed over a range of compression ratios. The comparison between LHA and nonlinear predictions provides vital information about the mathematical accuracy of the assumptions made in the LHA.

A comparison between the LHA and nonlinear CSMP predictions when losses are not coupled is given in Table 3.4. From top to bottom, the first, second, and third sets, respectively, represent predictions when the only losses are heat transfer, pressure drop, and mass leakage. Note first the effect of finite-cylinder heat transfer acting alone. For the mean gas temperature in the expansion $\overline{T}_e$ and compression $\overline{T}_c$ spaces, the LHA consistently overpredicts, except at the isothermal limit. The maximum discrepancy occurs for the adiabatic cylinders; however, the difference is very small, about 2.6 and 0.6 K or 0.3% and 0.2% in the expansion and compression spaces. Predictions of the heat input $\overline{\dot{Q}}_{in}$ and output $\overline{\dot{Q}}_{out}$, by the linear and nonlinear solutions, differ by only a fraction of 1%. As for the work output $\overline{\dot{W}}_{out}$, which is the difference between heat input and heat output, the agreement is also excellent, with the LHA showing a slightly lower value. A similar trend holds true for the efficiency. Overall, the LHA shows the worst effect, although a very small one, in calculating the work output and efficiency for cylinders with finite heat transfer rates.

Secondly, when the pressure drop acts alone, the LHA systematically overpredicts $\overline{T}_e$ and $\overline{T}_c$, but underpredicts $\overline{\dot{Q}}_{in}$ and $\overline{\dot{Q}}_{out}$. Consequently, this leads to an alternating prediction in work output and efficiency. The magnitude of the discrepancy in predicted work output and efficiency increases with increasing pressure drop coefficients, but it is always a small increase.

Finally, when mass leakage acts alone, the effects show the same trends as pressure drop. This is not surprising because both loss mechanisms are modeled in a similar way.

Table 3.4. Predicted performance comparison between LHA and CSMP for the RE-1000 Nominal engine with decoupled losses

h_e, h_c ($W/m^2 \cdot K$)	k_{pe}, k_{pc} ($Pa \cdot s/kg$)	k_{mc} ($kg/Pa \cdot s$)	$\bar{T}_e$ (K)		$\bar{T}_c$ (K)		$\bar{\dot{Q}}_{in}$ (W)		$\bar{\dot{Q}}_{out}$ (W)		$\bar{\dot{W}}_{out}$ (W)		Efficiency (%)	
			CSMP	LHA	CSMP	LHA	CSMP	LHA	CSMP	LHA	CSMP	LHA	CSMP	LHA
0	0	0	851.5	854.1	311.2	311.8	3,961	3,955	1,465	1,465	2,496	2,491	63.01	62.97
10,000	0	0	885.5	886.2	302.2	302.6	3,784	3,786	1,540	1,545	2,244	2,242	59.31	59.21
25,000	0	0	891.9	892.2	301.0	301.3	3,510	3,504	1,519	1,522	1,991	1,982	56.73	56.57
62,500	0	0	896.4	896.6	300.5	300.6	3,193	3,178	1,353	1,351	1,840	1,827	57.63	57.49
125,000	0	0	898.1	898.3	300.2	300.3	3,080	3,063	1,205	1,201	1,875	1,862	60.88	60.78
0.3D9	0	0	900.0	900.0	300.0	300.0	3,046	3,041	1,015	1,014	2,031	2,027	66.67	66.66
0	0	0	851.5	854.1	311.2	311.8	3,961	3,955	1,465	1,465	2,496	2,491	63.01	62.97
0	0.33333D7	0	856.7	858.4	312.4	313.3	3,589	3,586	1,647	1,640	1,942	1,945	54.11	54.25
0	0.66667D7	0	861.3	862.8	314.0	314.9	3,207	3,207	1,814	1,809	1,393	1,398	43.44	43.60
0	1.D7	0	866.0	867.3	315.3	316.4	2,825	2,821	1,977	1,968	848	853	30.02	30.24
0	1.33333D7	0	870.7	871.8	316.7	317.9	2,433	2,431	2,127	2,118	306	313	12.59	12.88
0	0	0	851.5	854.1	311.2	311.8	3,961	3,955	1,465	1,465	2,496	2,491	63.01	62.97
0	0	0.5D-8	851.9	854.5	311.7	313.3	3,794	3,790	1,734	1,733	2,060	2,057	54.29	54.28
0	0	1.D-8	853.6	855.9	312.8	314.2	3,550	3,545	1,944	1,942	1,605	1,603	45.23	45.23
0	0	2.D-8	859.2	861.3	313.3	314.5	2,929	2,928	2,170	2,168	759	760	25.93	25.96
0	0	3.D-8	866.3	868.2	312.6	313.6	2,297	2,297	2,186	2,182	111	115	4.82	4.99

More evidence supporting the accuracy of the LHA is provided in Table 3.5, which is intended to compare the two solution methods (LHA and CSMP) when two or more loss mechanisms are acting simultaneously. In Table 3.5, from top to bottom, the first, second, and third sets represent adiabatic, semiadiabatic, and isothermal cylinders, respectively; discussion will follow that order.

The comparison for the adiabatic cylinders is done so that the first line represents a calculation without pressure drop or mass leakage; the second line is mass leakage acting alone; the third line is pressure drop only; and the last line is pressure drop and mass leakage acting together. LHA overpredicts the mean gas temperatures but underpredicts heat absorption and heat rejection, which leads to mixed predictions in work output and efficiency. However, the magnitudes of all discrepancies are small (a fraction of 1%). The calculations for semiadiabatic and isothermal cylinders are applied similarly, and the predictions follow the same trends. The magnitude of the discrepancies is still small, but the discrepancies are larger than for adiabatic cylinders.

The comparison between LHA and nonlinear predictions of RE-1000 Nominal performance in Tables 3.4 and 3.5 can be summarized by examining three important performance parameters: heat input, heat output, and efficiency. Heat input and output are computed from the pressure-volume integrals in the expansion and compression spaces. All LHA predictions for heat input and output fall within +0.3% and −0.8% of the CSMP values. Efficiency is actually computed from the heat input and output. All LHA predictions for efficiency differ from CSMP values by no more than +0.29 and −0.33 percentage points. The discrepancies seem completely insignificant, considering that the best, and most carefully calibrated, numerical codes cannot predict Stirling engine performance to better than 10% or 20% because of a lack of knowledge of the processes and correlations involved in the computations. Therefore, it can be said with confidence that the LHA approximation is very reasonable over a wide range of loss coefficients, at least for low compression ratios.

A key assumption in the LHA is that the amplitudes of the oscillating variables are small compared with their mean values. The error that may be introduced by this assumption has been proven to be inconsequential for

Table 3.5. Predicted performance comparison between LHA and CSMP for the RE-1000 Nominal engine with coupled losses

h_e, h_c ($W/m^2 \cdot K$)	k_{pe}, k_{pc} ($Pa \cdot s/kg$)	k_{mc} ($kg/Pa \cdot s$)	$\overline{T}_e$ (K)		$\overline{T}_c$ (K)		$\overline{\dot{Q}}_{in}$ (W)		$\overline{\dot{Q}}_{out}$ (W)		$\overline{\dot{W}}_{out}$ (W)		Efficiency (%)	
			CSMP	LHA	CSMP	LHA	CSMP	LHA	CSMP	LHA	CSMP	LHA	CSMP	LHA
0	0	0	851.5	854.1	311.2	311.8	3,961	3,955	1,465	1,465	2,496	2,491	63.01	62.97
0	0	1.D-8	853.6	855.9	312.8	314.2	3,550	3,545	1,944	1,942	1,605	1,603	45.23	45.23
0	0.66667D7	0	861.3	862.8	314.0	314.9	3,207	3,207	1,814	1,809	1,393	1,398	43.44	43.60
0	0.66667D7	1.D-8	863.7	864.8	315.5	316.4	2,806	2,801	2,244	2,241	562	561	20.03	20.02
62,500	0	0	896.4	896.6	300.5	300.6	3,193	3,178	1,353	1,351	1,840	1,827	57.63	57.49
62,500	0	1.D-8	896.7	896.9	300.6	300.8	2,868	2,856	1,626	1,622	1,242	1,234	43.31	43.20
62,500	0.66667D7	0	897.2	897.4	300.6	300.8	2,452	2,434	1,636	1,632	816	802	33.27	32.95
62,500	0.66667D7	1.D-8	897.4	897.6	300.8	301.0	2,142	2,129	1,874	1,869	268	259	12.52	12.19
0.3D9	0	0	900.0	900.0	300.0	300.0	3,046	3,041	1,015	1,014	2,031	2,027	66.67	66.66
0.3D9	0	1.D-8	900.0	900.0	300.0	300.0	2,885	2,872	1,323	1,316	1,562	1,556	54.14	54.17
0.3D9	0.66667D7	0	900.0	900.0	300.0	300.0	2,279	2,261	1,270	1,262	1,010	998	44.29	44.16
0.3D9	0.66667D7	1.D-8	900.0	900.0	300.0	300.0	2,113	2,119	1,568	1,559	565	560	26.47	26.43

small volume compression ratios, but it might become significant for larger compression ratios. To address this possibility, a comparison between LHA and CSMP predictions for the RE-1000 Modified configuration, with adiabatic cylinders and no other losses, has been performed over a range of compression ratios. The compression ratio was varied by specifying piston amplitudes between 20% and 100% of the maximum values permitted by their mechanical constraints.

The results of the comparison, which are listed in Table 3.6, confirm our expectation that the errors associated with the LHA approximation become larger as the compression ratio is increased. However, even at the maximum compression ratio of 1.89, which is too high to be representative of practical engines, the LHA predictions for heat input and output are only 1.1% and 2.2%, respectively, below the CSMP values, and efficiency is overpredicted by only 0.5 percentage points. The LHA and CSMP efficiency predictions from Table 3.6 are plotted vs compression ratio in Fig. 3.2. The LHA calculations do not seem to create any noticeable error unless the compression ratio exceeds 1.6.

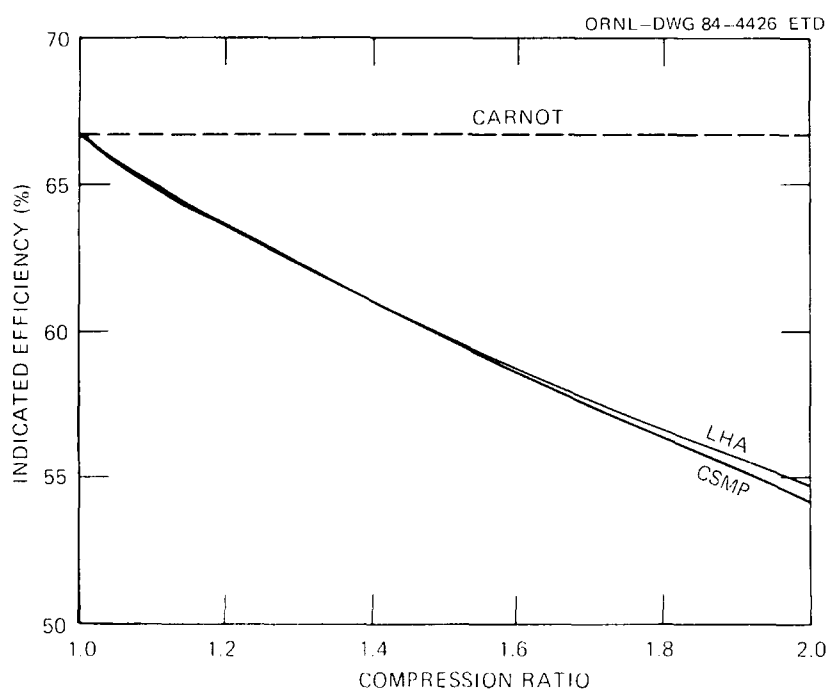

Fig. 3.2. Efficiency comparison between LHA and CSMP solution methods for RE-1000 Modified configuration.

Table 3.6. Predicted performance comparison between LHA and CSMP for the RE-1000 Modified configuration with adiabatic cylinders and no other losses

X_{pa}[a] / $\overline{X}_{pm}$	Compression ratio	$\overline{T}_e$ (K)		$\overline{T}_c$ (K)		$\overline{\dot{Q}}_{in}$ (W)		$\overline{\dot{Q}}_{out}$ (W)		$\overline{\dot{W}}_{out}$ (W)		Efficiency (%)	
		CSMP	LHA	CSMP	LHA	CSMP	LHA	CSMP	LHA	CSMP	LHA	CSMP	LHA
0.2	1.13	873.9	874.7	305.0	305.8	682.4	683.2	241.7	241.4	440.7	441.8	64.58	64.66
0.4	1.28	847.6	851.5	310.1	311.9	2,698	2,690	1,008	1,006	1,690	1,684	62.60	62.59
0.6	1.45	821.9	830.1	314.6	318.4	5,982	5,947	2,371	2,352	3,611	3,595	60.37	60.45
0.8	1.66	796.7	810.1	318.2	325.3	10,470	10,372	4,394	4,331	6,076	6,041	58.03	58.24
1.0	1.89	772.5	791.3	320.3	332.8	16,054	15,871	7,148	6,988	8,906	8,883	55.47	55.97

[a]Ratio between the power piston displacement amplitude and its maximum value.

Generally, the LHA solution method appears to provide very acceptable accuracy for Stirling engine applications. Much of the accuracy of the LHA solution can be attributed to the Fourier representation of the energy equations. Fourier analysis provides a logical way to represent arbitrary periodic functions in terms of a constant term and a first harmonic. Nonlinearities, such as the enthalpy flux discontinuity, are accounted for by the effect that they have on the constant term and the amplitude and phase of the first harmonic. Nonlinearities also create higher harmonics, but neglecting these effects seems to induce very little error. Unfortunately, the Fourier analysis creates the need for iteration; however, this minor complication seems to be worth the improved solution accuracy.

3.9 Vector Representation

Additional physical insight into Stirling engine processes can be gained by plotting results in a vector diagram.[27] A vector diagram provides information about the relative amplitudes of and phase relationships between harmonic variables. Generally, the length of a vector is proportional to the amplitude of the oscillation, and the direction of a vector represents the phase angle of the oscillation.

When harmonic variables are expressed in terms of $\sin(\omega t)$ and $\cos(\omega t)$ components, a vector diagram can be drawn easily by setting up a Cartesian coordinate system. The Cartesian coordinate, shown in Fig. 3.3, consists of two base vectors, $\sin(\omega t)$ and $\cos(\omega t)$, that are orthogonal functions. The sine axis lies in a horizontal direction, positive leftward, and the cosine axis lies in a vertical direction, positive downward. In this coordinate system, phase angles are positive in a counterclockwise direction. The cosine vector is rotated 90° ahead of the sine vector because $\cos(\omega t)$ reaches a maximum value of 90° before $\sin(\omega t)$.

The general form of a harmonic variable (e.g., pressure) is

$$P = \overline{P}_w + a \sin(\omega t) + b \cos(\omega t) \ .$$

Only the time-dependent portion of a harmonic variable can be represented in a vector diagram. Thus, the pressure oscillation is plotted (Fig. 3.3) by drawing a vector from the origin to the point (a,b). The length of the

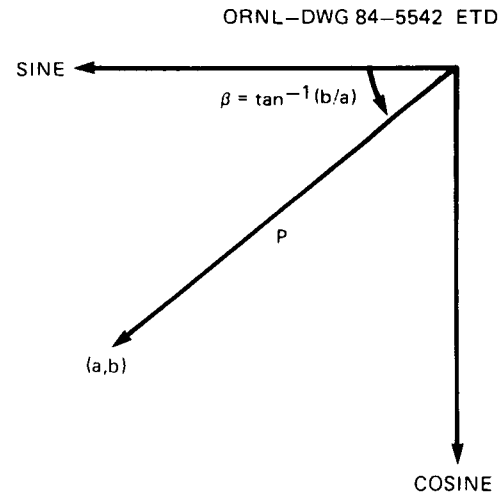

Fig. 3.3. Cartesian coordinate system with sine and cosine as orthogonal unit vectors.

vector is equal to the pressure amplitude ($\sqrt{a^2 + b^2}$), and the direction of the vector is at a phase angle $\beta = \tan^{-1}(b/a)$ from the sine axis.

A better understanding of vector presentation is provided by an example vector diagram for the RE-1000 Nominal engine with adiabatic cylinders and no other losses (Fig. 3.4). In the LHA, the piston motion was chosen as a reference with only a sine component; thus, the piston position vector is drawn along the sine axis. All other vectors are drawn relative to the piston position vector. In the RE-1000 Nominal engine, the displacer and piston amplitudes are equal, and the displacer phase angle β_d is 45°. Thus, the displacer position vector is drawn 45° ahead of and equal in length to the piston position vector. The expansion volume [Eq. (3.22)] reaches a maximum when the displacer position reaches a minimum. The expansion volume vector is drawn opposite the displacer position vector. The compression volume [Eq. (3.23)] is an area-weighted sum of the piston and displacer positions. The resultant compression volume vector lags the expansion volume vector by about 106°. The total volume vector is the vector sum of expansion and compression volume vectors. Most of the change in total volume is caused by the motion of the power piston; but some small change is also caused by the displacer motion acting through the area of the displacer rod (8.5% of the power piston area). The total volume vector is almost, but not exactly, 180° out of phase with

ORNL–DWG 84–5543 ETD

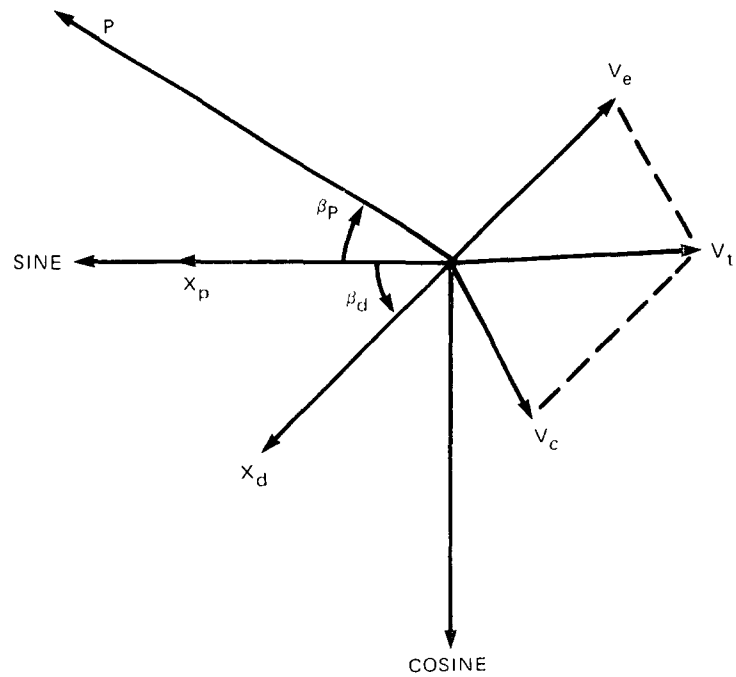

Fig. 3.4. Vector diagram showing relevant thermodynamic variables for RE-1000 Nominal engine with adiabatic cylinders and no other losses.

the piston position vector. The pressure vector shown in Fig. 3.4 was computed from the LHA analysis. The pressure phase angle β_p is important because it is a parameter that is measured in many experimental engines.

Heat input, heat output, work output, and efficiency can be computed from a vector diagram. Because these quantities are functions of only the pressure and volume vectors, some simplifications are made to the vector diagrams. For clarity, the two position vectors and the sine and cosine axes are omitted. Also, because only the relative amplitudes and phase angles between the vectors are important, the entire diagram can be rotated so that the total volume vector lies in the horizontal direction.

One final modification to the vector diagrams is the addition of the rate of change of volume $\dot{V}_t$ vector (Fig. 3.5). The derivative of a harmonic variable is always represented by a vector that lies 90° ahead of the variable. Thus, the $\dot{V}_t$ vector points upward and is normalized by the frequency to ensure a unit vector. The work output of an engine is equal to the dot product between the pressure and $\dot{V}_t$ vectors. Heat input and

ORNL–DWG 84–5541 ETD

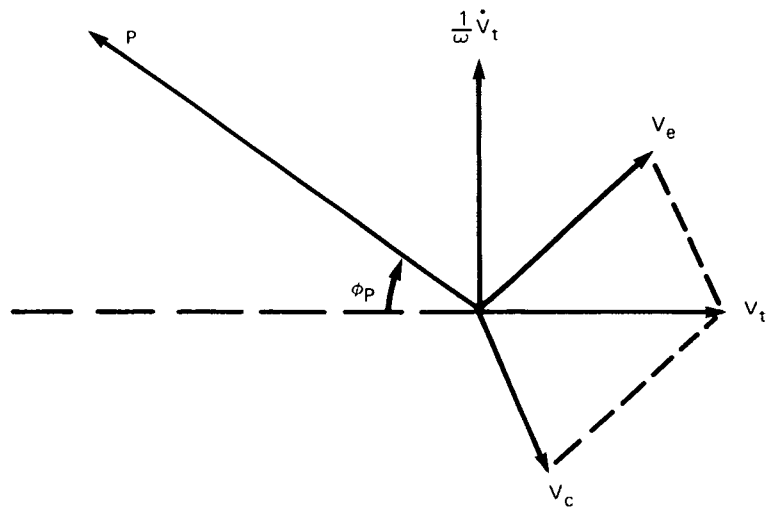

Fig. 3.5. Simplified vector diagram showing only pressure and volume vectors.

output are equal to the dot product between the pressure and $\dot{V}_e$ vectors and the negative dot product between the pressure and $\dot{V}_c$ vectors, respectively. Efficiency is related to the phase angle ϕ_P between the pressure vector and the negative total volume vector. The derivation of this relationship is given in Appendix B.

3.10 Summary of LHA Procedures

The LHA procedures can be summarized by nine steps.

1. The working space is divided into control volumes.
2. The conservation equations (mass, momentum, energy) are written for the control volumes.
3. It is assumed that P, m, T, and V have small amplitudes relative to their mean values, and a linear form of the ideal gas law is used to express P in terms of m, T, and V. V is expressed in terms of X; X is a specified harmonic function.
4. A complete transient solution is not pursued. The LHA method is restricted to steady state solutions. Harmonic solutions, in terms of undetermined coefficients (y_1, y_2, etc.), are assumed for m and T and are substituted into the governing equations.

5. Nonharmonic terms are represented in governing equations by truncated Fourier expansions.
6. The general form of each governing equation becomes:

$$\Sigma \text{ constant terms} + \Sigma \sin(\omega t) \text{ terms} + \Sigma \cos(\omega t) \text{ terms} = 0 \ .$$

A solution exists for all times only if

$$\Sigma \text{ constant terms} = 0 \ ,$$

$$\Sigma \sin(\omega t) \text{ terms} = 0 \ ,$$

$$\Sigma \cos(\omega t) \text{ terms} = 0 \ .$$

7. *Most* of the $\sin(\omega t)$, $\cos(\omega t)$ terms are linear functions of the undetermined coefficients (y_1, etc.). Nonlinear combinations of y_1, y_2, etc., are treated in a quasilinear manner. The resulting linear system of algebraic equations is solved using standard matrix theory to find the values of y_1, y_2, etc.
8. After y_1, y_2, etc., are obtained, the constant terms in the governing equations are solved to compute the values of other unknown parameters such as $\overline{T}_e$, $\overline{T}_c$, etc.
9. A few iterations are needed because of coupling between $\overline{T}_e$, $\overline{T}_c$, etc., in step (8) and the quasilinear approximations in step (7).

4. LOSS MECHANISMS

Four loss mechanisms that significantly affect engine performance will be discussed extensively. These losses are adiabatic effects, transient heat transfer, pressure drop, and mass leakage.

All results to be presented are direct applications of the LHA to the reference engines, RE-1000 Nominal and RE-1000 Modified, coupled with the entropy analysis for allocating individual loss mechanisms. In the course of discussions, vector diagrams will be used from time to time to illustrate the underlying physics, and considerations of the degree of coupling among losses will be provided.

4.1 Adiabatic Effects

This section includes a discussion of the thermodynamics of adiabatic cylinders and an analysis of the dependence of adiabatic efficiency loss on the compression and temperature ratios. The section will conclude with a discussion of the two mechanisms, revealed by entropy analysis, that are responsible for the adiabatic loss effects.

4.1.1 Thermodynamics of adiabatic cylinders

For a high-speed Stirling engine, the bulk of the gas in the cylinder behaves nearly adiabatically, while gas in the adjacent heat exchanger components acts more isothermally. The combination of adiabatic and isothermal volumes causes a loss mechanism, known loosely as the adiabatic loss, that reduces thermal efficiency.

As a numerical example illustrating the thermodynamics of adiabatic cylinders, the RE-1000 Nominal engine (see Tables 3.1 and 3.2 for operating conditions and dimensions) will be used. With adiabatic losses only (i.e., no pressure drop, mass leakage, or heat transfer to the cylinder walls), all the rate constants are set equal to zero in Eq. (3.92). Solving the matrix equation by the IBM subroutines DECOMP and SOLVE for the unknowns y_1—y_{10} determines completely the amplitude and phase information associated with all the thermodynamic variables. The results are illustrated over an entire cycle to show their interrelationship (Fig. 4.1).

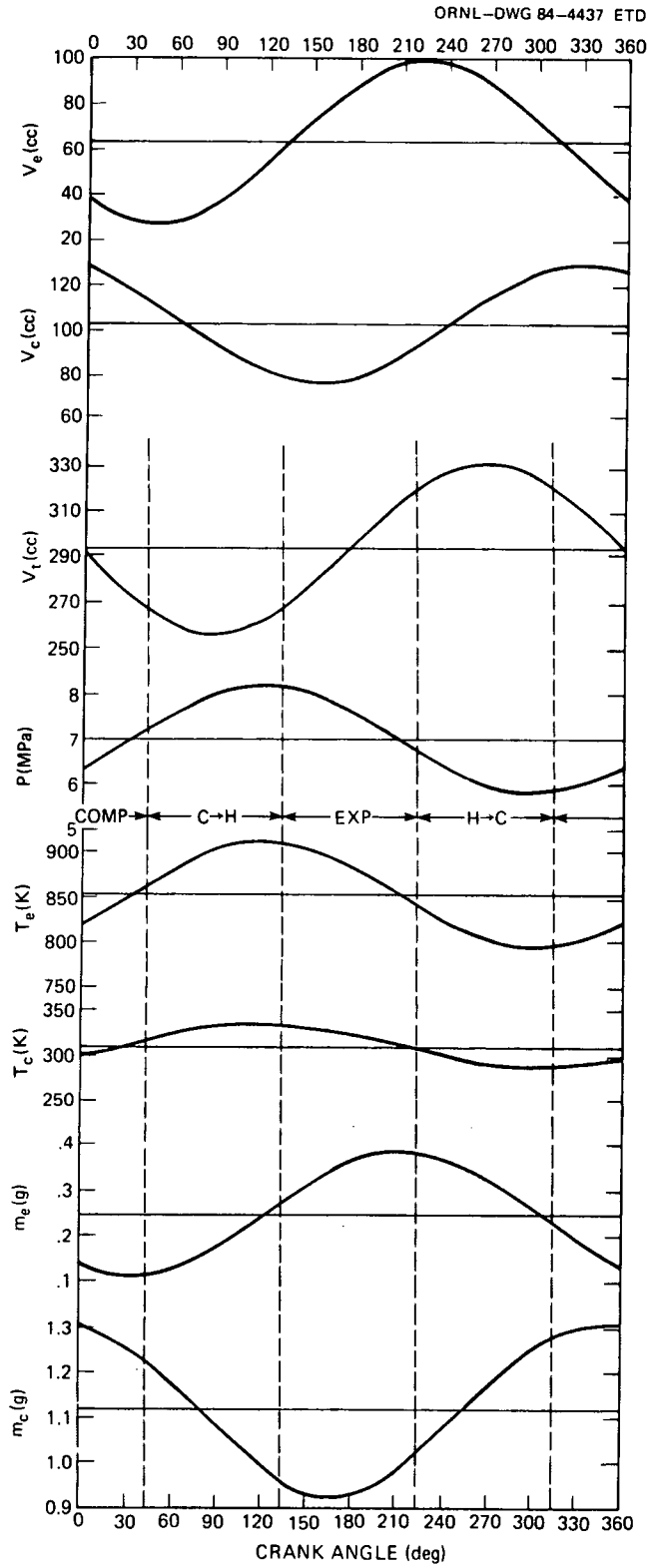

Fig. 4.1. Thermodynamics of RE-1000 Nominal engine with adiabatic cylinders.

For an engine with prescribed sinusoidal volume variations, LHA predicts sinusoidal variations around their mean values for all thermodynamic variables. General observations from Fig. 4.1 reveal that the pressure and temperature in both spaces are almost in phase (a characteristic of adiabatic cylinders) as expected. But, unlike the pressure and temperatures, masses in both spaces are neither in phase nor out of phase.

A more instructive understanding of the thermodynamics can be obtained if the cycle is broken down into four distinct regions of equal span. These regions are defined with respect to the total volume variation and are bounded by the vertical dashed lines in Fig. 4.1. Region 1, labeled as C → H, starting at a phase of about 42° and ending at 132°, represents the gas displacement from the cold cylinder to the hot cylinder. In this region, the total volume is near its minimum value and almost constant; however, a sharp rise and fall are observed in the mass inventories of the expansion and compression spaces. The pressures and temperatures are rising because the gas is being heated as it is displaced from the cold to hot cylinder. Region 2, labeled expansion (EXP) and spanning from 132° to 222°, is characterized by a large increase in total volume with small mass changes in the expansion and compression spaces. The pressures and temperatures in region 2 are decreasing because the gas in the cylinders expands adiabatically as the total volume increases. The trends in region 3 (gas displaced from hot to cold end) and region 4 (compression) are opposite to those of regions 1 and 2.

Observation of the temperature variations discloses some intrinsic properties of adiabatic cylinders. In the expansion space, there is a temperature overshoot above the heater temperature (900 K) over a fairly small fraction of the cycle (in this case, it lasts about 60°). The gas temperature stays below the heater temperature over the remaining times. Moreover, during the expansion phase, the working gas, with its peak allocation (m_e at maximum) in the expansion space, begins to expand adiabatically at a temperature close to heater temperature and falls well below that level. As a result, the mean gas temperature in the expansion space ($\overline{T}_e$ = 854 K) is considerably below the heater temperature of 900 K.

Conversely, there is a temperature undershoot below the cooler temperature (300 K) in the compression space. Unlike the temperature overshoot, the undershoot condition persists for a relatively long span (about one-third of a cycle). At other times, the gas temperature remains above the cooler temperature. Furthermore, during the compression phase, the working gas, with its peak allocation in the compression space (m_c at maximum), starts to compress adiabatically at a temperature close to the cooler temperature and rises above it. Consequently, this causes the mean temperature in the compression space ($\overline{T}_c$ = 312 K) to be higher than the cooler temperature of 300 K. These mean temperatures provide a measure of the degree of departure from isothermal cylinders: the larger the departure, the larger the adiabatic loss.

The PV-diagram of the RE-1000 Nominal engine with adiabatic cylinders is presented in Fig. 4.2. The large area enclosed by a curve in a clockwise direction represents the work produced by the expansion space. The expansion-space work output is equal to the heat input. The small area bounded by a curve in a counterclockwise direction denotes the work

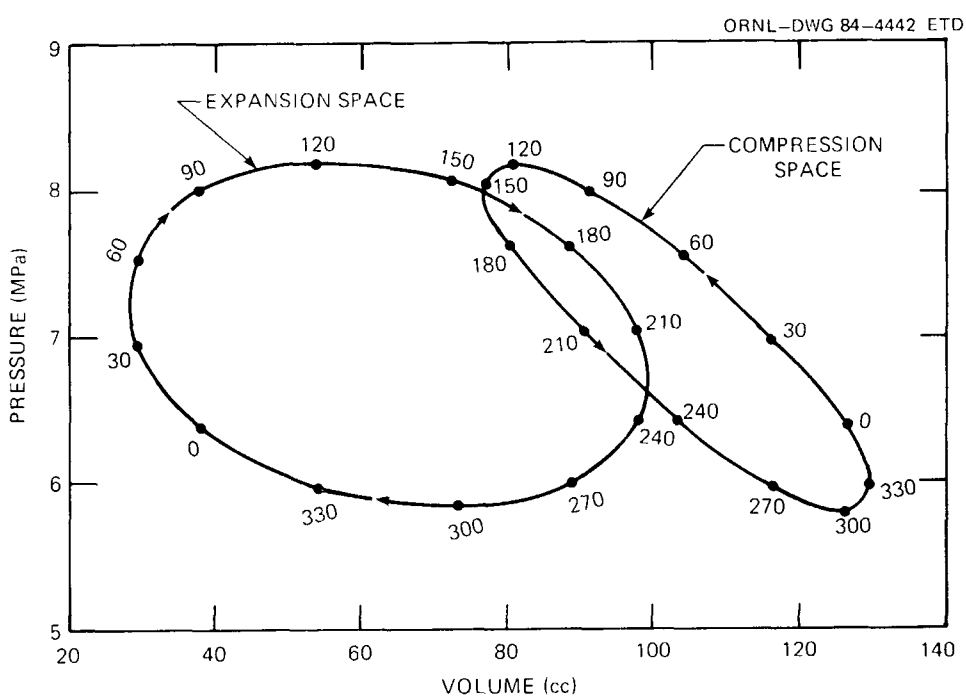

Fig. 4.2. P-V diagram for RE-1000 Nominal engine with adiabatic cylinders.

absorbed by the compression space, or the heat rejected. The algebraic sum of these two areas represents the net work performed by the engine.

Adiabatic and isothermal engines differ greatly in power output and efficiency. An adiabatic cylinder is a cylinder where no heat transfer occurs between the cylinder wall and the gas within the cylinder. An isothermal cylinder is a cylinder where an infinite heat transfer takes place between the cylinder wall and the gas so that a state of thermal equilibrium is maintained at all times. A comparison in RE-1000 Nominal engine performance between adiabatic and isothermal cylinders is shown in Table 4.1. The power output of the adiabatic engine is larger than that of an isothermal engine because the adiabatic cylinder produces a higher pressure amplitude than the isothermal cylinder for a given swept volume. However, the reverse holds true for efficiency. The efficiency of an isothermal engine is equal to the Carnot value, which is the maximum possible efficiency that any engine can achieve.

Table 4.1. RE-1000 Nominal engine performance comparison: adiabatic vs isothermal cylinders

Cylinder heat transfer	Power output (W)	Efficiency (%)
Isothermal	2027.0	66.67
Adiabatic	2636.9	62.97

4.1.2 Dependence of adiabatic efficiency loss on compression ratio

Three important variables that affect adiabatic efficiency losses are compression ratio, temperature ratio, and working fluid. In discussions to follow, the term "compression ratio" refers specifically to volume compression ratio, not pressure ratio. In this subsection, considerations will be restricted to the adiabatic loss dependence on compression ratios and working gases, while keeping the heat exchanger temperature ratio constant.

A study of the effects of adiabatic efficiency losses over a range of compression ratios requires changes from the RE-1000 Nominal configuration. This is achieved by a combined reduction of dead- and mean-compression volumes and an increase in power piston amplitude. The exact numerical values for the RE-1000 Modified engine are listed in Table 3.3 for reference. The combined modification produces a volume compression ratio ranging from 1 to 1.89.

Both monatomic and diatomic gases are studied. The heat capacity ratio of a diatomic gas, such as hydrogen or air, is 7:5, while the heat capacity ratio of a monatomic gas, such as helium, is 5:3.

When the LHA method is applied to the RE-1000 Modified configuration with no other losses, the results shown in Fig. 4.3 are obtained. The graph includes three curves: efficiencies for an isothermal cylinder engine (the Carnot efficiency is 67% for a temperature ratio of 3:1), an

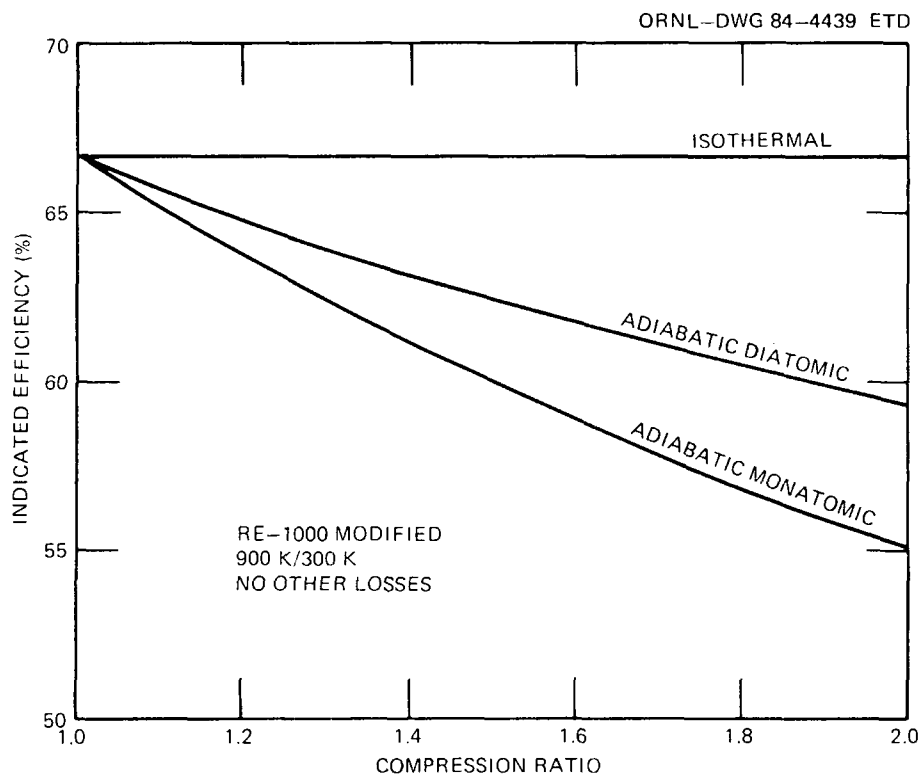

Fig. 4.3. Effects of compression ratio and working gas on efficiency of RE-1000 Modified configuration with isothermal and adiabatic cylinders.

adiabatic cylinder engine with a diatomic gas, and an adiabatic cylinder engine with a monatomic gas.

For engines with isothermal cylinders, the efficiency remains the same regardless of the compression ratio and the working gas used. However, for adiabatic cylinders, the efficiency depends on the working gas. An adiabatic cylinder is less efficient with a monatomic gas than with a diatomic one because for a given volume change, the monatomic gas will have larger fluctuations in both pressure and temperature.

It is important that the loss of efficiency caused by adiabatic gas behavior in the cylinders increases as the compression ratio increases. Such a loss is very significant. For example, at a compression ratio of 1.89 with helium (monatomic gas) as the working fluid, the loss in efficiency is more than 10 percentage points. Hence, Fig. 4.3 illustrates a major drawback of high compression ratio engines: they have much greater adiabatic efficiency losses than low compression ratio engines.

Figures 4.4 and 4.5 illustrate why this loss is high. Figure 4.4 shows the temperature fluctuation in the expansion space vs the phase angle of the power piston (i.e., the power piston position) for various compression ratios. When the pistons move sinusoidally, the gas undergoes periodic compression and expansion adiabatically; a temperature fluctuation develops, and the mean gas temperature shifts below the heater temperature. This effect intensifies when the compression ratio is increased. For instance, at a low compression ratio of 1.13 (case 1) corresponding to a piston amplitude that is one-fifth of the maximum possible value, the temperature amplitude $|T_e|$ and the mean gas temperature $\overline{T}_e$ are 34 and 875 K, respectively. Tripling the piston amplitude of case 1 (compression ratio = 1.45) almost triples the $|T_e|$ and lowers $\overline{T}_e$ substantially. A fivefold increase in the piston amplitude over case 1, equivalent to a compression ratio of 1.89, results in a significant increase in temperature swing ($|T_e|$ = 145 K) and also a very large fall in the mean gas temperature.

Similar and equally important effects have been observed in the compression space, except that the mean gas temperature shifts upward and remains above the cooler temperature (Fig. 4.5).

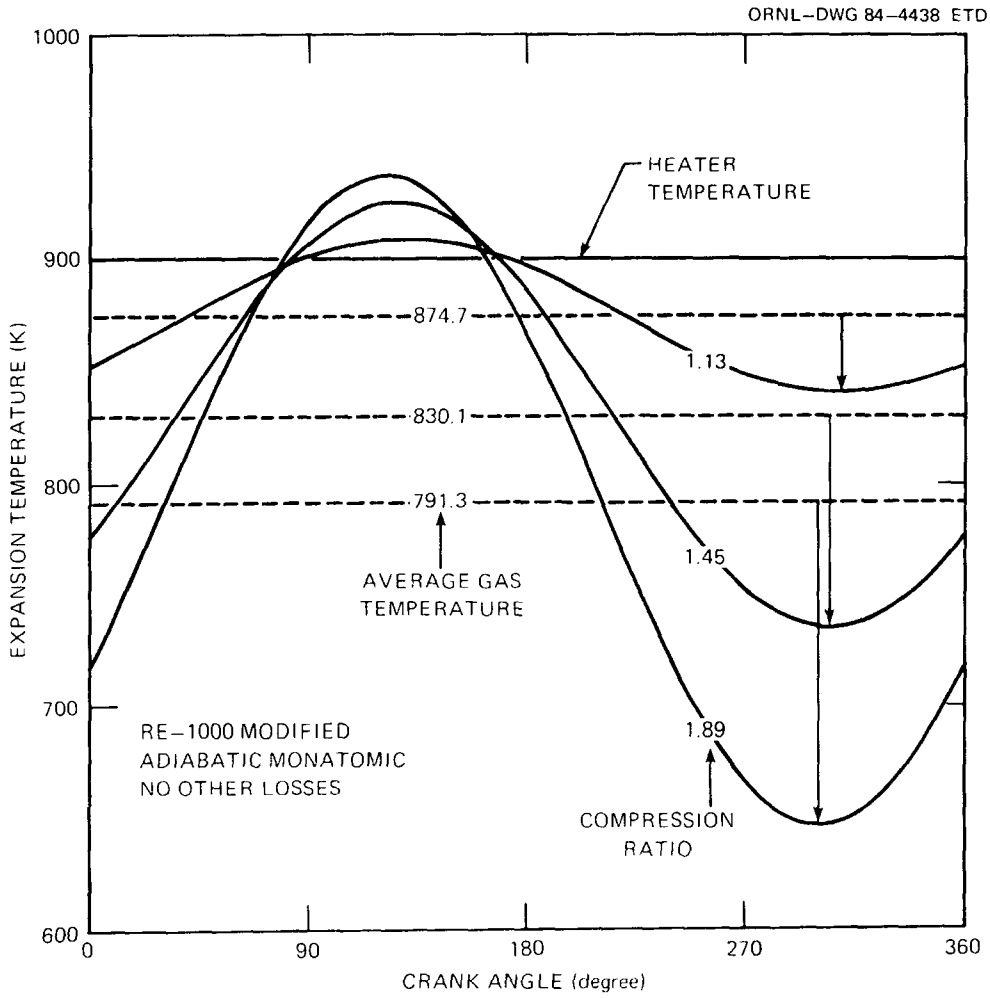

Fig. 4.4. Cyclic expansion space temperature variation for various compression ratios.

4.1.3 Dependence of adiabatic efficiency loss on temperature difference

In a typical engine with a large compression- expansion-space temperature difference, the adiabatic temperature fluctuations in the gas may be fairly small compared with the mean temperature difference. This means that adiabatic effects are relatively small; but for low temperature difference machines (including heat pumps), the adiabatic effects become very significant.

The adiabatic effects can be demonstrated by plotting efficiency vs heater temperature (Fig. 4.6); the effect of different working gases is also shown. For isothermal engines, the efficiency does not fall to zero

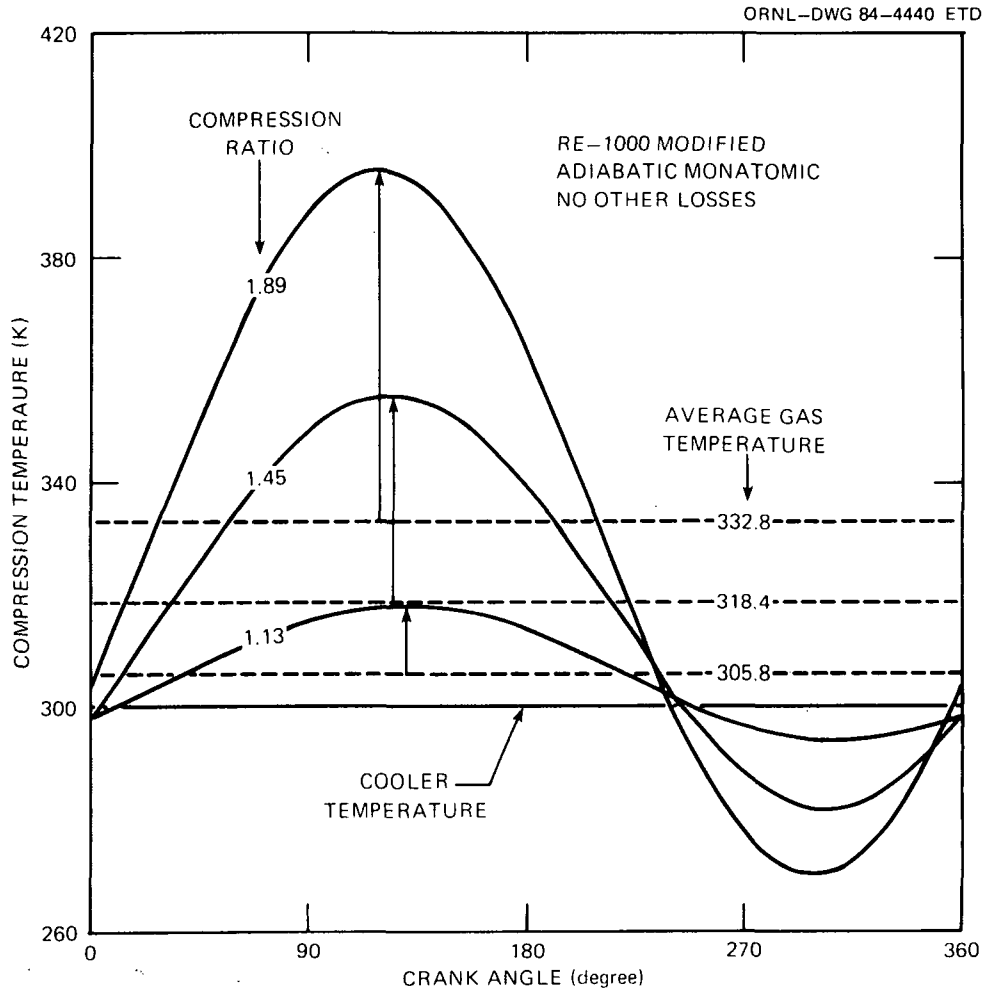

Fig. 4.5. Cyclic compression space temperature variation for various compression ratios.

until there is no temperature difference between the two spaces. However, for adiabatic engines, positive power is not produced unless a certain finite temperature difference between the heater and cooler is exceeded. In this particular instance, the minimum temperature difference for power production for the monatomic gas is about 34 K. The reduction in efficiency is less critical at higher heater temperatures; for example, for a monatomic gas at a heater temperature of 900 K, the reduction is 3.7 percentage points out of 67% Carnot efficiency. However, at a heater temperature of 350 K, the reduction is 9.3 percentage points out of 14% Carnot efficiency.

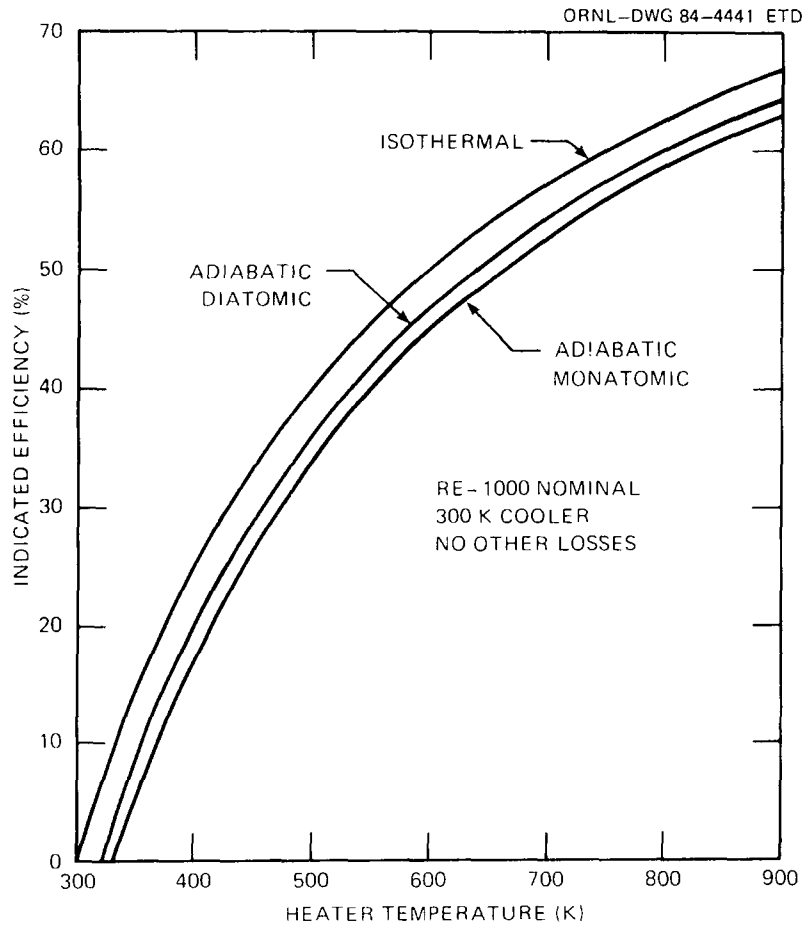

Fig. 4.6. Effects of heater temperature and working gas on efficiency of the RE-1000 Nominal engine with isothermal and adiabatic cylinders.

4.1.4 Mechanism for adiabatic efficiency loss

Fundamentally, the adiabatic effects leading to efficiency reduction below the Carnot value can be attributed to two distinct mechanisms: mixing and external heat transfer irreversibilities. The entropy production caused by each one will be derived and discussed.

4.1.4.1 Entropy production due to external heat transfer. Heat transfer across a finite temperature difference is an irreversible thermodynamic process because it results in an increase in entropy. There are four distinct regions where the external heat transfer irreversibilities occur in a typical Stirling engine:

1. Entropy change by heater heat transfer. During that part of the cycle where working gas flows out of the expansion space and into the

heater, the instantaneous entropy change may be represented by Eq. (2.35), if the heating (or cooling if there is a temperature overshoot) is so effective that the process will be completed almost spontaneously at the heater inlet.

$$\Delta\dot{S}_{QH} = c_p \left(-\frac{dm_e}{dt}\right) \int_{T_e}^{T_H} \frac{dT}{T} , \quad dm_e < 0 . \tag{4.1}$$

The average entropy production over that part of the cycle where mass flows out is, therefore,

$$\overline{\Delta\dot{S}}_{QH} = c_p \, \overline{m}_e \, f \int_{\theta_e}^{\theta_e + \pi} \frac{dm_e^*}{dt^*} \ln\left(\frac{T_e}{T_H}\right) dt^* , \tag{4.2}$$

with the integration intervals defined by

$$\theta_e = \begin{cases} \tan^{-1}\left(\frac{y_1}{y_2}\right), & y_2 > 0 \\ \tan^{-1}\left(\frac{y_1}{y_2}\right) + \pi , & y_2 < 0 \end{cases} . \tag{4.3}$$

2. Entropy change by cooler heat transfer. Similar expressions for the entropy production caused by cooler heat transfer irreversibility may be written as

$$\Delta\dot{S}_{QK} = c_p \left(-\frac{dm_c}{dt}\right) \int_{T_c}^{T_K} \frac{dT}{T} , \quad dm_c < 0 \tag{4.4}$$

for the instantaneous entropy change, and

$$\overline{\Delta\dot{S}}_{QK} = c_p \, \overline{m}_c \, f \int_{\theta_c}^{\theta_c + \pi} \frac{dm_c^*}{dt^*} \ln\left(\frac{T_c}{T_K}\right) dt^* \tag{4.5}$$

for the average value, where

$$\theta_c = \begin{cases} \tan^{-1}\left(\dfrac{y_5}{y_6}\right), & y_6 > 0 \\ \tan^{-1}\left(\dfrac{y_5}{y_6}\right) + \pi, & y_6 < 0 \end{cases} . \tag{4.6}$$

3. Entropy change by expansion-cylinder average heat transfer. As defined in Eq. (2.29), the instantaneous entropy change caused by this component is represented by

$$\Delta\dot{S}_{Qwe} = \frac{h_e \overline{A}_{se} \left(\overline{T}_{we} - \overline{T}_e\right)}{T_e} . \tag{4.7}$$

The average value may be obtained by integrating over an entire cycle

$$\overline{\Delta\dot{S}}_{Qwe} = \frac{h_e \overline{A}_{se}}{2\pi} \left(\frac{\overline{T}_{we}}{\overline{T}_e} - 1\right) \int_0^{2\pi} \frac{1}{T_e^*} \, dt^* . \tag{4.8}$$

After substituting Eq. (3.33) for T_e^*, a closed-form solution is possible;

$$\overline{\Delta\dot{S}}_{Qwe} = \frac{h_e \overline{A}_{se} \left(\dfrac{\overline{T}_{we}}{\overline{T}_e} - 1\right)}{\sqrt{1 - y_7^2 - y_8^2}} . \tag{4.9}$$

4. Entropy change by compression-cylinder average heat transfer. To avoid duplication, the derivations that are similar to those for the expansion cylinder will not be repeated. The cyclic entropy production caused by this contribution is

$$\overline{\Delta\dot{S}}_{Qwc} = \frac{h_c \overline{A}_{sc} \left(\dfrac{\overline{T}_{wc}}{\overline{T}_c} - 1\right)}{\sqrt{1 - y_9^2 - y_{10}^2}} . \tag{4.10}$$

With the derived entropy production caused by external heat transfer in the four regions, the average temperatures at which energy enters and leaves the cycle can be computed by use of Eqs. (2.25) and (2.26);

$$\overline{T}_{in} = \frac{\overline{\dot{Q}}_{in}}{\overline{\Delta\dot{S}}_{QH} + \overline{\Delta\dot{S}}_{Qwe}} , \tag{4.11}$$

and

$$\overline{T}_{out} = \frac{-\overline{\dot{Q}}_{out}}{\overline{\Delta\dot{S}}_{QK} + \overline{\Delta\dot{S}}_{Qwc}} . \tag{4.12}$$

Given the average temperatures, the efficiency reduction caused by the external heat transfer irreversibility can be computed from Eq. (2.22).

$$\Delta\eta_{EHT} = \frac{\overline{T}_{out}}{\overline{T}_{in}} - \frac{T_K}{T_H} . \tag{4.13}$$

4.1.4.2 Entropy production due to mixing. Mixing gases at different temperatures is another irreversible thermodynamic process. In a typical Stirling engine, mixing occurs when gas enters the expansion or compression spaces; however, the derivation and discussion will concentrate on the expansion space.

When a differential element of gas dm_e at the heater temperature T_H flows into the expansion space, it mixes with the gas in the cylinder at instantaneous mass m_e and temperature T_e. The entropy production caused by mixing can be better described by a heat transfer process as illustrated in Fig. 4.7. Assume that there is heat transfer at an instantaneous rate of $\dot{Q} = c_p \frac{dm_e}{dt} (T_H - T_e)$ between the gas added to the cylinder and the gas already in the cylinder so that the added mass is heated to T_e before it is mixed. Because the added mass is very small compared with the mass inside the cylinder (i.e., $dm_e \ll m_e$), the temperature of the larger mass m_e will be barely affected, while the infinitesimal mass

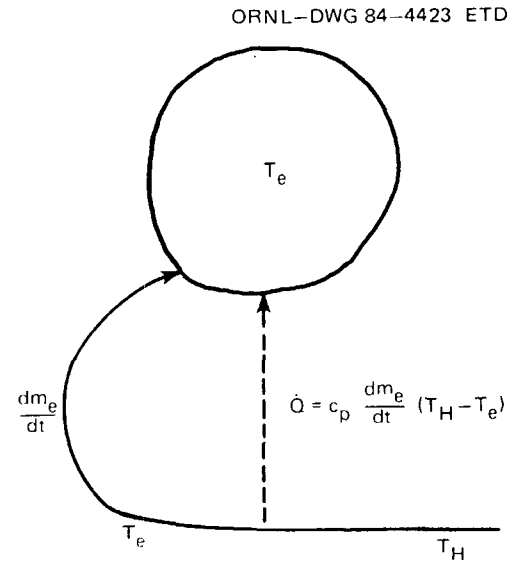

Fig. 4.7. Irreversible gas mixing in expansion space.

(dm_e) will either be cooled or heated, depending on the relative temperatures between the heater temperature and the instantaneous expansion gas temperature. During the process, the change of entropy for the mass of gas already in the cylinder may be approximated by

$$\Delta\dot{S} = \frac{\dot{Q}}{T_e} = \frac{c_p \frac{dm_e}{dt} (T_H - T_e)}{T_e} , \quad dm_e > 0 . \tag{4.14}$$

This approximation is reasonable because the temperature remains fairly constant during the heat transfer, for the reasons just given. The change of entropy for the small mass that is added to the cylinder can be computed from Eq. (2.35),

$$\Delta\dot{S} = c_p \frac{dm_e}{dt} \int_{T_H}^{T_e} \frac{dT}{T} , \quad dm_e > 0 . \tag{4.15}$$

Therefore, the net instantaneous rate of change of entropy in the expansion space caused by heat transfer between the two masses is the sum

of the changes calculated by Eqs. (4.14) and (4.15),

$$\Delta\dot{S}_{mixe} = \frac{c_p \frac{dm_e}{dt}(T_H - T_e)}{T_e} + c_p \frac{dm_e}{dt} \ln\left(\frac{T_e}{T_H}\right), \quad dm_e > 0 . \tag{4.16}$$

The average rate of entropy change over that part of the cycle where gas flows in may be obtained by integrating over the proper intervals. Thus,

$$\overline{\Delta\dot{S}}_{mixe} = c_p \, \overline{m}_e \, f \int_{\theta_e - \pi}^{\theta_e} \frac{dm_e^*}{dt^*} \left[\ln\left(\frac{T_e}{T_H}\right) + \frac{T_H}{T_e} - 1\right] dt^* , \tag{4.17}$$

where θ_e has been defined in Eq. (3.42).

A similar mixing process exists in the compression space. The derivation will not be repeated; however, the final result is

$$\overline{\Delta\dot{S}}_{mixc} = c_p \, \overline{m}_c \, f \int_{\theta_c - \pi}^{\theta_c} \frac{dm_c^*}{dt^*} \left[\ln\left(\frac{T_c}{T_K}\right) + \frac{T_K}{T_c} - 1\right] dt^* , \tag{4.18}$$

where θ_c was defined in Eq. (3.74).

These derivations are valid only for adiabatic mixing at constant pressure. For processes that involve nonconstant pressure, additional contributions due to that effect have to be incorporated in the full derivation of entropy changes (Sect. 2.5).

Numerical integration is inevitably needed to evaluate these integrals over the indicated intervals when mixing occurs. In the evaluations, temperature and mass oscillations were obtained from LHA predictions.

The total mixing-controlled entropy production in the engine is the algebraic sum of the contribution from each of the two spaces. The corresponding efficiency reduction may be allocated with reference to

Eq. (2.23),

$$\Delta\eta_{mix} = \frac{\bar{T}_{out}\left(\overline{\Delta\dot{S}}_{mixe} + \overline{\Delta\dot{S}}_{mixc}\right)}{\bar{\dot{Q}}_{in}} . \tag{4.19}$$

4.2 Transient Heat Transfer Loss

As the gas in the Stirling engine is compressed and expanded, the temperature of the gas oscillates up and down. Gas temperature oscillations create an oscillating temperature gradient between the gas and the cylinder wall that results in convective heat transfer. This presents an irreversible thermodynamic process and leads to a loss of both power and efficiency.

In an engine where there is a continuous displacement of the working fluid between the hot and cold cylinders, the losses caused by transient heat transfer are closely coupled to the losses caused by adiabatic cylinders. Gas springs can be used as an example to examine transient heat transfer losses in a more pure form because the adiabatic losses described in Sect. 4.1 do not exist in gas springs. This section will begin with a discussion of gas springs and will continue with a discussion of the working space of an engine.

4.2.1 Gas spring with sinusoidal motions

A gas spring undergoing a harmonic oscillation can be used to explain the transient heat transfer losses simply because it provides a closed-form solution for a perfect seal condition in which the mass remains constant. This analysis serves as a stepping-stone to dealing with the more complicated case of an engine working space where mass is displaced continuously.

A general gas spring analysis has been presented in Appendix A, where both transient heat transfer and seal leakage losses occurring simultaneously are treated. For the sake of illustrating transient heat transfer losses in a gas spring, consider the special case with no leakage. The analysis will assume that the piston undergoes a simple

harmonic motion in which only a sine component exists. Thus,

$$V_s^* = 1 + |V_s^*| \sin t^* , \tag{4.20}$$

where $|V_s^*| = |V_s|/\overline{V}_s$ is the dimensionless volume amplitude.

Under such conditions, the solution for pressure is greatly simplified from Eq. (A.36),

$$P_s^* = 1 - |V_s^*| \left[\left(1 + \frac{\gamma - 1}{1 + h_s^{*2}} \right) \sin t^* + \frac{(\gamma - 1)\, h_s^*}{1 + h_s^{*2}} \cos t^* \right] , \tag{4.21}$$

where the first term represents the mean pressure and the second term, in the square bracket, signifies the time-dependent component. It is this component that contains information on transient heat transfer loss, which will be investigated further.

The effects of transient heat transfer loss over a wide range of heat transfer coefficients h_s^* in a vector diagram (Fig. 4.8) can be shown by constructing an envelope containing the trajectory traced by the heads of pressure vectors for different heat transfer rates between wall and gas. The envelope is defined by Eq. (4.21) and turns out to be a

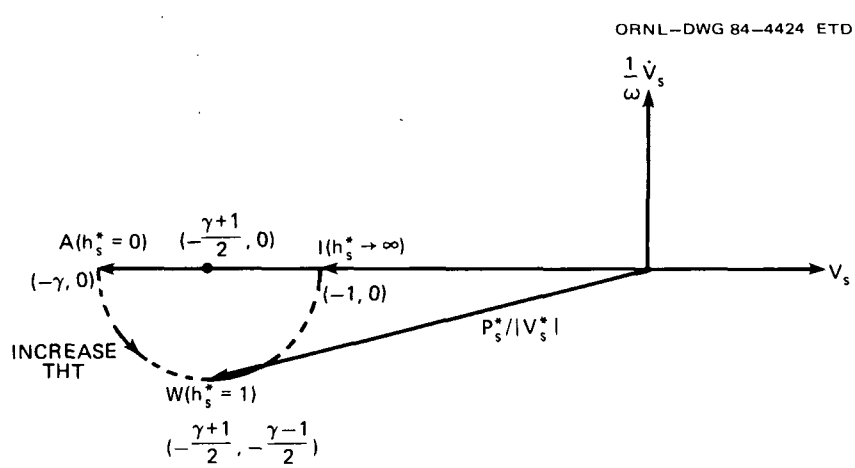

Fig. 4.8. Pressure and volume vectors for a gas spring with transient heat transfer loss only.

semicircle that is characterized by the following descriptions:

1. The two end points, marked A and I, represent the adiabatic and isothermal limits:

   $|P_s^*/|V_s^*|| = \gamma$, for $h_s^* \to 0$ (adiabatic cylinders),

   $|P_s^*/|V_s^*|| = 1$, for $h_s^* \to \infty$ (isothermal cylinders).

2. As the value of nondimensional heat transfer coefficients, (h_s^*) increases, the head of the pressure vector travels along the semicircle, which is centered at $\left(-\frac{\gamma+1}{2}, 0\right)$ and has a radius of $\frac{\gamma-1}{2}$.

3. The minimum, labeled W, occurs when $h_s^* = 1$ and is at a point on the graph defined by $\left(-\frac{\gamma+1}{2}, -\frac{\gamma-1}{2}\right)$.

This result is rather simple, but it has very significant implications. Recall that only that component of pressure in phase with the rate of change of volume $\dot{V}_s$ contributes to the work. At the adiabatic limit, the pressure and volume vectors are out of phase by 180°; the gas pressure attains its maximum when the volume becomes minimum. Because there is no component of pressure in phase with $\dot{V}_s$, there is no transient heat transfer loss, and no net work is required to drive the piston. Furthermore, the spring force is proportional to γ, as it should be for an adiabatic gas spring. Because there is no transient heat transfer loss, the spring is said to be perfect.

The other extreme is the isothermal limit ($h_s^* \to \infty$). Again, pressure is 180° out of phase with volume, and the gas acts as a spring but with a lower spring rate than before. The ratio of the pressure vector length, and, therefore, the spring force, for the adiabatic and isothermal cases is γ. There is no component of pressure in phase with velocity, and, therefore, no transient heat transfer loss.

Immediately away from these two extremes, the pressure vector in general has two components: one, 180° out of phase with the volume vector; and the other, 180° out of phase with the rate of change of volume vector.

When the heat transfer coefficient between wall and gas increases, the head of the pressure vector rotates counterclockwise. The downward vertical component, in a negative $\dot{V}_s$ direction, increases until it

reaches the minimum point W and then decreases all the way to the isothermal limit. This leads to a transient heat transfer loss that increases from zero to a maximum and then decreases back to zero. Therefore, there exists a worst case W that produces a maximum transient heat transfer loss.

From the previous discussions, it has been shown that there is no transient heat transfer loss for an isothermal or adiabatic gas spring, but that it does take finite net work to drive a piston with an intermediate cylinder. To derive the expression for power loss, the pressure-volume integral must be evaluated. This is given by

$$\overline{\dot{W}}_s = \frac{1}{2\pi} \int_0^{2\pi} P_s \frac{dV_s}{dt} dt^* , \tag{4.22}$$

or in dimensionless form,

$$\overline{\dot{W}}_s = \frac{\omega \overline{P}_w \overline{V}_s}{2\pi} \int_0^{2\pi} P_s^* \frac{dV_s^*}{dt^*} dt^* . \tag{4.23}$$

Substituting Eq. (4.21) for P_s^* and Eq. (4.20) for volume variation and evaluating the integral results in

$$\overline{\dot{W}}_s = - \frac{\omega \overline{P}_w \overline{V}_s}{2} |V_s^*|^2 \frac{(\gamma - 1) h_s^*}{1 + h_s^{*2}} . \tag{4.24}$$

This relation reveals that

1. Work has to be performed on the piston externally as indicated by the negative sign; therefore, it is a power loss.
2. The power loss is, among other factors, proportional to the square of the volume amplitude.
3. No power loss exists for an adiabatic gas spring because of a vanishing heat transfer coefficient ($h_s^* \to 0$); nor does it exist for an isothermal one because of an infinite heat transfer coefficient ($h_s^* \to \infty$).

Equation (4.24) can be further simplified by the following manipulations. Recall that the mass inside the cylinder remains constant if the seal is perfect. For such a case, the linearized ideal gas law [Eq. (3.7)] reduces to

$$\frac{\Delta T_s}{\overline{T}_s} = \frac{\Delta P_s}{\overline{P}_w} + \frac{\Delta V_s}{\overline{V}_s} \ . \tag{4.25}$$

Using Eqs. (4.20), (4.21), and (4.25), the temperature amplitude can be related to the volume amplitude by

$$|T_s^*|^2 = \frac{(\gamma - 1)^2}{1 + h_s^{*2}} \, |V_s^*|^2 \ . \tag{4.26}$$

Replacing the volume amplitude with the temperature amplitude in Eq. (4.24) results in

$$\overline{\dot{W}}_s = - \frac{h_s \overline{A}_{ss} \overline{T}_s}{2} \left(\frac{|T_s|}{\overline{T}_s} \right)^2 \ . \tag{4.27}$$

Equation (4.27) shows that the power loss is uniquely characterized by the product of the square of the relative temperature amplitude, with $h_s \overline{A}_{ss} \overline{T}_s$ as the proportionality constant. Again, there is no power loss for both adiabatic and isothermal gas springs, but different interpretations must be applied. For adiabatic gas springs, even though the temperature fluctuation attains a maximum, the zero heat transfer coefficient makes the power loss vanish. On the other hand, for the isothermal gas springs, although the heat transfer coefficient approaches infinity, the zero temperature oscillation nullifies the power loss.

4.2.2 Working space of a Stirling engine

Transient heat transfer losses in the working space of a Stirling engine depend primarily on the heat transfer rates between the cylinder walls and the working fluid. Unfortunately, adiabatic losses are also affected by the heat transfer rates. Thus, unlike a gas spring where the

adiabatic and transient heat transfer losses do not interact, it is not meaningful to investigate the transient heat transfer losses separately from the adiabatic losses in an engine.

Engine performance results, as a function of heat transfer coefficients and based on the RE-1000 Nominal configuration with no other losses, are presented in Fig. 4.9. There is no transient heat transfer loss at the adiabatic extreme (left side of plot) because there is no heat transfer between the gas and the walls. However, the adiabatic

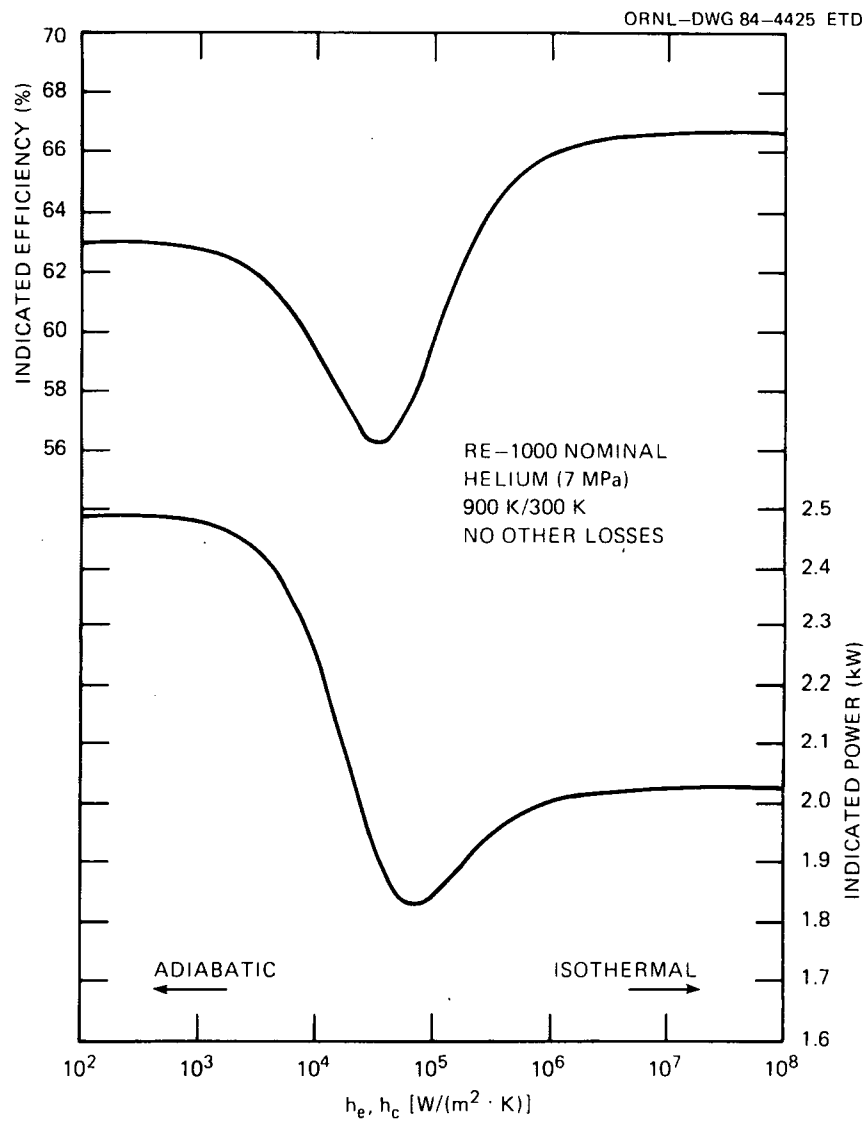

Fig. 4.9. Power output and efficiency vs heat transfer coefficients for RE-1000 Nominal engine.

losses that were discussed previously (Sect. 4.1) are present, the efficiency is less than the Carnot value, and the power output is greater than for the isothermal engine. There is no transient heat transfer loss at the isothermal limit (right side of the plot) because the temperature of the gas equilibrates with the local wall temperature. Both efficiency and power output show a worst case in the semiadiabatic region. This result for the engine might have been anticipated based on the gas spring analyses. The minimum efficiency occurs at a slightly lower heat transfer rate than the minimum power.

Heat transfer rates in the expansion and compression spaces have a very strong effect on the temperature oscillations of the working fluid. Figures 4.10 and 4.11 show, respectively, the expansion- and compression-

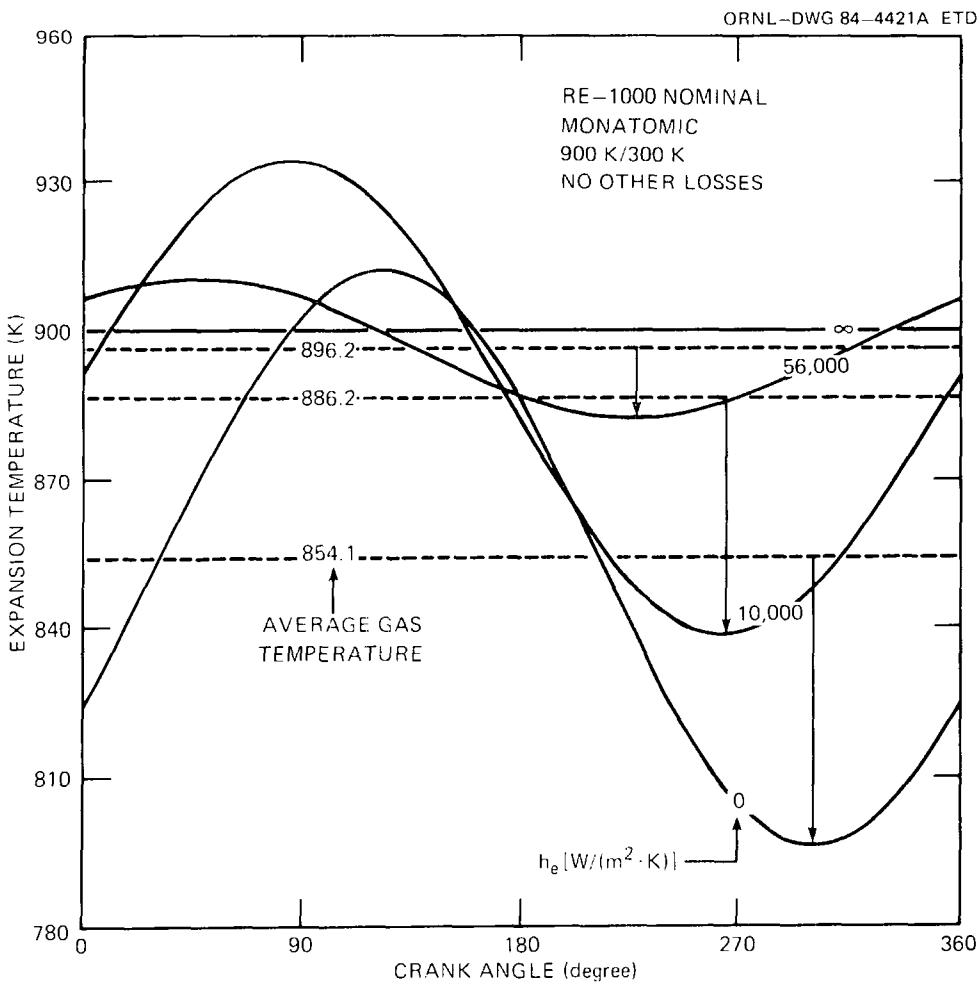

Fig. 4.10. Cyclic expansion-space temperature variation for various heat transfer coefficients.

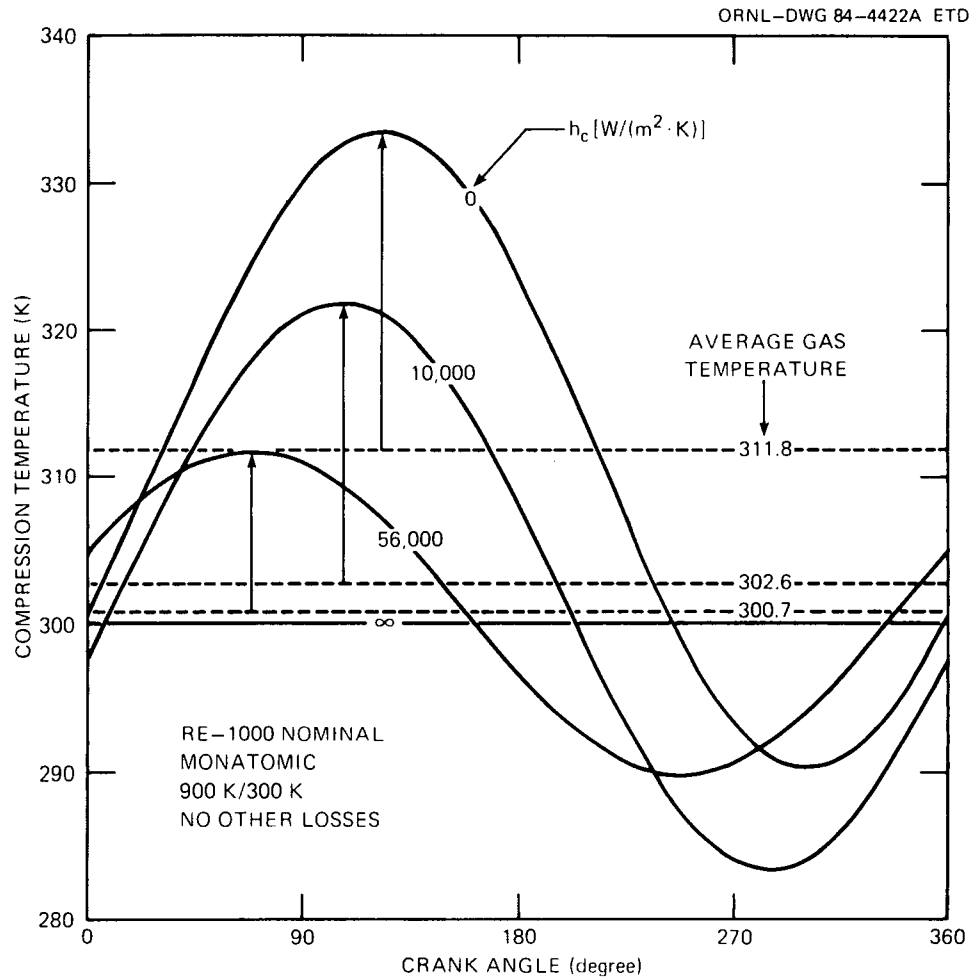

Fig. 4.11. Cyclic compression-space temperature variation for various heat transfer coefficients.

space temperature waves for a wide range of heat transfer coefficients. Three effects can be seen as the heat transfer rate increases: (1) The amplitudes of the temperature oscillations decrease. (2) The mean gas temperatures become closer to their respective adjacent heat exchanger temperatures. (3) The phases of the temperature waves shift. At the isothermal limit, the gas temperatures become constant and equal to the heat exchanger temperatures.

For additional insight, the same results are presented in a vector diagram (Fig. 4.12). There are three major differences between the vector diagrams of a gas spring and the working space:

1. In the gas spring, the pressure vectors lie in the third quadrant with a downward vertical component 180° away from the $\dot{V}$ vectors and

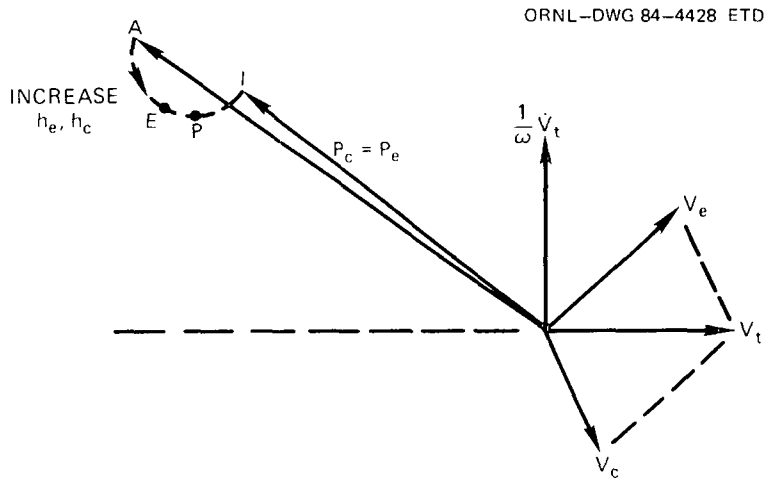

Fig. 4.12. Pressure and volume vectors for RE-1000 Nominal engine with transient heat transfer loss only.

represent a damping force. The product of this damping force with $\dot{V}$ produces a negative power or loss. For an engine, the pressure vectors lie in the second quadrant with upward vertical components in phase with $\dot{V}$. This represents a driving force, and positive work is produced from the engines.

2. In the analysis of the gas spring with sinusoidal motions, it has been shown that adiabatic springs produce a larger pressure swing than isothermal ones, but with the same phase. This is not the case for an engine working space. Although the trend for the pressure amplitude is similar for isothermal and adiabatic spaces, the two vectors do not coincide. In fact, the adiabatic pressure vector rotates counterclockwise away from the isothermal one, which leads to a loss in efficiency as described in Appendix B.

3. For the gas spring, the envelope traced by the pressure vector as h* varies is a semicircle. This is not true in the working space where the envelope is somewhat modified and becomes a pseudo-semicircle.

With reference to Fig. 4.12, two significant features of the engine performance, power output and efficiency, can be inferred. With respect to power output, the projection of the pressure vector onto the rate of change of total volume vector is proportional to the amount of work that the engine produces. Thus, adiabatic cylinders will generate substantially more power than isothermal cylinders because the vertical pressure

component is greater. The vector diagram can be used to explain the worst case lying between ideally isothermal and adiabatic cylinders. As h* increases, the head of the pressure vector travels along the pseudo-semicircle, and its component in the $\dot{V}_t$ direction first assumes a maximum at point A for the adiabatic cylinders, then decreases to a minimum at point P for the worst case, and then rises back to the isothermal limit at the point I. The vector diagram confirms the characteristics described previously.

Efficiency can be proven to depend on the phase angle between the pressure vector and the negative total volume vector (Appendix B). The angle is maximal for isothermal cylinders, representing the Carnot efficiency. As h* increases, the head of the pressure vector moves counterclockwise along the locus. The phase angle, and, hence, the efficiency, decreases until the worst case (point E), where the pressure vector is tangential to the curve, and then recovers back to the Carnot limit. The points P and E define the worst case for the power output and efficiency, respectively, and correspond to different h* values. The efficiency minimum is at a smaller h* than the power minimum, as discussed earlier.

4.2.3 Entropy production due to transient heat transfer

Transient heat transfer is an irreversible thermodynamic process that gives away heat at high temperatures and regains it at lower temperatures. The entropy change in the expansion space caused by this process has been defined in the second component of Eq. (2.29) and is repeated here:

$$\Delta\dot{S}_{TQe} = \frac{h_e\overline{A}_{se}\left(\overline{T}_e - T_e\right)}{T_e} \; . \tag{4.28}$$

The cyclic entropy production may be computed by integrating Eq. (4.28) over a cycle,

$$\overline{\Delta\dot{S}}_{TQe} = \frac{h_e\overline{A}_{se}}{2\pi} \int_0^{2\pi} \left(\frac{1}{\overline{T}_e^*} - 1\right) dt^* \; . \tag{4.29}$$

Substituting the solution for T_e^* from Eq. (3.33) into Eq. (4.29) gives

$$\overline{\Delta\dot{S}}_{TQe} = \frac{h_e\overline{A}_{se}}{2\pi} \int_0^{2\pi} \left(\frac{1}{1 + y_7 \sin t^* + y_8 \cos t^*} - 1 \right) dt^* \ . \tag{4.30}$$

This integration can be performed explicitly, leading to a closed-form solution

$$\overline{\Delta\dot{S}}_{TQe} = h_e\overline{A}_{se} \left(\frac{1}{\sqrt{1 - y_7^2 - y_8^2}} - 1 \right) \ . \tag{4.31}$$

Note that $(y_7^2 + y_8^2)$ represents the square of the relative temperature amplitude, and $(y_7^2 + y_8^2) < 1$ for small oscillations. Thus, the previous exact solution can be approximated by

$$\overline{\Delta\dot{S}}_{TQe} \simeq h_e\overline{A}_{se} \left[1 + \frac{1}{2} (y_7^2 + y_8^2) - 1 \right] \ , \tag{4.32}$$

or

$$\overline{\Delta\dot{S}}_{TQe} \simeq \frac{h_e\overline{A}_{se}}{2} \left(\frac{|T_e|}{\overline{T}_e} \right)^2 \ , \tag{4.33}$$

where

$$\frac{|T_e|}{\overline{T}_e} = \sqrt{y_7^2 + y_8^2} \ . \tag{4.34}$$

Equation (4.33) shows that the cyclic entropy production caused by the transient heat transfer in the expansion space of an engine is characterized by the product of the square of the relative temperature amplitude, with $h_e\overline{A}_{se}$ as the proportionality constant. The corresponding power loss [Eq. (2.24)] can be obtained if Eq. (4.33) is multiplied by $\overline{T}_{out}$, which represents the average temperature at which energy is

rejected:

$$\overline{\Delta \dot{W}}_{TQe} \simeq \frac{h_e \overline{A}_{se} \overline{T}_{out}}{2} \left(\frac{|T_e|}{\overline{T}_e} \right)^2 . \tag{4.35}$$

Suprisingly, eq. (4.35), for the expansion space of the engine, is similar in form to Eq. (4.27), for the simple gas spring. This is not coincidental because both are uniquely characterized by two key parameters: conductance (i.e., product of heat transfer coefficiency h and area A) and temperature amplitude. However, note that the temperature fluctuation in the expansion space of the engine is affected by the continuous mass movement in and out of the cylinder. This effect has been accounted for in the LHA analysis.

There is no transient heat transfer entropy production for either truly adiabatic or perfectly isothermal cylinders. For the adiabatic cylinders, no heat is exchanged with the walls although the amplitude of the temperature swing inside the cylinder reaches its maximum. For the isothermal cylinders, the reason for the absence of transient heat transfer loss differs. Here, there is absolutely no temperature oscillation although the conductance approaches infinity.

Similarly, the counterpart of those equations for the compression space can be derived:

$$\overline{\Delta \dot{S}}_{TQc} = h_c \overline{A}_{sc} \left(\frac{1}{\sqrt{1 - y_9^2 - y_{10}^2}} - 1 \right) , \tag{4.36}$$

representing the exact solution for the cyclic entropy change, and

$$\overline{\Delta \dot{S}}_{TQc} \simeq \frac{h_c \overline{A}_{sc}}{2} \left(\frac{|T_c|}{\overline{T}_c} \right)^2 \tag{4.37}$$

for the approximate solution.

The corresponding power loss over a cycle is

$$\overline{\Delta \dot{W}}_{TQc} \simeq \frac{h_c \overline{A}_{sc} \overline{T}_{out}}{2} \left(\frac{|T_c|}{\overline{T}_c} \right)^2 . \tag{4.38}$$

Finally, it can be stated that the total efficiency reduction [Eq. (2.23)] by transient heat transfer for an engine is

$$\Delta\eta_{THT} = (\overline{\Delta\dot{S}}_{TQe} + \overline{\Delta\dot{S}}_{TQc})\,\overline{T}_{out}/\overline{\dot{Q}}_{in} \quad . \tag{4.39}$$

4.3 Effect of Combined Adiabatic and Transient Heat Transfer Losses on Efficiency

So far, formulae for allocating losses due to the effects of mixing, external heat transfer irreversibility, and transient heat transfer have been derived and discussed, as a result of the Second-Law analysis. It remains to be shown how the theory is applicable to typical Stirling engines. Thus, calculations are performed by use of the reference engine (RE-1000 Nominal) to quantify efficiency reduction by individual and/or combined mechanisms over a wide range of heat transfer rates (with no other losses such as pressure drop and mass leakage losses).

The results (Fig. 4.13) are summarized in a composite plot to show the relative importance among individual loss mechanisms in relation to the overall. Remember that the effect of interactions between the adiabatic and transient heat transfer losses is fully taken into account by the LHA even though it remains possible to allocate the total loss between the individual mechanisms. The ordinate in Fig. 4.13 indicates the efficiency loss below the Carnot value in percentage points. The abscissa signifies the heat transfer coefficient between cylinder wall and gas in a log scale. At the operating condition of the RE-1000 Nominal engine, both heat transfer coefficients in the expansion and compression space are about equal and estimated by the authors to be near 1000 $W/(m^2 \cdot K)$.

Figure 4.13 consists of four curves. Curves 1 to 3 represent, respectively, the efficiency loss allocation due to transient heat transfer only, external heat transfer irreversibility only, and mixing only. Curve 4 represents the total of curves 1 to 3.

Curve 1 is a bell-shaped curve that represents the efficiency loss due to the effects of transient heat transfer alone. This curve is

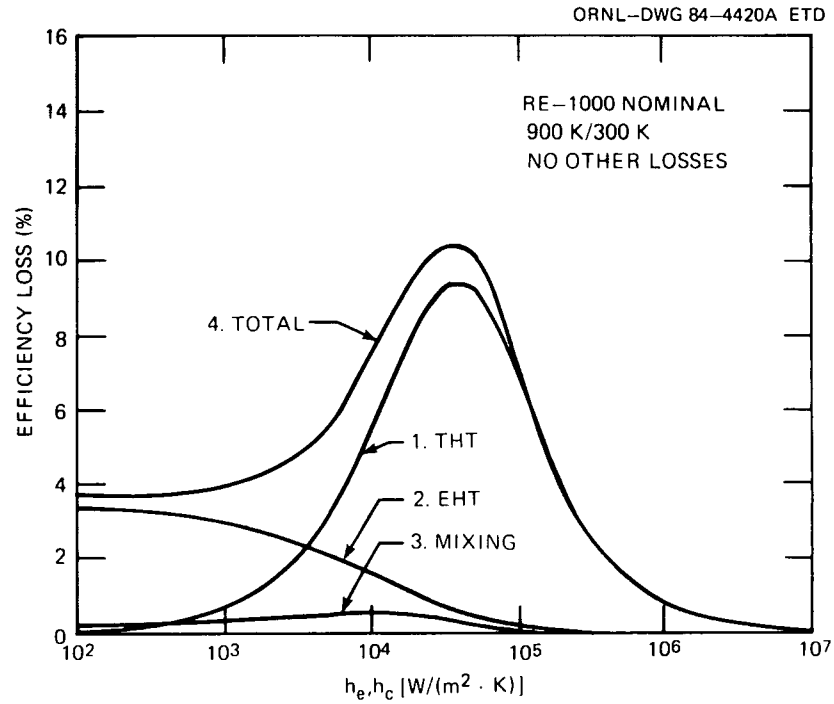

Fig. 4.13. Efficiency loss allocation vs cylinder heat transfer.

produced by a three-step calculation:

1. calculate cyclic entropy change in the expansion space by Eq. (4.31),
2. calculate cyclic entropy change in the compression space by Eq. (4.36), and
3. calculate the efficiency loss due to transient heat transfer only by Eq. (4.39).

As expected, there is no transient heat transfer loss for perfectly adiabatic or perfectly isothermal cylinders, but there exists a worst case for semiadiabatic cylinders with finite heat transfer rates. The worst case occurs right at the line of symmetry of the bell-shaped curve because it represents the maximum efficiency loss. For this particular example, the worst case occurs at a cylinder-to-gas heat transfer coefficient of 40,000 W/(m^2•K) in both spaces and produces a very significant efficiency loss of about 9.5 percentage points. At 1000 W/(m^2•K), close to the value estimated for the real engine, the loss is 0.7 percentage points.

Curve 2 represents the effect of external heat transfer irreversibility. To generate the curve, a string of calculations is required:

First, in the expansion space

1. calculate cyclic entropy change due to heater heat transfer by Eq. (4.2),
2. calculate cyclic entropy change due to the average component of the wall heat transfer by Eq. (4.9), and
3. calculate the average temperature at which gas enters the system by Eq. (4.11).

Second, in the compression space

1. calculate cyclic entropy change due to cooler heat transfer by Eq. (4.5),
2. calculate cyclic entropy change due to the average component of the wall heat transfer by Eq. (4.10), and
3. calculate the average temperature at which gas leaves the system by Eq. (4.12).

Third, calculate the efficiency loss due to external heat transfer irreversibility by Eq. (4.13).

The efficiency loss revealed by these calculations attains its maximum at the adiabatic limit, then decreases gradually as the heat transfer coefficient increases, and finally vanishes at the isothermal extreme.

Curve 3 denotes the effect of mixing inside cylinders. Like curve 1, this curve results from a three-step calculation:

1. calculate cyclic entropy change in the expansion space by Eq. (4.17),
2. calculate cyclic entropy change in the compression space by Eq. (4.18), and
3. calculate the efficiency loss due to mixing by Eq. (4.19).

The behavior of the efficiency loss as a result of mixing is rather intriguing. It has a finite value near the adiabatic limit, then rises to a maximum as the heat transfer coefficient is increased. After the maximum, the mixing loss declines slowly and eventually diminishes when it approaches the isothermal extreme, where no mixing should exist. The

reason for this maximum can be attributed to the complex effects of temperature overshoot in the expansion space and temperature undershoot in the compression space over different parts of the cycle. The mixing loss is small over the entire heat transfer range, which may be somewhat of a surprise because the loss due to adiabatic cylinders is commonly called mixing loss. Based on the Second-Law analysis, the "adiabatic loss" is the sum of the mixing and external heat transfer (EHT) losses; and most of the adiabatic loss is due to heat transfer rather than mixing irreversibilities.

Curve 4, the outermost envelope, represents the total sum of the individual loss mechanisms and gives the overall efficiency loss.

In summary, the following general conclusions may be stated:

1. the effects of external heat transfer irreversibility dominate in the range of small heat transfer coefficients,
2. the effects of transient heat transfer dominate in the range of intermediate heat transfer coefficients, and
3. the effects of mixing remain small in magnitude through the whole spectrum of heat transfer coefficients and, thus, are the least important.

4.4 Pressure Drop Loss

4.4.1 Effects of pressure drop on engine performance

Up to this point, all the examples have assumed a common pressure in the engine. In reality, however, an oscillating pressure difference exists between the compression and expansion spaces. This pressure difference is caused by fluid friction and acceleration as the working gas flows through the heater, cooler, and regenerator.

The effects of pressure drop on engine performance are shown in Fig. 4.14 as a function of the pressure drop coefficients. The LHA predictions are for the RE-1000 Nominal configuration with adiabatic cylinders and no other losses. The range of pressure drop coefficients is selected to cover the range of positive engine power output. With zero pressure

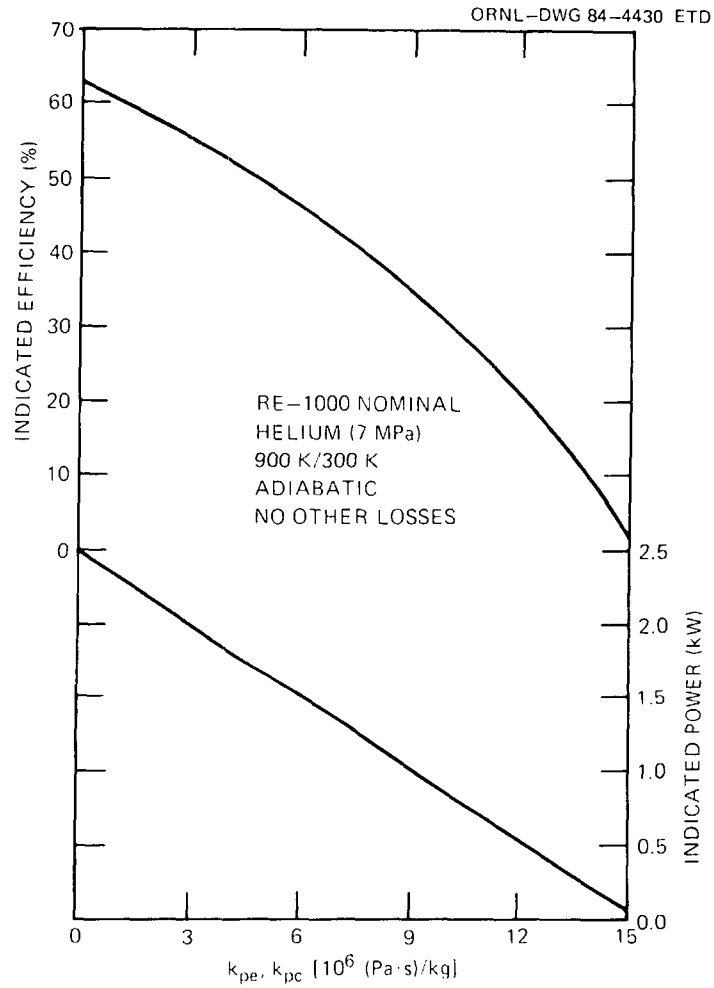

Fig. 4.14. Power output and efficiency vs pressure drop coefficients for RE-1000 Nominal engine.

drop, the performance of the engine is equal to that of the ideal adiabatic engine. As pressure drop increases, both power output and efficiency fall until they both reach zero. However, power output shows a more linear relationship than efficiency.

The effect of pressure drop is also shown in a vector diagram in Fig. 4.15. The pressure vector labeled $P_e = P_c$, represents uniform pressure and is found where there is no pressure drop. As the pressure drop coefficient increases, the pressure oscillations in the expansion and compression spaces are no longer identical. The expansion-space pressure amplitude becomes smaller, and the vector rotates clockwise. Concurrently, the compression-space vector becomes larger and rotates

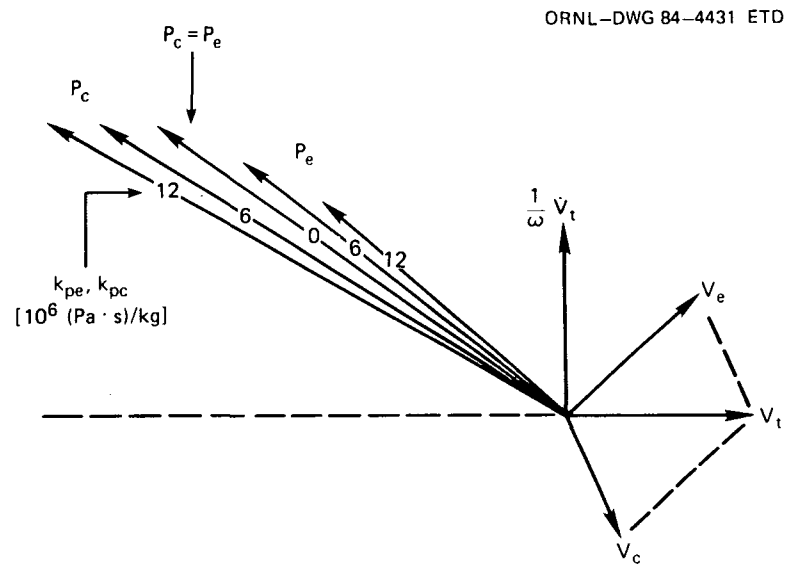

Fig. 4.15. Pressure and volume vectors for RE-1000 Nominal engine with pressure drop loss only.

counterclockwise. The outermost pair of nonuniform pressure vectors [$k_{pe} = k_{pc} = 12 \times 10^{-6}$ (Pa•s)/kg] shown in the diagram corresponds to a case where the power output is about 0.5 kW.

The vector difference ($P_c - P_e$) between the two nonuniform pressure vectors represents the amplitude and phase angle of the oscillating pressure drop across the heat exchanger components. This vector is displayed in Fig. 4.16 to show its relationship with three other vectors: displacer position, displacer velocity, and expansion volume. Recall that the displacer position vector is opposed to the expansion volume vector because they are out of phase by 180° (i.e., when the volume is at a maximum, the displacer position is at a minimum). Furthermore, the displacer velocity (symbolically represented by $\dot{X}_d$) is ahead of the displacer position by 90° for harmonic motion.

From the vector diagram, some key thermodynamic parameters can be identified:

1. Expansion-space work integral
   $= \oint P_e dV_e$
   = heat addition
   = component of P_e that lies in the direction of $\dot{V}_e$.

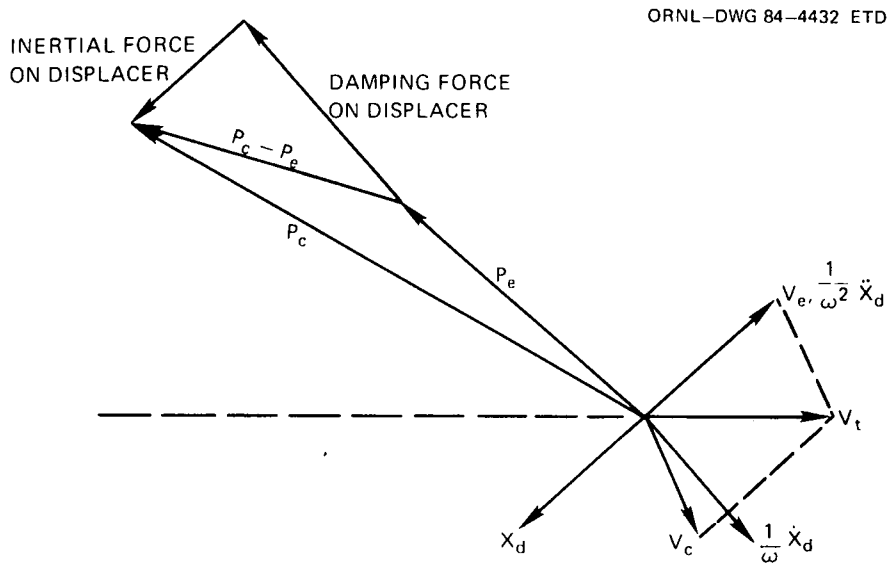

Fig. 4.16. Damping and inertial components of pressure drop on displacer.

As pressure drop increases, the positive work component decreases monotonically. Consequently, the area of the work diagram in the expansion space (clockwise) is reduced.

2. Compression-space work integral
   $= \oint P_c dV_c$
   = heat rejection
   = component of P_c that lies in the direction of $\dot{\overline{V}}_c$.

As pressure drop increases, the negative work component increases. Hence, the area of the work diagram in the compression space (counterclockwise) is enlarged.

3. Pressure drop loss
   $= (A_d - A_r) \oint (P_c - P_e)\, dX_d$
   = displacer loss that must be balanced by a displacer drive force
   = component of $(P_c - P_e)$ that lies in $\dot{X}_d$ direction.

The pressure drop vector $(P_c - P_e)$ actually has two components. One component lies in the $-\dot{X}_d$ direction. This component acts like a damper or dashpot. The other component lies in the X_d (or $-\ddot{X}_d$) direction and acts like an inertial force or added mass.

4.4.2 Entropy production due to pressure drop

Mass flowing across a pressure differential is an irreversible thermodynamic process. In the present study, pressure drop through the heat exchangers is represented by two throttling processes: one between the expansion and dead volumes, the other between the compression and dead volumes. During a throttling process the enthalpy remains unchanged, and for an ideal gas, the temperature remains unchanged as well. The applicable formula for entropy production is Eq. (2.38), which is repeated here,

$$\Delta\bar{\dot{S}} = \frac{R}{2\pi} \int_0^{2\pi} \left(-\frac{dm}{dt}\right) \ln\left(\frac{P_{final}}{P_{initial}}\right) dt^* \ . \tag{4.40}$$

Therefore, the entropy production due to pressure drop between the expansion and dead volumes becomes

$$\overline{\Delta\dot{S}}_{PDe} = R\bar{m}_w f \int_0^{2\pi} \left(\frac{\bar{m}_e}{\bar{m}_w}\right) \frac{dm_e^*}{dt^*} \ln\left(\frac{P_d^*}{P_e^*}\right) dt^* \ , \tag{4.41}$$

and between the compression and dead volumes

$$\overline{\Delta\dot{S}}_{PDc} = R\bar{m}_w f \int_0^{2\pi} \left(\frac{\bar{m}_e}{\bar{m}_w} \frac{dm_e^*}{dt^*} + \frac{\bar{m}_d}{\bar{m}_w} \frac{dm_d^*}{dt^*}\right) \ln\left(\frac{P_c^*}{P_d^*}\right) dt^* \ . \tag{4.42}$$

It is interesting to observe that the magnitude of the entropy generation depends on the operating frequency as well as the mass-weighted pressure drop between the initial and final states; the higher the frequency and pressure drop, the larger the entropy production. Also, note that in Eq. (4.42) the total mass flow between the compression space and the dead volume is the combined rate of change of mass inventory in the expansion space and the dead volume [i.e., $d/dt\ (m_e + m_d)$] and not just the mass inventory in the dead volume (i.e., dm_d/dt).

The total pressure-drop-induced entropy production within the engine thus equals the sum of these two components:

$$\overline{\Delta \dot{S}}_{\Delta P} = \overline{\Delta \dot{S}}_{PDe} + \overline{\Delta \dot{S}}_{PDc} \ . \tag{4.43}$$

4.5 Mass Leakage Loss

4.5.1 Gas spring with sinusoidal motions

Isothermal gas springs with seal leakage provide an elegant closed-form solution as shown in Appendix A; therefore, the effects of mass leakage can be illustrated analytically. Consider a gas spring that undergoes harmonic motion with only a sine component as expressed by Eq. (4.20). Under such conditions, the pressure wave solution for an isothermal spring with seal leakage [Eq. (A.30)] simplifies to:

$$P^*_s = 1 - |V^*_s| \left(\frac{1}{1 + k^{*2}_{ms}} \sin t^* + \frac{k^*_{ms}}{1 + k^{*2}_{ms}} \cos t^* \right) , \tag{4.44}$$

where the first and second terms, respectively, represent the mean pressure and the fluctuating component. The fluctuating pressure wave, in general, consists of sine as well as cosine components. It is this fluctuating pressure wave that contains interesting information on the mass leakage loss. This will be studied further by use of a vector diagram.

In the vector diagram (Fig. 4.17), a family of pressure vectors emanating from the origin will rotate counterclockwise as the mass leakage coefficient increases. The head of the normalized pressure vector traces a semicircle over the whole spectrum of coefficients. A normalized pressure vector is defined as the pressure vector divided by the dimensionless volume amplitude or more specifically, $P^*_s/|V^*_s|$.

The two end points of the semicircle will be established first. At the limit of a perfect seal ($k^*_{ms} = 0$), the cosine term of Eq. (4.44) vanishes and only the sine term survives; the normalized pressure vector is in the negative sine direction with a magnitude of 1 (left-end point), which represents the maximum pressure excursion as an isothermal gas

ORNL–DWG 84–4433 ETD

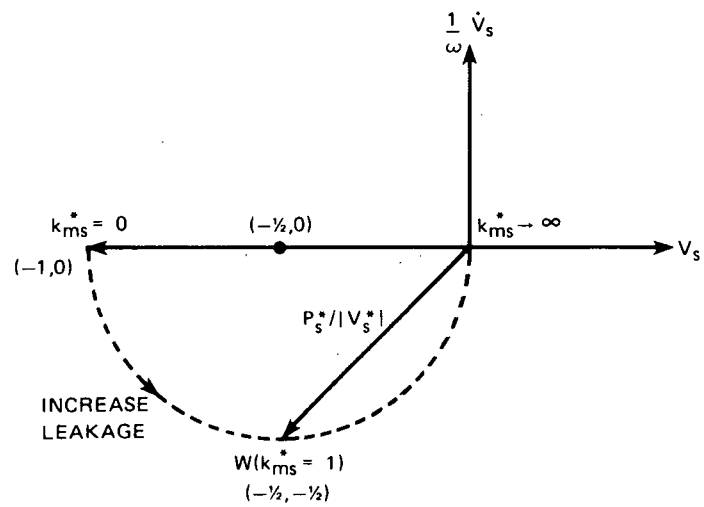

Fig. 4.17. Pressure and volume vectors for isothermal gas spring with seal leakage.

spring. For such a case, there is no power loss because the pressure vector is perpendicular to the $\dot{V}_s$ vector. At the other extreme where there is no seal ($k^*_{ms} \to \infty$), both terms of Eq. (4.44) vanish. Thus, the pressure vector degenerates to the point of origin (right-end point) where the pressure amplitude is zero. Such a case represents a constant pressure resulting from pressure equalization between the cylinder and buffer spaces (see Fig. A.1). Again, there is no power loss because of no pressure variation.

A gas spring with intermediate mass leakage shows a worst case labeled as W. The worst case occurs where the normalized pressure vector attains a maximum component that lies in the negative $\dot{V}_s$ direction, therefore, leading to a maximum power loss. The coordinates of the worst case are shown to be (−1/2, −1/2) when the mass leakage coefficient assumes a value of unity (i.e., $k^*_{ms} = 1$).

4.5.2 Effects of mass leakage on engine performance

In the formulation, leakage is allowed to occur between the working space and the buffer space where a state of constant pressure and temperature is maintained. The change of the working space mass is further assumed to be in linear proportion to the pressure difference between the

two spaces. The magnitude of the mass change is controlled by a leakage coefficient.

Engine performance can be very markedly affected by leakage. The extent has been quantified by varying the leakage coefficient between zero and a value that results in no net power. The results predicted by the LHA method are shown in Fig. 4.18. Again, the predictions are for the RE-1000 Nominal configuration with adiabatic cylinders and no other losses.

The vector representation of the leakage loss is shown in Fig. 4.19. Some similarities to the isothermal gas spring with leakage are apparent. The locus of the heads of the pressure vectors corresponding to various leak coefficients is nearly semicircular. As the leakage rises, the

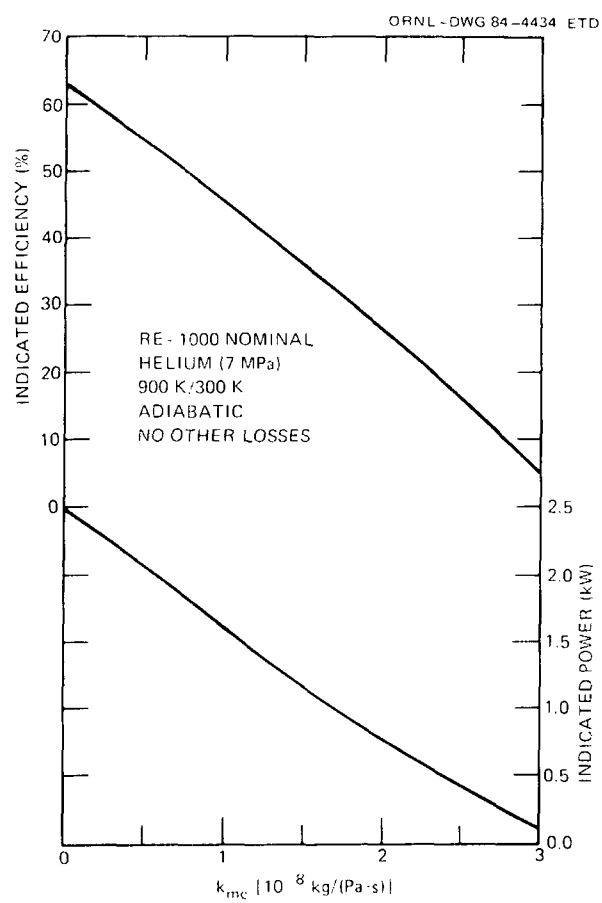

Fig. 4.18. Power output and efficiency vs mass leakage coefficients for RE-1000 Nominal engine.

ORNL–DWG 84–4435 ETD

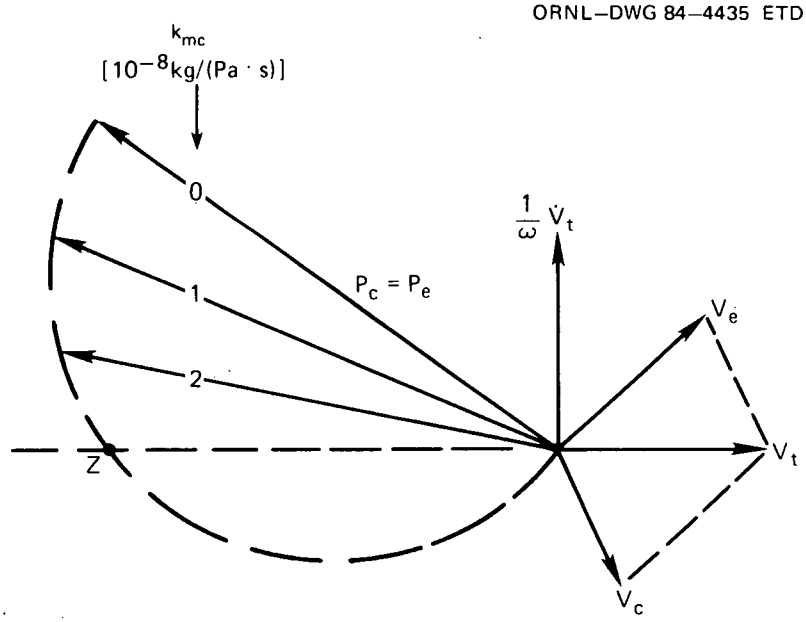

Fig. 4.19. Pressure and volume vectors for RE-1000 Nominal engine with mass leakage only.

pressure vectors rotate counterclockwise, and the work component falls monotonically and vanishes at the point Z, where the pressure vector is normal to the $\dot{V}_t$ vector. Beyond that point, power is needed to drive the engine because of a negative work component. Concurrently, the phase angle that is proportional to efficiency, between the pressure vector and negative total volume vector, shrinks as does the efficiency. Moreover, that phase angle changes from positive to negative as the pressure vector crosses the zero net power point. This illustration confirms the performance predictions described previously. If the pressure vector lags the negative V_t vector, power is produced from an engine; on the other hand, if the pressure vector leads the negative V_t vector, power is absorbed.

4.5.3 Entropy production due to mass leakage

Mass leakage between the compression space (where pressure fluctuates) and the buffer space (where pressure remains constant) is another irreversible thermodynamic process. Such a process is irreversible because mass is lost at a high pressure and regained at low pressure. The cyclic entropy change associated with this process presents no difference

in principle from that of pressure drop. Thus,

$$\overline{\Delta\dot{S}}_{MLc} = R\bar{m}_w f \int_0^{2\pi} \left(\frac{\bar{m}_e}{\bar{m}_w} \frac{dm_e^*}{dt^*} + \frac{\bar{m}_d}{\bar{m}_w} \frac{dm_d^*}{dt^*} + \frac{\bar{m}_c}{\bar{m}_w} \frac{dm_c^*}{dt^*} \right) \ln \left(\frac{1}{P_c^*} \right) dt^* \ . \qquad (4.45)$$

4.6 Coupling of Losses

Until now, the transient heat transfer, pressure drop, and leakage losses have been examined independently. The Second Law of Thermodynamics provides a rational means to allocate the individual loss mechanisms when two or more of the losses are coupled together. Thus, the Second-Law analysis, coupled with the LHA method, has been applied directly to the RE-1000 Nominal configuration for various loss combinations. The loss coefficients for 12 cases studied are listed in Table 4.2. In the table, the rate constants for both the pressure drop and seal leakage are chosen to exaggerate the coupling effects beyond those to be expected in a well-designed and -constructed engine. The highlights of the results are summarized in Tables 4.3 and 4.4; one shows the efficiency loss allocations [Eqs. (2.19) and (2.27)], whereas the other shows the power losses [Eq. (2.24)].

Table 4.2. Loss coefficients for coupling studies

Cylinder heat transfer	Heat transfer coefficient, $h_e = h_c$ [W/(m^2·K)]	Pressure drop, $k_{pe} = k_{pc}$ [(Pa·s)/kg]	Seal leakage, k_{mc} [kg/(Pa·s)]
Adiabatic	0	0	0
	0	0	1.0×10^{-8}
	0	6.7×10^6	0
	0	6.7×10^6	1.0×10^{-8}
Semiadiabatic	62,500	0	0
	62,500	0	1.0×10^{-8}
	62,500	6.7×10^6	0
	62,500	6.7×10^6	1.0×10^{-8}
Isothermal	3×10^8	0	0
	3×10^8	0	1.0×10^{-8}
	3×10^8	6.7×10^6	0
	3×10^8	6.7×10^6	1.0×10^{-8}

Table 4.3. Coupled efficiency loss for RE-1000 Nominal engine

Cylinder heat transfer	Carnot efficiency (%)	Adiabatic		THT	Pressure drop	Seal leakage
		EHT[a]	Mixing			
Adiabatic	66.67	−3.45	−0.25	0.00	0.00	0.00
	66.67	−3.51	−0.21	0.00	0.00	−17.72
	66.67	−3.37	−0.29	0.00	−19.40	0.00
	66.67	−3.34	−0.23	0.00	−16.90	−26.18
Semiadiabatic	66.67	−0.34	−0.18	−8.67	0.00	0.00
	66.67	−0.32	−0.19	−8.94	0.00	−14.01
	66.67	−0.32	−0.26	−13.12	−20.02	0.00
	66.67	−0.30	−0.26	−13.53	−18.17	−22.22
Isothermal	66.67	0.00	0.00	0.00	0.00	0.00
	66.67	0.00	0.00	0.00	0.00	−12.49
	66.67	0.00	0.00	0.00	−22.50	0.00
	66.67	0.00	0.00	0.00	−19.83	−20.40

[a]External heat transfer irreversibility consists of four heat transfer components: heater, cooler, average expansion cylinder, and average compression cylinder.

Table 4.4. Coupled power loss for RE-1000 Nominal engine

Cylinder heat transfer	Reference power[a] (W)	Adiabatic		THT	Pressure drop	Seal leakage
		EHT	Mixing			
Adiabatic	2636.9	−136.3	−9.9	0.0	0.0	0.0
	2363.7	−124.4	−7.4	0.0	0.0	−628.4
	2137.9	−108.1	−9.3	0.0	−622.2	0.0
	1867.6	−93.4	−6.5	0.0	−473.4	−733.5
Semiadiabatic	2118.9	−10.9	−5.8	−275.0	0.0	0.0
	1904.2	−9.2	−5.3	−255.4	0.0	−400.3
	1622.9	−7.7	−6.3	−319.5	−487.3	0.0
	1419.0	−6.4	−5.6	−288.0	−386.7	−472.9
Isothermal	2027.0	0.0	0.0	−0.1	0.0	0.0
	1914.4	0.0	0.0	−0.1	0.0	−358.7
	1507.0	0.0	0.0	−0.1	−508.6	0.0
	1412.3	0.0	0.0	−0.1	−420.2	−432.2

[a]Reference power is defined as the heat input multiplied by the Carnot efficiency.

The tables reveal some interesting loss interactions. First of all, pressure drop appears to have a significant effect on the other losses. Compare the cases that have seal leakage and no pressure drop with the cases that have both seal leakage and pressure drop. An increased pressure drop causes an increase in the seal leakage losses, both in efficiency and power. These effects hold true for the adiabatic, semiadiabatic, and isothermal cases. The physical explanation is that pressure drop causes the amplitude of the pressure wave in the compression space to increase (see Fig. 4.15). As a result, a larger pressure difference exists across the piston seal, which leads to a larger leakage loss. In addition, an increased pressure drop tends to increase the transient heat transfer loss for those cylinders that are semiadiabatic.

Secondly, seal leakage appears to have a reverse effect on pressure drop losses. Compare the cases that have pressure drop and no seal leakage with the cases that have both. An increased seal leakage causes a reduction in the pressure drop loss. However, it is difficult to infer a physical reason. In fact, all of the trends discussed so far may not hold true for all Stirling machines. Nevertheless, for the RE-1000 Nominal configuration presented here, the results show rather convincingly that the losses do seem to couple in a highly complex manner.

Some final comments about the Second-Law analysis and loss allocation are in order. Efficiency losses are subtracted from the Carnot efficiency to arrive at an overall efficiency. The Carnot value depends only on the heater and cooler temperatures and represents the maximum efficiency that any engine can achieve. The 12 cases shown in Table 4.3 all have the same Carnot value. On the other hand, power losses are subtracted from a reference power output that is defined as the heat input to the engine multiplied by the Carnot efficiency. The reference powers shown in Table 4.4 vary from case to case because the engine heat inputs, which are equal to the expansion-space pressure-volume integrals, are different. Thus, a comparison of power losses from case to case might be less meaningful than an efficiency loss comparison because the reference power outputs vary, whereas the reference efficiencies remain the same. This should certainly be remembered when second-order, or decoupled, Stirling machine analyses are undertaken.

5. CONCLUSIONS

The LHA has proved to be a simple but very effective method for Stirling cycle engine analyses. The present theoretical formulation, which focuses on thermodynamic development, retains three control volumes (an expansion space, a compression space, and a dead volume made up of the three heat exchanger components), while encompassing four of the most significant loss mechanisms (adiabatic effects, transient heat transfer loss, pressure drop loss, and mass leakage loss). The simplicity of LHA is a consequence of the underlying assumptions of pressure linearization and harmonically oscillating state variables. The effectiveness of LHA refers to its ability to provide a better understanding of loss mechanisms while offering a stable, efficient, accurate, and economical solution to the governing equations.

LHA provides the opportunity to obtain a better physical understanding of loss mechanisms than do nodal or numerical methods. This is a direct consequence of the semi-closed-form solution. In some cases, relations between causes and effects can be expressed analytically, leading to a better feel for the underlying physical processes. Also, the controlling variables that undergo harmonic variations can be directly and effectively represented in vector diagrams to provide still further insight. Thus, the LHA can be used as an analytical tool to explore new phenomena, especially in free-piston Stirling engine applications.

Even with its simplicity, LHA gives rather accurate solutions to the equations. The arithmetical accuracy has been checked independently by a well-established numerical method, the CSMP, which does not assume linear pressure terms and harmonic variables. The cross comparisons were made among key thermodynamic parameters such as efficiency, power output, heat input, heat output, and mean gas temperatures in the expansion and compression spaces, at different loss levels over a wide range of loss rates. The general agreement is satisfactory; the worst discrepancy in heat input and heat output at a compression ratio of 1.89 is 1.1% and 2.2%, respectively.

LHA offers a stable solution and is not subject to the computational instabilities that are possible with numerical integration methods. This stability comes from the harmonic representation of the state variables and the imposed conditions for a steady state solution.

Based on LHA predictions, a Second-Law analysis has been used to quantify how individual loss mechanisms contribute to the total loss when two or more losses are acting simultaneously. The allocation of losses is based on entropy production. Three irreversible thermodynamic processes that occur in typical Stirling engines were identified: heat transfer across a finite temperature difference, mixing gases at two temperatures, and mass flow over a pressure drop. All these processes lead to entropy production and efficiency and power losses. The analysis shows that (1) efficiency losses are computed with respect to the Carnot efficiency as the reference value, and (2) the reference power is the heat input to the engine multiplied by the Carnot efficiency; individual power losses are quantified with respect to this reference value.

Some highlights on the loss mechanisms are summarized below:

1. Adiabatic effects
   a. are caused by external heat transfer and mixing irreversibilities. Mixing occurs when the working gas enters the expansion and compression spaces. Irreversibilities caused by external heat transfer consist of four components: heater, cooler, expansion-cylinder, and compression-cylinder average heat transfer. The heater (cooler) heat transfer irreversibility occurs when the gas enters the heater (cooler). For the RE-1000 Nominal free-piston engine, the mixing is relatively insignificant compared with the external heat transfer irreversibility by one order of magnitude.
   b. require a consideration of the coupled effects of mean temperature shifts, mixing loss, and transient heat transfer loss.
   c. dominate efficiency reduction in cylinders with poor heat transfer.
   d. cause the pressure vector to rotate counterclockwise away from that of the isothermal vector (Carnot efficiency) so that the

phase angle between the pressure and the negative total volume vectors decreases, leading to an efficiency reduction.

e. depend strongly upon the compression ratio; the larger the ratio, the larger the efficiency reduction. For the RE-1000 Modified engine with a ratio of 1.8:1, the reduction is about 10 percentage points.

f. depend strongly upon the temperature difference between heater and cooler. For low temperature difference machines, such as heat pumps, the adiabatic effect becomes very significant.

g. cause the mean gas temperature to shift downwards in the expansion and upwards in the compression space; the larger the adiabatic effects, the larger the shifts.

2. Transient heat transfer loss

a. is a loss because giving up heat at a high temperature and regaining it at a low temperature is an irreversible thermodynamic process.

b. reduces adiabatic loss effects.

c. is not present in ideally adiabatic or ideally isothermal cylinders but shows worst cases for both power and efficiency at some intermediate points between these two extremes.

d. causes an entropy production that is uniquely characterized by the square of the relative temperature amplitudes in the respective spaces.

e. dominates efficiency reduction in the intermediate cylinder heat transfer ranges.

f. causes the pressure vector to rotate counterclockwise away from the adiabatic vector until reaching the worst efficiency point, then to rotate clockwise toward the isothermal vector (Carnot efficiency) so that the phase angle between the pressure vector and the negative total volume vector first decreases, then increases, leading to an efficiency reduction below the Carnot value.

3. Pressure drop loss
   a. results from mass flowing through a pressure drop — an irreversible thermodynamic process.
   b. decreases the pressure amplitude in the expansion space and increases it in the compression space.
   c. causes the expansion-space pressure vector to rotate clockwise and concurrently causes the compression-space pressure vector to rotate counterclockwise from the uniform (common) pressure vector.
4. Mass leakage loss
   a. results from mass lost at high pressure and regained at low pressure — an irreversible thermodynamic process.
   b. causes the pressure vector to rotate counterclockwise away from the lossless (perfect seal) pressure vector so that the phase angle between the pressure and the negative total volume vectors decreases, leading to an efficiency reduction.

REFERENCES

1. F. H. Speckhart and W. L. Green, *A Guide to Using CSMP — The Continuous System Modeling Program*, Prentice-Hall, Inc., Englewood Cliffs, New Jersey, 1976.

2. I. Urieli and D. M. Berchowitz, *Stirling Cycle Engine Analysis*, Adam Hilger, Ltd., Bristol, 1984.

3. T. Finkelstein, "Generalized Thermodynamic Analysis of Stirling Engines," SAE Paper No. 118B, Society of Automotive Engineers, January 1960.

4. E. B. Qvale, *An Analytical Model of Stirling-Type Engine*, Ph.D. thesis, Massachusetts Institute of Technology, Cambridge, 1967.

5. P. A. Rios, *An Analytical and Experimental Investigation of the Stirling Cycle*, Ph.D. thesis, Massachusetts Institute of Technology, Cambridge, 1969.

6. W. R. Martini, *Stirling Engine Design Manual*, 2d ed., DOE/NASA 3094-1; NASA CR-168088, January 1983.

7. N. C. J. Chen and F. P. Griffin, *A Review of Stirling Engine Mathematical Models*, ORNL/CON-135, Union Carbide Corp. Nuclear Div., Oak Ridge Natl. Lab., August 1983.

8. H. Fokker and J. A. M. van Eekelen, "The Description of the Stirling Cycle in a Vector Diagram," pp. 1739—45 in *Proceedings of the 13th IECEC*, Paper No. 789112, 1978.

9. J. S. Rauch, "Harmonic Analysis of Stirling Engine Thermodynamics," pp. 1696—1700 in *Proceedings of the 15th IECEC*, Paper No. 809335, 1980.

10. C. J. Rallis and I. Urieli, *Optimum Compression Ratios of Stirling Cycle Machines*, Report No. 68, School of Mechanical Engineering, University of the Witwatersrand, Johannesburg, South Africa, June 1976.

11. C. D. West, *The Stirling Engine with One Adiabatic Cylinder*, ORNL/TM-8022, Union Carbide Corp. Nuclear Div., Oak Ridge Natl. Lab., March 1982.

12. E. H. Cooke-Yarborough, *A Proposal for a Heat-Powered Non-Rotating Electrical Alternator*, Harwell AERE-M1881, 1967.

13. J. S. Rauch, "Steady State Analysis of Free-Piston Stirling Engine Dynamics," pp. 961—65 in *Proceedings of the 10th IECEC*, Paper No. 759144, 1975.

14. T. J. Marusak and W. S. Chiu, "The Matching of a Free Piston Stirling Engine Coupled with a Free Piston Linear Compressor for a Heat Pump Application," pp. 1820—25 in *Proceedings of the 13th IECEC*, Paper No. 789272, 1978.

15. D. M. Berchowitz and G. F. Wyatt-Mair, "Closed-Form Solutions for a Coupled Ideal Analysis of Free-Piston Stirling Engines," pp. 1114—19 in *Proceedings of the 14th IECEC*, Paper No. 799241, 1979.

16. L. F. Goldberg, "A State Space Analysis of a Symmetrical Compounded Free Piston Stirling Engine," pp. 2251—57 in *Proceedings of the 15th IECEC*, Paper No. 809450, 1980.

17. R. Vincent, W. Rifkin, and G. Benson, "Analysis and Design of Free-Piston Stirling Engines — Thermodynamics and Dynamics," pp. 1686—1711 in *Proceedings of the 15th IECEC*, Paper No. 809334, 1980.

18. C. D. West, "Dynamic Analysis of the Fluidyne," pp. 779—84 in *Proceedings of the 18th IECEC*, Paper No. 839126, 1983.

19. D. R. Gedeon, "The Optimization of Stirling Cycle Machines," pp. 1784—90 in *Proceedings of the 13th IECEC*, Paper No. 789193, 1978.

20. J. E. Giansante, *A Free Piston Stirling Engine Performance Code*, 81TR17, prepared for NASA-Lewis by Mechanical Technology, Inc., November 1980.

21. General Electric, *Development and Demonstration of a Stirling/Rankine Heat Activated Heat Pump*, GE Document No. 83-AEP-004 vol. 1, 1984.

22. J. S. Rauch, "Harmonic Analysis of Stirling-Cycle Performance: A Comparison with Test Data," to be published in *Proceedings of the 19th IECEC*, 1984.

23. J. Schreiber, *Testing and Performance Characteristics of a 1-kW Free Piston Engine*, NASA TM-8299, April 1983.

24. J. L. Crowley, *Efficiency Terms for Stirling Engine Systems*, ORNL/CON-131, Union Carbide Corp. Nuclear Div., Oak Ridge Natl. Lab., June 1983.

25. G. J. Van Wylen and R. E. Sonntag, *Fundamentals of Classical Thermodynamics*, 2d ed., John Wiley and Sons, Inc., New York, 1973, p. 373.

26. R. D. Banduric and N. C. J. Chen, *Nonlinear Analysis of Stirling Engine Thermodynamics*, ORNL/CON-154, Martin Marietta Energy Systems, Inc., Oak Ridge Natl. Lab., June 1984.

27. G. Walker, *Stirling Engines*, Clarendon Press, Oxford, 1980, pp. 254—86.

Appendix A

GAS SPRING ANALYSIS

As a proof of principle, the LHA procedure has been applied to a gas spring. There are two reasons for this choice: first, to provide a better understanding of loss mechanisms and second, to provide necessary information for free-piston Stirling engine dynamic analysis. A gas spring system is simpler than an engine, yet it experiences some significant loss mechanisms similar to those occurring in engines. When compared with an engine, which is characterized by two spaces (expansion and compression), two temperature levels (source and sink), and the potential for producing work, the attributes of a gas spring include a single space, a single temperature, and no power production. However, a gas spring does show a transient heat transfer loss and mass leakage.

Consider a typical gas spring as shown in Fig. A.1, in which a piston separating two volumes undergoes a cyclic motion. The space enclosed by the cylinder and the moving piston is referred to as the gas spring, whereas the space above the piston with an open end is the buffer space. The buffer space is maintained at a constant pressure (e.g., the average

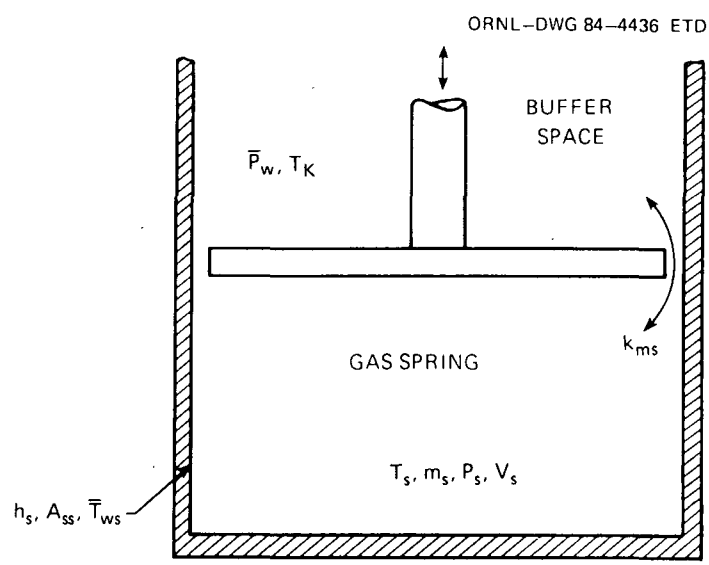

Fig. A.1. Schematic of gas spring.

system pressure $\overline{P}_w$) and a constant temperature (the cooler temperature T_K). This is true because the effective volume of the buffer space is very large in comparison with piston-swept volume.

The state of the gas spring is completely defined by two variables: temperature T_s and mass m_s, if the volume variation V_s is prescribed. Solving for these two variables requires two governing equations, which are the mass and energy conservation equations. They may be written in dimensionless forms similar to those used in the engine formulation:

$$\frac{dm_s^*}{dt^*} = k_{ms}^* \left(1 - m_s^* - T_s^* + V_s^*\right) , \tag{A.1}$$

$$\frac{d(m_s^* T_s^*)}{dt^*} + (\gamma - 1)\left(m_s^* + T_s^* - V_s^*\right) \frac{dV_s^*}{dt^*}$$

$$= \gamma T_{s\ flux}^* \frac{dm_s^*}{dt^*} + h_s^* \left(\overline{T}_{ws}^* - T_s^*\right) , \tag{A.2}$$

where

$$T_{s\ flux}^* = \begin{Bmatrix} T_K^*, \text{ if } dm_s^* > 0 \\ T_s^*, \text{ if } dm_s^* < 0 \end{Bmatrix} . \tag{A.3}$$

The meanings of each term and variable in Eqs. (A.1)—(A.3) remain the same as defined in the engine formulation except with a subscript s for gas spring.

Note that in the energy equation, Eq. (A.2), there exists an enthalpy flux discontinuity. The discontinuity arises from the alternating mass flow into and out of the cylinder, which, in turn, is caused by an oscillating pressure through an imperfect seal between the cylinder and the piston.

Since only a steady state solution is pursued, harmonic oscillations of all variables, dependent and independent, will be considered:

$$m_s^* = 1 + y_{s1} \sin t^* + y_{s2} \cos t^* , \tag{A.4}$$

$$T_s^* = 1 + y_{s3} \sin t^* + y_{s4} \cos t^* , \tag{A.5}$$

$$V_s^* = 1 + y_{s5} \sin t^* + y_{s6} \cos t^* . \tag{A.6}$$

It should be pointed out that, for generality, the volume variation is assumed to be composed of sine and cosine components even though the coefficients y_{s5} and y_{s6} are specified. Finally, the linearized pressure wave can be calculated by

$$P_s^* = m_s^* + T_s^* - V_s^* . \tag{A.7}$$

Following the same procedures for Fourier representation as outlined in Chap. 3, the mass and energy equations, respectively, transform to

$$(k_{ms}^* y_{s1} - y_{s2} + k_{ms}^* Y_{s3} - k_{ms}^* y_{s5}) \sin t^* + (y_{s1} + k_{ms}^* y_{s2} + k_{ms}^* y_{s4} - k_{ms}^* y_{s6}) \cos t^* = 0 , \tag{A.8}$$

$$\begin{aligned} \dot{\bar{W}}_s^* - \dot{\bar{H}}_s^* - \dot{\bar{Q}}_{ws}^* &+ \{FF(7) y_{s1} + [-1 + \gamma\tau_s + FF(8)] y_{s2} \\ &+ h_s^* y_{s3} - y_{s4} - (\gamma - 1) y_{s6}\} \sin t^* + \{[1 - \gamma\tau_s \\ &+ FF(9)] y_{s1} + [-FF(7)] y_{s2} + y_{s3} \\ &+ h_s^* y_{s4} + (\gamma - 1) y_{s5}\} \cos t^* = 0 , \end{aligned} \tag{A.9}$$

where

$$\tau_s = \frac{1}{2} (1 + T_K^*) , \tag{A.10}$$

$$FF(7) = -\frac{2\gamma}{3\pi} (y_{s4} \cos^3 \theta_s - y_{s3} \sin^3 \theta_s) , \tag{A.11}$$

$$FF(8) = \frac{2\gamma}{3\pi} [y_{s3} \cos \theta_s (\sin^2 \theta_s + 2) - y_{s4} \sin^3 \theta_s] , \tag{A.12}$$

$$FF(9) = -\frac{2\gamma}{3\pi} [y_{s3} \cos^3 \theta_s - y_{s4} \sin \theta_s (\cos^2 \theta_s + 2)] , \tag{A.13}$$

$$\sin\ \theta_s = \frac{y_{s1}}{\sqrt{y_{s1}^2 + y_{s2}^2}}\ , \tag{A.14}$$

$$\cos\ \theta_s = \frac{y_{s2}}{\sqrt{y_{s1}^2 + y_{s2}^2}}\ . \tag{A.15}$$

The constant terms in Eq. (A.9) merely represent, respectively, the cyclic averages of the work output, enthalpy flux, and heat input, the sum of which should be zero, as demanded by the steady state criterion. Thus, it follows that the gas spring must satisfy the integrated energy equation:

$$\overline{\dot{H}}_s^* + \overline{\dot{Q}}_{ws}^* = \overline{\dot{W}}_s^*\ , \tag{A.16}$$

and, concurrently, a system of fluctuating equations:

$$\begin{bmatrix} k_{ms}^* & -1 & k_{ms}^* & 0 \\ 1 & k_{ms}^* & 0 & k_{ms}^* \\ FF(7) & -1 + \gamma\tau_s + FF(8) & h_s^* & -1 \\ 1 - \gamma\tau_s + FF(9) & -FF(7) & 1 & h_s^* \end{bmatrix} \begin{bmatrix} y_{s1} \\ y_{s2} \\ y_{s3} \\ y_{s4} \end{bmatrix} = \begin{bmatrix} k_{ms}^* y_{s5} \\ k_{ms}^* y_{s6} \\ (\gamma - 1) y_{s6} \\ -(\gamma - 1) y_{s5} \end{bmatrix} . \tag{A.17}$$

The gas mean temperature is defined implicitly by the integrated energy equation [Eq. (A.16)]. Therefore, it requires expression of each term in that equation in fundamental variables. This can be done by evaluating the zero-order terms in the Fourier expansions. The procedure is similar to that for the complete engine analysis

$$\overline{\dot{H}}_s = Z1(5)(T_K - \overline{T}_s) + Z1(6)\ , \tag{A.18}$$

$$\overline{\dot{Q}}_{ws} = h_s \overline{A}_{ss}\ (\overline{T}_{ws} - \overline{T}_s)\ , \tag{A.19}$$

$$\overline{\dot{W}}_s = \frac{\omega}{2}\ \overline{P}_w \overline{V}_s\ [y_{s5}\ (y_{s2} + y_{s4}) - y_{s6}\ (y_{s1} + y_{s3})]\ , \tag{A.20}$$

$$Z1(5) = \frac{\omega}{\pi}\ c_p\ \overline{m}_s \sqrt{y_{s1}^2 + y_{s2}^2}\ , \tag{A.21}$$

$$Z1(6) = \frac{\gamma}{4(\gamma - 1)} \omega \overline{P}_w \overline{V}_s \left(y_{s1} y_{s4} - y_{s2} y_{s3}\right) . \tag{A.22}$$

With the aid of Eqs. (A.18)—(A.22), the cyclic mean gas temperature can now be solved:

$$\overline{T}_s = \frac{Z1(5) T_K + Z1(6) + h_s \overline{A}_{ss} \overline{T}_{ws} - \overline{\dot{W}}_s}{Z1(5) + h_s \overline{A}_{ss}} . \tag{A.23}$$

Some interactions exist between the cyclic mean temperature and fluctuating components. On one hand, the temperature and mass amplitudes are needed to evaluate the mean gas temperature. Conversely, some elements in the matrix equation depend on the mean gas temperature. Therefore, an iterative process is necessary for a complete solution. However, two special cases that render closed-form solutions will constitute the rest of this appendix.

Case 1: <u>Isothermal cylinder ($h_s^* \to \infty$) with leakage ($k_{ms}^* \neq 0$)</u>

For this limiting case, the gas inside the cylinder behaves isothermally with no temperature fluctuations. In other words, the system can be described only by the mass equation with the energy equation discarded. Therefore, a simple analytical solution becomes available.

One interesting consequence from the cyclic gas temperature [Eq. (A.23)] will be shown. Divide each term in the numerator and denominator by h_s and then take the limit for $h_s \to \infty$, resulting in

$$\overline{T}_s = \overline{T}_{ws} . \tag{A.24}$$

This confirms the notion that for isothermal cylinders, the heat transfer is so effective that the gas bulk temperature inside the cylinder equilibrates with the wall temperature at all times.

In the meantime, if each term in the last two equations in Eq. (A.17) is divided by h_s^* and then h_s^* approaches infinity, the matrix equation

will simplify to

$$\begin{bmatrix} k^*_{ms} & -1 & k^*_{ms} & 0 \\ 1 & k^*_{ms} & 0 & k^*_{ms} \\ 0 & 0 & 1 & 0 \\ 0 & 0 & 0 & 1 \end{bmatrix} \begin{bmatrix} y_{s1} \\ y_{s2} \\ y_{s3} \\ y_{s4} \end{bmatrix} = \begin{bmatrix} k^*_{ms} y_{s5} \\ k^*_{ms} y_{s6} \\ 0 \\ 0 \end{bmatrix} . \tag{A.25}$$

The solutions read

$$y_{s1} = \frac{k^*_{ms}(k^*_{ms} y_{s5} + y_{s6})}{1 + k^{*2}_{ms}} , \tag{A.26}$$

$$y_{s2} = \frac{k^*_{ms}(k^*_{ms} y_{s6} - y_{s5})}{1 + k^{*2}_{ms}} , \tag{A.27}$$

$$y_{s3} = 0 , \tag{A.28}$$

$$y_{s4} = 0 . \tag{A.29}$$

The first two represent the mass amplitudes, whereas the last two are the temperature amplitudes. Not surprisingly, it just reconfirms that there are no temperature fluctuations for isothermal gas springs.

Finally, by use of Eq. (A.7), the pressure wave may be computed:

$$p^*_s = 1 + \left[\frac{k^*_{ms}(k^*_{ms} y_{s5} + y_{s6})}{1 + k^{*2}_{ms}} - y_{s5}\right] \sin t^* + \left[\frac{k^*_{ms}(k^*_{ms} y_{s6} - y_{s5})}{1 + k^{*2}_{ms}} - y_{s6}\right] \cos t^* . \tag{A.30}$$

This completes the analysis of an isothermal gas spring with mass leakage acting alone. The significant implications were discussed in Sect. 4.5.1.

Case 2: Finite heat transfer cylinders ($h_s^* \neq 0$) with perfect seal ($k_{ms}^* = 0$)

For cylinders with a perfect seal, the gas spring will be subject to transient heat transfer loss only. Under this extreme, the system can be characterized solely by the energy equation, with the mass equation disregarded since the mass within the cylinder remains constant. Furthermore, the cyclic enthalpy flux term in the integrated energy equation no longer exists because no mass flows into or out of the cylinder. Consequently, the integrated energy equation simplifies to

$$\bar{\dot{Q}}_{ws}^* = \bar{\dot{W}}_s^* \tag{A.31}$$

or equivalently to the relation

$$\bar{T}_s = \bar{T}_{ws} - \frac{\bar{\dot{W}}_s}{h_s \bar{A}_{ss}} , \tag{A.32}$$

which is obtained from Eq. (A.23) by setting both functions Z(5) and Z(6) equal to zero because of no mass oscillation ($y_{s1} = y_{s2} = 0$). Concurrently, the system of the fluctuating equations can be proven to reduce to a 2 × 2 matrix equation:

$$\begin{bmatrix} h_s^* & -1 \\ 1 & h_s^* \end{bmatrix} \begin{bmatrix} y_{s3} \\ y_{s4} \end{bmatrix} = \begin{bmatrix} (\gamma - 1) y_{s6} \\ -(\gamma - 1) y_{s5} \end{bmatrix} . \tag{A.33}$$

An elegant closed-form solution for Eq. (A.33) reads

$$y_{s3} = \frac{(\gamma - 1)\ (h_s^* y_{s6} - y_{s5})}{1 + h_s^{*2}} , \tag{A.34}$$

$$y_{s4} = \frac{-(\gamma - 1)\ (h_s^* y_{s5} + y_{s6})}{1 + h_s^{*2}} . \tag{A.35}$$

Finally, the pressure wave can be expressed from Eq. (A.7) as

$$P_s^* = 1 + \left[\frac{(\gamma - 1)(h_s^* y_{s6} - y_{s5})}{1 + h_s^{*2}} - y_{s5}\right] \sin t^*$$

$$+ \left[\frac{-(\gamma - 1)(h_s^* y_{s5} + y_{s6})}{1 + h_s^{*2}} - y_{s6}\right] \cos t^* \ . \qquad (A.36)$$

This pressure wave equation is the most important relation for studying the transient heat transfer loss in semiadiabatic cylinders. In the first place, it can be used to calculate the amount of work required to drive the piston externally during a cycle (or the power loss). Second, by vector representations, it can be used to explain a worst case. The significant implications were discussed in Sect. 4.2.1.

The average gas temperature can now be derived more explicitly from the reduced integrated energy equation, that is, Eq. (A.32). Substitution of Eq. (A.20) for the cyclic work term, coupled with the solutions for the temperature amplitudes given by Eqs. (A.34) and (A.35), results in

$$\bar{T}_s = \bar{T}_{ws} + \frac{(\gamma - 1)^2 \ (y_{s5}^2 + y_{s6}^2)}{2(1 + h_s^{*2})} \bar{T}_s \ , \qquad (A.37)$$

or

$$\bar{T}_s = \bar{T}_{ws} + \frac{(\gamma - 1)^2}{2(1 + h_s^{*2})} \ |V_s^*|^2 \ \bar{T}_s \ ; \qquad (A.38)$$

or solve for the cyclic gas temperature explicitly:

$$\bar{T}_s = \frac{\bar{T}_{ws}}{1 - \dfrac{(\gamma - 1)^2}{2(1 + h_s^{*2})} \ |V_s^*|^2} \ . \qquad (A.39)$$

This relation reveals that for a nearly adiabatic cylinder ($h_s^* \to 0$), the mean gas temperature inside the cylinder depends on the square of

the relative volume amplitude; the larger the amplitude (or the piston-swept volume), the higher the mean gas temperature. This may be a somewhat surprising result, but it is a consequence demanded by the underlying physics. Recall that steady state operation is ensured only if the overall energy of the system is balanced; that is, work output equals heat input. When the mean gas temperature is greater than that of the wall, heat is transferred in an amount exactly equal to the work supplied externally to the piston to overcome the losses.

Appendix B

DERIVATION OF THE EFFICIENCY AND PRESSURE PHASE RELATION

For an engine with a uniform pressure, the relationships of the pressure, total volume, and expansion volume vectors may be depicted by Fig. B.1, in which the expansion-space volume vector leads the total volume vector by an angle of θ, and the pressure vector lags the negative total volume vector by an angle of ϕ.

The work output from the engine during one cycle is:

$$\bar{\dot{W}}_{out} \propto |P||V_t| \sin(180° - \phi) \propto |P||V_t| \sin \phi \ , \qquad (B.1)$$

where

$|P|$ = amplitude of the pressure,

$|V_t|$ = amplitude of total volume,

ϕ = phase angle between P and negative V_t.

Similarly, the heat input to the engine over a cycle may be represented by

$$\bar{\dot{Q}}_{in} \propto |P||V_e| \sin(180° - \theta - \phi) \propto |P||V_e| \sin(\theta + \phi) \ , \qquad (B.2)$$

ORNL–DWG 84–4429 ETD

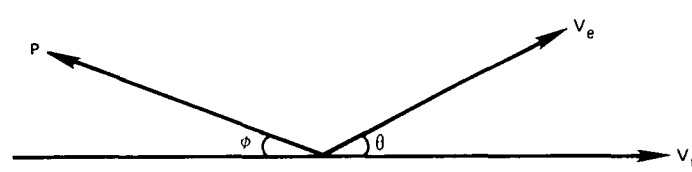

Fig. B.1. General relationship between pressure and volume vectors in Stirling engine.

where, in addition

$|V_e|$ = amplitude of expansion-space volume,

θ = phase angle between V_e and V_t.

By Eq. (2.15), the efficiency is defined by

$$\eta = \frac{\bar{\dot{W}}_{out}}{\bar{\dot{Q}}_{in}} . \tag{B.3}$$

Substituting Eqs. (B.1) and (B.2) into Eq. (B.3), after some simplification, results in:

$$\eta = \frac{|V_t|}{|V_e| \sin\theta \, (\cot\theta + \cot\phi)} . \tag{B.4}$$

This establishes the relationship between efficiency and pressure phase angle ϕ. For an engine with fixed dimensions, the volume amplitudes and phase angle θ are constant; the efficiency then depends only on the pressure phase angle. Rotating the pressure vector counterclockwise reduces ϕ. This, in turn, increases cot ϕ and therefore increases the denominator in Eq. (B.4), thus reducing η.

Appendix C

NOMENCLATURE

A_d	Displacer cross-sectional area (m^2)
A_p	Power piston cross-sectional area (m^2)
A_r	Displacer rod cross-sectional area (m^2)
A_{sc}	Wall heat transfer surface area in compression space (m^2)
A_{se}	Wall heat transfer surface area in expansion space (m^2)
a_1, a_2, a_3	Nondimensional volume constants defined in Eq. (3.17)
b_i	A nonhomogeneous vector involving specified volumes as components defined in Eq. (3.92)
c_p	Specific heat at constant pressure [J/(kg•K)]
c_v	Specific heat at constant volume [J/(kg•K)]
D(i,j)	Matrix elements defined in Eqs. (3.92) and (3.93)
FF(n)	n = 1,2,...9 Fourier correction factors
f	Frequency (Hz)
$\dot{H}_c$	Enthalpy flux rate into the compression space (W)
$\dot{H}_e$	Enthalpy flux rate into the expansion space (W)
h	Specific enthalpy (J/kg)
h_c	Cylinder wall to gas heat transfer coefficient in compression space [W/(m^2•K)]
h_e	Cylinder wall to gas heat transfer coefficient in expansion space [W/(m^2•K)]
k_{mc}	Mass leakage coefficient between compression and buffer spaces [kg/(Pa•s)]
k_{pc}	Pressure drop coefficient between compression and dead spaces [(Pa•s)/kg]
k_{pe}	Pressure drop coefficient between expansion and dead spaces [(Pa•s)/kg]
m	Mass of gas (kg)
m_c	Mass of gas in compression space (kg)
m_d	Mass of gas in dead volume (kg)
m_e	Mass of gas in expansion space (kg)
m_w	Total mass of gas in working space (kg)

P	Pressure (Pa)
P_c	Pressure in compression space (Pa)
P_d	Pressure in dead volume (Pa)
P_e	Pressure in expansion space (Pa)
$\overline{P}_w$	Cyclic average pressure in working space (Pa)
$\dot{Q}$	Heat transfer rate (W)
$\overline{\dot{Q}}_{in}$	Cyclic average total heat input rate, $\overline{\dot{Q}}_{in} = \overline{\dot{H}}_e + \overline{\dot{Q}}_{we}$ (W)
$\overline{\dot{Q}}_{out}$	Cyclic average total heat output rate, $\overline{\dot{Q}}_{out} = -\overline{\dot{H}}_c - \overline{\dot{Q}}_{wc}$ (W)
$\dot{Q}_{wc}$	Cylinder wall heat transfer rate in compression space (W)
$\dot{Q}_{we}$	Cylinder wall heat transfer rate in expansion space (W)
R	Gas constant [J/(kg•K)]
s	Specific entropy [J/(kg•K)]
T	Gas temperature (K)
T_c	Gas temperature in compression space (K)
$T_{c\ flux}$	Enthalpy flux temperature between compression and dead spaces (K)
$\overline{T}_d$	Constant temperature in dead space, $\overline{T}_d = \overline{V}_d/[\overline{V}_H/T_H + \overline{V}_R \ln (T_H/T_K)/(T_H - T_K) + \overline{V}_K/T_K]$ (K)
T_e	Gas temperature in expansion space (K)
$T_{e\ flux}$	Enthalpy flux temperature between expansion and dead spaces (K)
T_H	Heater temperature (K)
$\overline{T}_{in}$	Cyclic average gas temperature at which heat is absorbed into the engine (K)
T_K	Cooler temperature (K)
$\overline{T}_{out}$	Cyclic average gas temperature at which heat is rejected out of the engine (K)
$\overline{T}_{wc}$	Average wall temperature in compression space (K)
$\overline{T}_{we}$	Average wall temperature in expansion space (K)
t	Time (s)

v	Specific volume (m^3/kg)
V	Volume (m^3)
V_c	Prescribed compression volume (m^3)
$\overline{V}_c$	Average volume in compression space with pistons at mid-strokes (m^3)
$\overline{V}_d$	Constant dead space volume, $\overline{V}_d = \overline{V}_K + \overline{V}_H + \overline{V}_R$ (m^3)
V_e	Prescribed expansion volume (m^3)
$\overline{V}_e$	Average volume in expansion space with pistons at mid-strokes (m^3)
$\overline{V}_H$	Constant heater volume (m^3)
$\overline{V}_K$	Constant cooler volume (m^3)
$\overline{V}_R$	Constant regenerator volume (m^3)
V_t	Total volume in working space, $V_t = V_e + V_c + \overline{V}_d$ (m^3)
$\dot{W}_c$	PV power by gas in compression space (W)
$\dot{W}_e$	PV power by gas in expansion space (W)
$\overline{\dot{W}}_{out}$	Cyclic average total power output (W)
X_d	Prescribed displacer position, zero at midstroke (m)
X_{da}	Displacer amplitude, 1/2 displacer stroke (m)
X_p	Prescribed power piston position, zero at midstroke (m)
X_{pa}	Power piston amplitude, 1/2 power piston stroke (m)
X_{pm}	Maximum power piston amplitude allowable by mechanical constraint (m)
y_n	$n = 1,2,\ldots,14$, amplitudes of harmonic components defined in Eq. (3.33)
Z1(n)	$n = 1,2,\ldots,6$, defined in Eqs. (3.83)—(3.86), also Eqs. (A.21) and (A.22)

Superscripts

—	Average over a cycle
•	Derivative with respective to time or d/dt
*	Nondimensional quantities defined in Eqs. (3.10)—(3.18)
||	Amplitude of a variable

Subscripts

s	Gas spring

Greek

$\alpha_0, \alpha_1, \alpha_2$	Fourier coefficients
β	Phase angle relative to power piston (deg)
β_d	Displacer phase angle relative to power piston (deg)
β_P	Pressure phase angle relative to power piston (deg)
γ	Ratio of specific heats of gas, $\gamma = c_p/c_v$
Δm	Fluctuating mass component (kg)
ΔP	Fluctuating pressure component (Pa)
$\Delta\dot{S}_{loss}$	Entropy production due to internal irreversibilities defined in Eq. (2.27) (W/K)
$\Delta\dot{S}_{mixc}$	Entropy production due to mixing in compression space (W/K)
$\Delta\dot{S}_{mixe}$	Entropy production due to mixing in expansion space (W/K)
$\Delta\dot{S}_{MLc}$	Entropy production due to mass leakage (W/K)
$\Delta\dot{S}_{PDc}$	Entropy production due to pressure drop between compression and dead spaces (W/K)
$\Delta\dot{S}_{PDe}$	Entropy production due to pressure drop between expansion and dead spaces (W/K)
$\Delta\dot{S}_{Qc}$	Entropy production due to heat transfer in compression space ($\Delta\dot{S}_{Qc} = \Delta\dot{S}_{Qwc} + \Delta\dot{S}_{TQc}$) (W/K)
$\Delta\dot{S}_{Qe}$	Entropy production due to heat transfer in expansion space ($\Delta\dot{S}_{Qe} = \Delta\dot{S}_{Qwe} + \Delta\dot{S}_{TQe}$) (W/K)
$\Delta\dot{S}_{QH}$	Entropy production due to heater heat transfer (W/K)
$\Delta\dot{S}_{QK}$	Entropy production due to cooler heat transfer (W/K)
$\Delta\dot{S}_{Qwc}$	Entropy production due to average heat transfer in compression space (W/K)
$\Delta\dot{S}_{Qwe}$	Entropy production due to average heat transfer in expansion space (W/K)
$\Delta\dot{S}_{TQc}$	Entropy production due to transient heat transfer in compression space (W/K)

$\Delta\dot{S}_{TQe}$	Entropy production due to transient heat transfer in expansion space (W/K)
$\Delta\dot{S}_{\Delta P}$	Entropy production due to pressure drop ($\Delta\dot{S}_{\Delta P} = \Delta\dot{S}_{PDc} + \Delta\dot{S}_{PDe}$) (W/K)
ΔT	Fluctuating temperature component (K)
ΔV	Fluctuating volume component (m^3)
$\Delta\dot{W}_{TQc}$	Power loss due to transient heat transfer in compression space (W)
$\Delta\dot{W}_{TQe}$	Power loss due to transient heat transfer in expansion space (W)
$\Delta\eta_{EHT}$	Efficiency loss due to external heat transfer
$\Delta\eta_{loss}$	Efficiency loss due to various losses
$\Delta\eta_{mix}$	Efficiency loss due to mixing
$\Delta\eta_{THT}$	Efficiency loss due to transient heat transfer
η	Indicated thermal efficiency
η_c	Carnot efficiency
θ	Phase angle between V_e and V_t (deg)
θ_c	Defined in Eq. (3.74)
θ_e	Defined in Eq. (3.42)
τ_c	Temperature ratio associated with compression space, $\tau_c = (T_K + \overline{T}_c)/2\,\overline{T}_c$
τ_e	Temperature ratio associated with expansion space, $\tau_e = (T_H + \overline{T}_e)/2\,\overline{T}_e$
ϕ_P	Phase angle between pressure vector and negative total volume vector (deg)
ω	Frequency (rad/s)

Internal Distribution

1. F. C. Chen
2-11. N. C. J. Chen
12. F. A. Creswick
13. J. L. Crowley
14. N. Domingo
15. P. D. Fairchild
16. W. Fulkerson
17-26. F. P. Griffin
27. D. S. Griffith
28. F. R. Kalhammer (Consultant)
29. S. V. Kaye (Consultant)
30. T. R. LaPorte (Consultant)
31. R. E. MacPherson
32. J. W. Michel
33. R. J. Minturn
34. L. I. Moss (Consultant)
35. R. W. Murphy
36. G. T. Privon
37. H. E. Trammell
38. D. B. Trauger
39-48. C. D. West
49. W. H. Williams (Consultant)
50-59. Materials and Systems Technology, Building 9108, MS-2
60. ORNL Patent Office
61. Central Research Library
62. Document Reference Section
63-64. Laboratory Records Department
65. Laboratory Records (RC)

External Distribution

66. D. Alter, NASA Lewis Research Center, 21000 Brookpark Road, Mail Stop 500-215, Cleveland, OH 44135
67. Thierry Alleau, Commissariat a l'Energie Atomique, Centre d'Etudes Nuclearies de Grenoble, Service des Transferts Termiques, 85X, 38041 GRENOBLE CEDEX, France
68. W. Beale, Sunpower, Inc., 6 Byard St., Athens, OH 45701
69. G. M. Benson, Energy Research and Generation, Inc., Lowell & 57th Street, Oakland, CA 94608
70. D. M. Berchowitz, Sunpower, Inc., 6 Byard St., Athens, OH 45701
71. D. G. Beremand, Stirling Engine Project Office, National Aeronautics and Space Administration, Lewis Research Center, Cleveland, OH 44135
72. Stig G. Carlqvist, Societe ECA, 17 Avenue du Chateau, 92190 Meudon-Bellevue, France
73. W. Chiu, General Electric Company, Advanced Energy Programs Department, P.O. Box 527, King of Prussia, PA 19406
74. Lt. Cmdr. Mike Clarke, Royal Naval Engineering College, Manadon, Plymouth, Devon PL5 3AQ, United Kingdom
75. Mike Clinch, Gas Research Institute, 8600 W. Bryn Mawr Avenue, Chicago, IL 60631

76. E. H. Cooke-Yarborough, Instrumentation and Applied Physics Division, Atomic Energy Research Establishment, Harwell, Didcot, Oxon OX11, ORA, England
77. J. G. Daley, Components Technology Division, Argonne National Laboratory, 9700 South Cass Ave., Argonne, IL 60439
78. Adriano de Cicco, Instituto di Macchine E Technologie Meccaniche, Universita de Roma, Rome, Italy
79. G. Dochat, Mechanical Technology, Inc., 968 Albany-Shaker Rd., Latham, NY 12110
80. H. B. Faulkner, Department of Mechanical Engineering, Massachusetts Institute of Technology, Cambridge, MA 02139
81. O. R. Fauvel, University of Calgary, 2500 University Drive NW, Calgary, Alberta, Canada T2N 1N4
82. T. Finkelstein, TCA, P.O. Box 643, Beverly Hills, CA 90213
83. R. J. Fiskum, Program Manager, Energy Conversion Equipment Branch, CE113.2, Rm. GH068, Department of Energy, 1000 Independence Ave. S.W., Washington, DC 20585
84. D. B. Gedeon, Sunpower, Inc., 6 Byard St., Athens, OH 45701
85. L. Goldberg, University of Minnesota, 28 Appleby Hall, 128 Pleasant St. SE, Minneapolis, MN 55455
86. B. Goldwater, Mechanical Technology, Inc., 968 Albany-Shaker Road, Latham, NY 12110
87. Marv. Gunn, ECUT, Department of Energy, 1000 Independence Ave. S.W., Washington, D.C. 20585
88. A. C. Harvey, Foster-Miller Associates, Inc., 350 Second Ave., Waltham, MA 02154
89. J. Hogan, General Electric Co., P.O. Box 8666, Philadelphia, PA 19101
90. R. E. Holtz, Components Technology Division, Bldg. 330, Argonne National Laboratory, 9700 South Cass Ave., Argonne, IL 00439
91. W. F. Hughes, Mechanical Engineering Department, Carnegie-Mellon University, Schenley Park, Pittsburgh, PA 15213
92. Y. Ishizaki, Cryogenic Systems, 253-5 Yamanouchi, Kamakura 247, Japan
93. Naotsugu Isshiki, 2-29-6 Kyodo Setagayaku, Tokyo 156, Japan
94. E. Keshock, Mechanical and Aerospace Engineering Department, University of Tennessee, Knoxville, TN 37996
95. Nobuhide Kasagi, University of Tokyo, Department of Mechanical Engineering, Bunkyo-Ku, Tokyo 113, Japan
96. Bill Krauss, Gas Research Institute, 8600 W. Bryn Mawr Avenue, Chicago, Il 60631
97. Kangpil Lee, Facility and Manufacturing Automation, P.O. Box 809, Sudbery, MA 01776
98. K. L. Lewis, School of Mechanical Engineering, University of the Witwatersrand, Johannesburg, South Africa
99. Tom J. Marusak, Mechanical Technology, Inc., 986 Albany-Shaker Road, Latham, NY 12110
100. W. Martini, Martini Engineering, 2303 Harris, Richland, WA 99352
101. R. C. Meier, Advanced Energy Programs Dept., General Electric Company, P.O. Box 527, King of Prussia, PA 19406
102. Naomasa Nakajima, Department of Mechanical Engineering, University of Tokyo, Bunkyo-ku, Tokyo 113, Japan

103. Vincenzo Naso, Universita Degli Studi Di Roma, Instituto di Macchine E Technologie Meccaniche, Rome, Italy
104. N. P. Nightingale, Stirling Engine Systems Division, Mechanical Technology, Inc., 968 Albany-Shaker Rd., Latham, NY 12110
105. Herbert Nilsson, United Stirling AB, Box 856, S-201 80 Malmo, Sweden
106. W. Perceval, United Stirling, Inc., 211 Strand, Alexandria, VA 22314
107. C. J. Rallis, University of Witwatersrand, School of Mechanical Engineering, 1 Jan Smuts Avenue, Johannesburg 2001, South Africa
108. W. H. Raser, Data Trace, Inc., 6451 W. 83rd Street, Los Angeles, CA 90045
109. Lt. Cmdr. G. T. Reader, Royal Naval Engineering College, Manadon, Plymouth, Devon PL5 3AQ, United Kingdom
110. D. A. Renfroe, University of Arkansas, Mechanical Engineering & Engineering Science Department, Fayetteville, AR 72701
111. G. Rice, Department of Engineering, University of Reading, Reading, Berkshire, England
112. P. Riggle, University of Washington, Richland, WA 99352
113. Franco Rispoli, Instituto di Macchine E Technologie Meccaniche - A.T.I., Sezione Laziale, Rome, Italy
114. D. H. Rix, University Engineering Department, Trumpington St., Cambridge, CB2 1PZ, England
115. A. Ross, Ross Enterprises, 37 West Broad Street, Suite 360, Columbus, OH 43215
116. J. D. Ryan, Acting Chief, Energy Conversion Equipment Branch, CE113.2, Rm. GH068, Department of Energy, 1000 Independence Ave. S.W., Washington, DC 20585
117. J. G. Schrieber, Stirling Engine Project Office, National Aeronautics and Space Administration, Lewis Research Center, Cleveland, OH 44135
118. D. J. R. Senft, Department of Mathematics/Computer Science, University of Wisconsin, River Falls, WI 54022
119. Lt. Cmdr. M. G. Short, Royal Naval Engineering College, Manadon Plymouth, Devon P15 3AQ, England
120. R. Shoureshi, Department of Mechanical Engineering, College of Engineering, Wayne State University, Detroit, MI 48202
121. M. A. Simetkosky, Stirling Engine System Division, Mechanical Technology, Inc., 968 Albany-Shaker Rd., Latham, NY 12110
122. J. G. Slaby, National Aeronautics and Space Administration, Lewis Research Center, Cleveland, OH 44135
123. S. Srinivasan, Department of Mechanical Engineering, University of Calgary, 2920 24th Ave. NW, Calgary, Canada T2N1N4
124. Chin-Chia Su, University Engineering Department, Trumpington St., Cambridge, CB2 1PZ, England
125. P. F. Swenson, Director, Energy Systems Research, Consolidated Natural Gas Service Co., 11001 Cedar Ave., Cleveland, OH 44106
126. D. R. Taylor, Royal Naval Engineering College, Manadon Plymouth, Devon PL5 3AQ, England
127. Roy Tew, National Aeronautics and Space Administration, Lewis Research Center, Cleveland, Ohio 44135
128. Israel Urieli, Sunpower, Inc., 6 Byard St., Athens, OH 45701

129. V. J. Van Griethuysen, Energy Conversion Branch, Aerospace Power Division - Aero Propulsion Laboratory, Department of the Air Force, Wright-Patterson Air Force Base, OH 45433
130. D. A. Vaughn, Department of the Army, U.S. Army Mobility Equipment R&D Command, Fort Belvoir, VA 22060
131. G. Walker, Department of Mechanical Engineering, University of Calgary, 2920 24th Ave. NW, Calgary, Canada T2N1N4
132. B. P. Wang, Mechanical Engineering Dept., University of Texas at Arlington, P.O. Box 19023, Arlington, TX 76019
133. Seiichi Watanabe, Welding Laboratory, Central Research Laboratories, Sumitomo Metal Industries Ltd., No. 3 1-Chome, Nishinagasu Hondori, Amagasaki, Japan
134. M. A. White, University of Washington, Richland, WA 99352
135. Les Wright, Gas Research Institute, 8600 W. Bryn Mawr Avenue, Chicago, Il 60631
136. Office of Assistant Manager for Energy Research and Development, Department of Energy, ORO, Oak Ridge, TN 37831

137-163. Technical Information Center, DOE, Oak Ridge, TN 37831